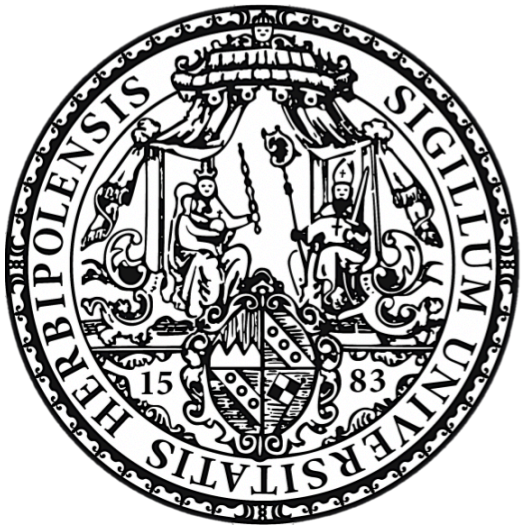

Cadherin-13 Deficiency Impacts Murine Serotonergic Circuitries and Cognitive Functions

Cadherin-13 Defizienz beeinflusst serotonerge Netzwerke und kognitive Funktionen der Maus

Dissertation for a doctoral degree
at the Graduate School of Life Sciences,
Julius-Maximilians-Universität Würzburg,
Section Neuroscience

submitted by

Hsing-Ping Ku

from
Kaohsiung, Taiwan

Würzburg, 2021

Submitted on:

Members of the *thesis committee*:

Chairperson: Prof. Dr. Matthias Gamer

Primary Supervisor: Prof. Dr. Klaus-Peter Lesch

Supervisor (Second): PD Dr. Robert Blum

Supervisor (Third): Prof. Dr. Esther Asan

Date of Public Defense:
Date of Receipt of Certificates: .....

ACKNOWLEDGEMENTS

I would first like to thank my colleague and a very dear friend, Dr. Andrea Forero, for all her support, ideas, and input during this project. Also, I would also like to thank Dr. Olga Rivero for being a great mentor in every aspect of my research and life. I would furthermore like to thank my supervisor, Professor Dr. Klaus-Peter Lesch, for his advice during this PhD, along with my committee members, PD Dr. Robert Blum and Professor Dr. Esther Asan, for their valuable suggestions. I would like to thank all the members of my lab who provided great technical assistance; all the colleagues with whom I held discussions and had fun; my students and interns for the great teaching experience and for their feedback. Last but not least, a thank you to all my friends and family, who have been so supportive throughout my whole PhD period. I could not have done this without you.

ABSTRACT

Cadherin-13 (CDH13) is a member of the cadherin superfamily that lacks the typical transmembrane domain for classical cadherins and is instead attached to the cell membrane with a GPI-anchor. Over the years, numerous genome-wide association (GWA) studies have identified CDH13 as a risk factor for neurodevelopmental disorders, including attention-deficit/hyperactivity disorder (ADHD) and autism spectrum disorder. Further evidence using cultured cells and animal models has shown that CDH13 plays important roles in cell migration, neurite outgrowth and synaptic function of the central nervous system. Research in our laboratory demonstrated that the CDH13 deficiency resulted in increased cell density of serotonergic neurons of the dorsal raphe (DR) in developing and mature mouse brains as well as serotonergic hyperinnervation in the developing prefrontal cortex, one of the target areas of DR serotonergic neurons. In this study, the role of CDH13 was further explored using constitutive and serotonergic system-specific CDH13-deficient mouse models. Within the adult DR structure, the increased density of DR serotonergic neurons was found to be topographically restricted to the ventral and lateral-wing, but not dorsal, clusters of DR. Furthermore, serotonergic hyperinnervation was observed in the target region of DR serotonergic projection neurons in the lateral wings. Unexpectedly, these alterations were not observed in postnatal day 14 brains of CDH13-deficient mice. Additionally, behavioral assessments revealed cognitive deficits in terms of compromised learning and memory ability as well as impulsive-like behaviors in CDH13-deficient mice, indicating that the absence of CDH13 in the serotonergic system alone was sufficient to impact cognitive functions and behavioral competency. Lastly, in order to examine the organization of serotonergic circuitries systematically and to tackle limitations of conventional immunofluorescence, a pipeline of the whole-mount immunostaining in combination with the iDISCO+ based rapid tissue clearing techniques was established. This will facilitate future research of brain neurotransmitter systems at circuitry and/or whole-brain levels and provide an excellent alternative for visualizing detailed and comprehensive information about a biological system in its original space. In summary, this study provided new evidence of CDH13's contribution to proper brain development and cognitive function in mice, thereby offering insights into further advancement of therapeutic approaches for neurodevelopmental disorders.

ZUSAMMENFASSUNG

Cadherin-13 (CDH13) ist ein Mitglied der Cadherin-Superfamilie, dem die für klassische Cadherine typische Transmembran-Domäne fehlt und das stattdessen mit einem GPI-Anker an der Zellmembran befestigt ist. Im Laufe der Jahre wurde CDH13 in mehreren genom-weiten Assoziationsstudien (GWAS) als Risikofaktor für neurologische Entwicklungsstörungen, einschließlich Aufmerksamkeitsdefizit-/Hyperaktivitätsstörung (ADHS) und Autismus-Spektrum-Störung, identifiziert. Weitere Nachweise in Zellkulturen und Tiermodellen zeigten, dass CDH13 eine wichtige Rolle bei der Zellmigration, dem Wachstum von Neuriten und der synaptischen Funktion des zentralen Nervensystems spielt. Untersuchungen in unserem Labor haben gezeigt, dass CDH13-Defizienz zu einer erhöhten Zelldichte serotonerger Neuronen der dorsalen Raphe (DR) in sich entwickelnden und reifen Mäusegehirnen sowie zu einer serotonergen Hyperinnervation im sich entwickelnden präfrontalen Kortex, einem der Zielgebiete der serotonergen Neuronen der DR, führt. In dieser Studie wurde die Rolle von CDH13 weiter untersucht, indem konstitutive und für das serotonerge System spezifische CDH13-defiziente Mausmodelle verwendet wurden. Innerhalb der adulten DR-Struktur zeigte sich, dass die erhöhte Dichte serotonerger DR-Neurone topographisch auf die ventralen und lateralen, nicht aber dorsalen Cluster der DR beschränkt ist. Außerdem wurde eine serotonerge Hyperinnervation in der Zielregion der serotonergen Projektionsneuronen der DR in den Seitenflügeln beobachtet. Unerwarteterweise wurden diese Veränderungen nicht in den Gehirnen von CDH13-defizienten Mäusen nach dem 14. postnatalem Tag. Darüber hinaus zeigten Verhaltensuntersuchungen bei CDH13-defizienten Mäusen kognitive Defizite in Form von beeinträchtigter Lern- und Gedächtnisfähigkeit sowie impulsivem Verhalten, was darauf hindeutet, dass das Fehlen von CDH13 im serotonergen System allein ausreicht, um kognitive Funktionen und Verhaltenskompetenz zu beeinträchtigen. Um die Organisation der serotonergen Netzwerke systematisch zu untersuchen und die Grenzen der konventionellen Immunfluoreszenz zu überwinden, wurde eine Pipeline für die Ganzkörper-Immunfärbung in Kombination mit der auf iDISCO+ basierenden raschen und effizienten Gewebereinigungstechnik eingerichtet. Dies wird die künftige Erforschung der Neurotransmitter-Systeme des Gehirns auf Netzwerk- und/oder Ganzhirnebene erleichtern und eine hervorragende Alternative für die Visualisierung detaillierter und umfassender Informationen über ein biologisches System in seinem ursprünglichen Raum bieten. Zusammenfassend lässt sich sagen, dass diese Studie neue Hinweise für den Beitrag von CDH13 zur korrekten Entwicklung des Gehirns und der kognitiven Funktionen bei Mäusen lieferte und damit Einblicke in die weitere Entwicklung von therapeutischen Ansätzen für Entwicklungsstörungen des Nervensystems bietet.

CONTENTS

ABBREVIATIONS

-ir	Immunoreactive
°C	Degree celsius
3D	Three-dimensional
5-CSRTT	Five-choice serial reaction time task
5-HT	5-hydroxy--tryptamine
5-HTT	Serotonin transporter
ADHD	Attention-deficit/hyperactivity disorder
AKT	Protein kinase B
AmyBL	Basolateral complex of amygdala
ANOVA	Analysis of variance
B2m	Beta 2 microglobulin
B7d	The dorso-median clusters of serotonergic neurons in DR
B7l	The serotonergic-neuron clusters of lateral wings of DR
B7v	The ventral cluster of serotonergic neurons in DR
BDNF	Brain-derived neurotrophic factor
BM	Barnes maze
BSA	Bovine serum albumin
CA	Cornu ammonis
CAM	Cell adhesion molecules
CB	Cerebellum
CCD	Charge-coupled device
CDH13	Cadherin-13
Cdh13 cKO	Serotonergic system-specific CDH13 knockout mice
CELSR1	Cadherin EGF LAG seven-pass G-type receptor 1
CG	Cingulate cortex
CLARITY	Clear lipid-exchanged acrylamide-hybridized rigid imaging / immunostaining / in situ-hybridization-compatible tissue hydrogel
CNS	Central nervous system

CNV	Copy number variants
CPu	Caudate putamen
Ctx	Cortex
Cy3	Cyanine 3
Cy5	Cyanine 5
DAPI	4′,6-diamidino-2-phenylindole
D	Day
dATP	Deoxyadenosine triphosphate
DCM	Dichloromethane
dCTP	Deoxycytidine triphosphate
DEPC	Diethylpyrocarbonate
DG	Dentate gyrus
dGTP	Deoxyguanosine triphosphate
DMSO	Dimethyl sulfoxide
DNA	Deoxyribonucleic acid
DNP	Dinitrophenyl
dNTP	Deoxynucleoside triphosphate
DR	Dorsal raphe
DTT	Dithiothreitol
dTTP	Deoxythymidine triphosphate
E	Embryonic day
E/I	Excitation and inhibition
EC	Extracellular cadherin
ec	External capsule
EGF	Epidermal growth factor
EGFP	Enhanced green fluorescent protein
EphA5	Erythropoietin-producing hepatocellular carcinoma receptor A5
EPM	Elevated plus maze
GABA	Gamma-Aminobutyric acid

GAP-43	Growth-associated protein-43
GC	Guanine-cytosine
GFP	Green fluorescent protein
GPI	Glycosylphosphatidylinositol
GWAS	Genome-wide association studies
H_2O_2	Hydrogen peroxide
Hb	Hindbrain
H	Habituation phase
iDISCO	Immunolabelling-enabled three-dimensional imaging of solvent cleared organs
iDISCO+	Improved immunolabelling-enabled three-dimensional imaging of solvent cleared organs
Ig	Immunoglobulin
IL	Infralimbic cortex
iPSC	Induced pluripotent stem cells
ITI	Inter-trial interval
KO	Knockout
LDB	Light-dark box
LMD	Laser microdissection
LoF	Loss of function
LSFM	Light sheet fluorescence microscopy
Mb	Midbrain
mle	Medial lemniscus
mfb	Medial forebrain bundle
mPFC	Medial prefrontal cortex
mtg	Mamillotegmental tract
n	Sample size
NCAM	Neural cell adhesion molecule
OB	Olfactory bulb
OF	Open field test

OR	Object recognition test
P	Postnatal day
p	P-value
PBS	Phosphate-buffered saline
Pcdhαc2	Protocadherin alpha subfamily C, 2
PCR	Polymerase chain reaction
PEN	Polyethylene-naphthalate
PET1 (=FEV)	FEV transcription factor, ETS family member
PFA	Paraformaldehyde
PFC	Prefrontal cortex
PI3K/AKT	Phosphoinositide-3-kinase
PTwH	PBS/0.2% Tween-20 with 10 µg/ml heparin buffer
qRT-PCR	Real-time quantitative reverse transcription PCR
RFP	Red fluorescent protein
RI	Refractive index
RNA	Ribonucleic acid
RNAi	RNA interference
ROI	Region of interest
ROUT	Robust regression and outlier removal
Rplp0	Ribosomal protein lateral stalk subunit P0
RT	Room temperature
S100B	S100 calcium binding protein B
SB	Social behavior test
scs	Supracallosal striae
SDS	Sodium dodecyl sulfate
SERT	Serotonin transporter
SIM	Structured illumination microscopy
sm	Stria medullaris
SNP	Single nucleotide polymorphism

SN	Substantia nigra
SNV	Single nucleotide variation
StD	Stimulus duration
TBS	Tris-buffered saline
Th	Thalamus
TH	Tyrosine hydroxylase
ThaLD	Laterodorsal nucleus of thalamus
ThaPV	Paraventricular nucleus of thalamus
TM	Transmembrane domain
TPH2	Tryptophan hydroxylase 2
Tris	Tris (hydroxymethyl)-aminomethane
UKW	Universitätsklinikum würzburg
VA-044	2,2'-Azobis[2-(2-imidazolin-2-yl)propane] dihydrochloride
VTA	Ventral tegmental area
WES	Whole exome sequencing
WT	Wild-type

LIST OF TABLES

LIST OF FIGURES

CHAPTER 1 INTRODUCTION

1.1 Classical cadherins and Cadherin-13

Cell-cell recognition and adhesion are crucial processes in the formation and maintenance of complex neural networks in the central nervous system (CNS). Among all cell adhesion molecules, the cadherin superfamily, a group of calcium-dependent transmembrane proteins, has been identified as a critical player in these processes. Ever since the first cadherin was discovered by Yoshida and Takeichi (1982), many other molecules sharing amino acid sequences with the cadherins have been identified, some having been extensively studied. We are now aware of over 130 types of cadherins in the superfamily that work together in synchrony towards functions such as neural tube formation, cell migration, boundary formation, cell differentiation, neurite elongation and branching, axon guidance, target recognition, and synaptogenesis (Hirano and Takeichi, 2012). Despite sharing gross functional abilities, their individual roles vary due to their differences in structure, expression, and anatomical location.

Cadherin-13 (CDH13), an atypical member of the cadherin superfamily, was first characterized by Ranscht and Dours-Zimmermann (1991) in chick embryos. Instead of having transmembrane and cytoplasmic domains typical of classical cadherins, CDH13 anchors to the plasma membrane via a glycosylphosphatidylinositol (GPI) moiety (Fig. 1). It has therefore been labelled "T-cadherin", short for truncated cadherin. Without the strand-swapping sequence signatures on which the binding mechanism of classical cadherins depends, CDH13 engages in intercellular recognition through a homophilic interface that is distinct from that of classical cadherins. Namely, it forms *trans*-dimers at the non-swapped interface near the extracellular cadherin (EC) 1 and 2 calcium binding sites (Ciatto et al., 2010). Like other GPI-anchored membrane proteins, cell surface CDH13 is localized to the so-called lipid rafts where it interacts with signal transduction proteins that control various cellular functions (Arnemann et al., 2006; Doyle et al., 1998; Philippova et al., 2008). Despite lacking the transmembrane domain, the cellular position of CDH13 indicates that it may mediate intracellular signaling, presumably via interaction with integrin β1, and thereby activate the PI3K/AKT pathway (Rivero et al., 2013; Sacristan et al., 1993). Taken together, these findings imply the importance of CDH13 in intracellular signaling and its role in mechanical adhesion.

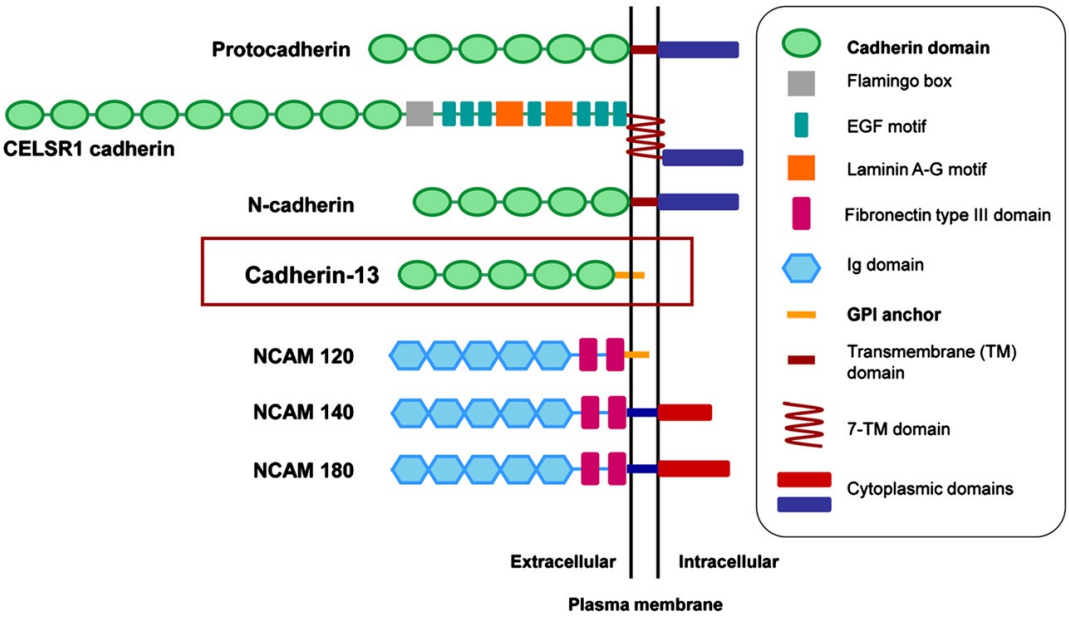

Figure 1. Structure of cell adhesion molecules (CAM).
Mature classical (type I) cadherins, such as N-cadherin, have ectodomains consisting of five EC repeats, a single transmembrane domain (TM), and a cytoplasmic domain that interacts with β-catenin (which is linked to the actin cytoskeleton via F-actin binding protein α-catenin). This transmembrane assembly of cadherin-catenin complex with the cytoskeleton is crucial for the stabilization and adhesion-mediated signaling (Conacci-Sorrell et al., 2002; Shapiro and Weis, 2009). Numerous nonclassical cadherins have also been characterized, including the clustered and non-clustered protocadherins, flamingo cadherins with receptor-like seven-pass TMs (e.g. CELSR1), and CDH13 (shown in the red boxed area), which attaches to the cell membrane via a GPI-anchor rather than the typical TM. CELSR1, Cadherin EGF LAG seven-pass G-type receptor 1; NCAM, neural cell adhesion molecule; EGF, epidermal growth factor; Ig, immunoglobulin; GPI, glycosylphosphatidylinositol. Reprinted from "Impact of the ADHD-susceptibility gene CDH13 on development and function of brain networks," by Rivero et al., 2013. *European Neuropsychopharmacology*, 23(6), p. 16. Copyright (2012), with permission from Elsevier (License number: 5112971445345).

1.2 The role of CDH13 in the central nervous system

Several studies investigating the function of CDH13 during neurodevelopment have implicated it in cell migration, neurite outgrowth, and synaptic function. Early studies on neurite outgrowth of motor neurons in chick embryos indicated that CDH13 is localized at the growth cones and serves as a negative regulator that works in concert with other molecules to guide motor axons to their peripheral targets (Fredette et al., 1996; Fredette and Ranscht, 1994). In vascular cells, CDH13 was found to be redistributed to the leading edge of migrating cells, suggesting its involvement in directed locomotion and cell-cell recognition (Philippova et al., 2003). Knocking down CDH13 using an RNAi-based technique in hippocampal cultures resulted in decreased synapse density of glutamatergic and GABAergic neurons, indicating the importance of CDH13 in synaptic development (Paradis et al., 2007). In murine embryos, it was shown that loss of CDH13 resulted in altered axonal formation of cortical neurons and a reduced number of cortical GABAergic interneurons (Hayano et al., 2014; Killen et al., 2017). Moreover, Forero et al. (2017) found an increased number of serotonergic neurons as well as their projections to the developing cortex when CDH13 was absent in mouse embryos, suggesting its role in the

accurate development of serotonergic neurons. Despite all of the efforts made in the past decade, the function of CDH13 during neurodevelopment remains unclear.

The temporal and spatial expressions of CDH13 in mice have been investigated in certain developmental stages by several independent studies. Initially expressed in restricted areas such as the dorsal raphe (DR) at embryonic day (E) 13.5, the presence of CDH13 shifts rostrally to the forebrain at E17.5 (Fig. 2) and later widely distributes in many areas in the adult mouse brain (Forero et al., 2017; Rivero et al., 2015; Rivero et al., 2013). First detected at E13.5, the expression of *Cdh13* mRNA in the whole mouse brain peaks at postnatal (P) day 7 and gradually downregulates, but persists, in brain areas exhibiting synaptic plasticity such as the hippocampus (Rivero et al., 2015). Takeuchi et al. (2000) found *Cdh13* transcripts in prefrontal cortex, medulla, thalamus and midbrain as well as CDH13 in cellular membranes and neurites of the cerebral cortex, medulla oblongata and nucleus olivaris in the human adult brain. Interestingly, in the same study, the authors found CDH13 expression level to be higher in the adult brain than in the developing brain, although this effect has not been seen in mice and new world monkeys (Matsunaga et al., 2013; Rivero et al., 2015). Nonetheless, the fact that the expression of CDH13 persists after the completion of neuronal circuit formation suggests a likely involvement of CDH13 in the maintenance of synapses and/or the coordination of processes critical for synaptic plasticity (Rivero et al., 2015). Indeed, CDH13 is present on inhibitory pre- and postsynaptic sites of cultured hippocampal neurons; loss of CDH13 resulted in increased inhibitory synaptic transmission due to altered number of inhibitory synapses formed onto CA1 pyramidal cells in postnatal hippocampal slices of the mouse (Rivero et al., 2015). A recent publication using human-derived iPSCs also demonstrated an important role for CDH13 in excitation and inhibition (E/I) balance, possibly the key structure underlying the neural code and cognition (Mossink et al., 2021). More research is needed to broaden the understanding of CDH13's role in mature CNS.

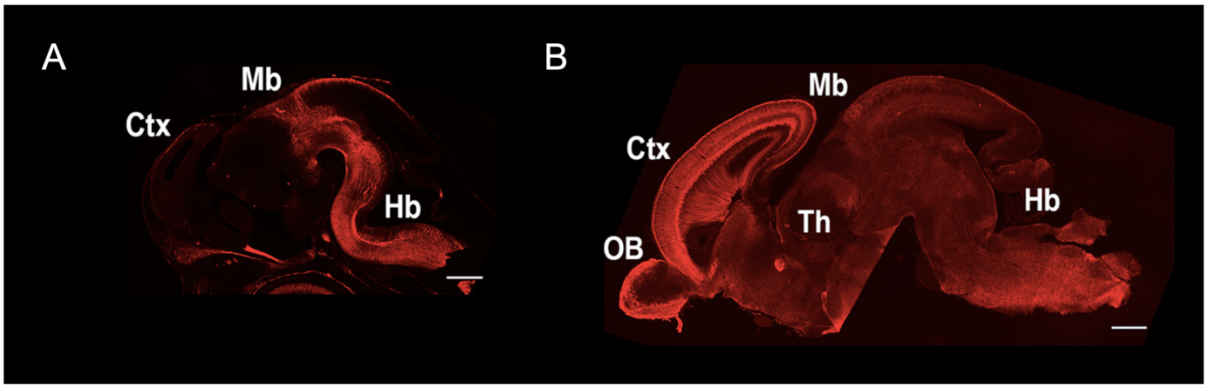

Figure 2. Distribution of CDH13 protein in the embryonic mouse brain.
At E13.5, CDH13 immunoreactivity is mainly found in the hindbrain (A), while it shifts rostrally to the forebrain at E17.5 (B). Ctx, cortex; Hb, hindbrain; Mb, midbrain; Th, thalamus; OB, olfactory bulb. Scale bar = 500 µm. Adapted from "Cadherin-13 Deficiency Increases Dorsal Raphe 5-HT Neuron Density and Prefrontal Cortex Innervation in the Mouse Brain," by Forero et al., 2017. *Front Cell Neurosci.,* 11(307). Copyright © 2017 Forero, Rivero, Wäldchen, Ku, Kiser, Gärtner, Pennington, Waider, Gaspar, Jansch, Edenhofer, Resink, Blum, Sauer and Lesch.

1.3 Clinical importance of CDH13

About 5% children worldwide suffer from attention-deficit/hyperactivity disorder (ADHD), of which around 50% have symptoms that persist into adulthood, bringing about a substantial individual and societal burden (Childress and Berry, 2012; Lai et al., 2014). ADHD may occur either as an isolated disorder or be accompanied by comorbid conditions, including mood, anxiety, substance abuse, and personality disorders (Katzman et al., 2017; Spencer, 2006). Results from meta-analysis of multiple twin studies estimated ADHD's heritability to be 74%, which prompted the search for common genetic variants determining ADHD susceptibility (Faraone and Larsson, 2019). As a result, several genome-wide association studies (GWAS), meta-analysis, and whole exome sequencing (WES) studies identified CDH13 as a risk gene for neurodevelopmental disorders (Fig. 3) (Franke et al., 2009; Mavroconstanti et al., 2013; Neale, Medland, Ripke, Asherson, et al., 2010; Salatino-Oliveira et al., 2015; Zhou, Asherson, et al., 2008). In a cohort of ADHD-affected children, Arias-Vasquez *et al.* found an intron-variant within *CDH13,* rs11150556, to be genome-wide associated with performance on verbal working memory. Supportively, CDH13 is found in areas that are important for verbal working memory, such as the fronto-parietal network and the cerebellum (Emch et al., 2019; Eriksson et al., 2015). Notwithstanding the link between *CDH13* and ADHD, many of the associated single nucleotide polymorphisms (SNPs) are located in non-coding regions (e.g. intron-variants) of the gene. It is said that rather than causing alterations in protein function, the variant SNPs cause changes in gene expression levels, which may ultimately contribute to disruption of proper brain function (Hawi et al., 2018; Tak and Farnham, 2015).

Moreover, convergent evidence from brain imaging, behavioral, and molecular genetic studies indicate that the neuropathophysiology of ADHD originates from complex multisystem abnormalities from multiple cortical and subcortical areas that are structurally and functionally connected to each other. Although it has not been examined systematically in mature human CNS, CDH13 expression pattern in mice overlaps largely with the underlying neural networks that mediate cognitive control, attention, timing and working memory (such as the fronto-cingulo-striato-thalamic and fronto-parieto-cerebellar networks), as well as regions showing volumetric reductions in children with ADHD (such as the nucleus accumbens, amygdala, caudate, hippocampus, putamen, cerebellum, and prefrontal cortex) (Greven et al., 2015; Hoogman et al., 2017; Konrad and Eickhoff, 2010; Valera et al., 2007). It is therefore of considerable relevance to understand the role of CDH13 in brain development and physiological function.

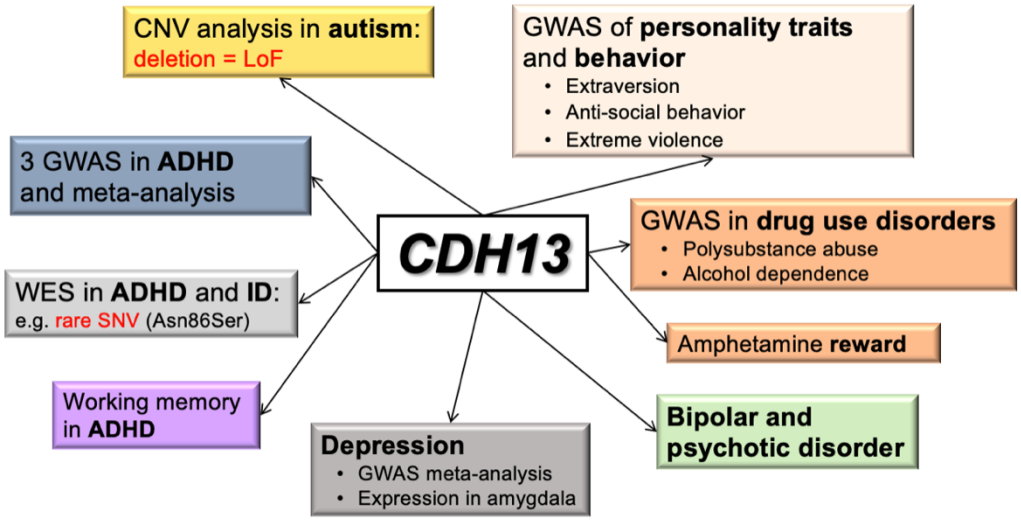

Figure 3. Studies using different methodological approaches support a role of CDH13 in the pathophysiology of neurodevelopmental and psychiatric disorders.
Numerous GWAS, meta-analysis, and WES studies have associated CDH13 with ADHD (Corominas et al., 2020; Demontis et al., 2016; Neale et al., 2008; Neale, Medland, Ripke, Anney, et al., 2010; Neale, Medland, Ripke, Asherson, et al., 2010; Rivero et al., 2013; Zhou, Dempfle, et al., 2008). A clinical study that recruited ADHD-affected children provided further evidence of the link between CDH13 and working memory performance (Arias-Vasquez et al., 2011). In addition to ADHD, variants in CDH13 have also been implicated in autism spectrum disorders, drug use disorders, bipolar and psychotic disorders, and depression, as well as in specific personality traits (Matsunami et al., 2013; Sanders et al., 2015; Sibille et al., 2009; Terracciano et al., 2010; Tiihonen et al., 2015; Uhl, Drgon, Johnson, et al., 2008; Uhl, Drgon, Liu, et al., 2008; Xu et al., 2014). CNV, copy number variants; SNV, single nucleotide variation; LoF, loss of function. Adapted from "Impact of the ADHD-susceptibility gene CDH13 on development and function of brain networks," by Rivero et al., 2013. *European Neuropsychopharmacology*, 23(6), p. 16. Copyright (2012), with permission from Elsevier (License number: 5112971445345). Credit for the updated version: K.P. Lesch.

1.4 The development of the serotonergic system and its role in adult brain function

Serotonin, also known as 5-hydroxy-tryptamine (5-HT), is a neurotransmitter synthesized from tryptophan that participates in most biological functions. The maturation of serotonergic neurons begins with the initiation of 5-HT synthesis and extends up to at least the first three weeks of life with continuous plasticity at the terminals throughout the lifetime in order to adjust to environmental events (Deneris and Gaspar, 2018). Being one of the earliest cell types to express a specific neurotransmitter, serotonergic neurons release 5-HT soon after they acquire serotonergic neuron identity at E 9.5 to E12 in mice (E10.5 to E13 in rats; 5th to 7th week of gestation in humans), thereby regulating the ingrowth and terminal development of neurons of itself and other monoamines, in particular dopamine (Benes et al., 2000; Whitaker-Azmitia, 2001). As early as E10, they migrate from their birthplace, the ventricular zone of the rhombencephalon, to their final destination near the pial surface via somal translocation (Hawthorne et al., 2010; Sodhi and Sanders-Bush, 2004; Whitaker-Azmitia, 2001). Through continued proliferation, migration and maturation of serotonergic neurons, the typical sigmoidal anatomical structure of the rostral raphe nuclei, consisting of the ascending serotonergic system of the DR and median raphe nuclei, begins to surface at E12.5 (Hawthorne

et al., 2010). Subsequently, fiber bundles along the rostrocaudal axis are formed by extending axons that are predominately thin, highly branched, and unmyelinated (Jacobs and Azmitia, 1992). Instead of creating new paths, the axons travel along the preexisting non-serotonergic fiber bundles when they are available (Fig. 4a) (Cases et al., 1995; Deneris and Gaspar, 2018). At the time of birth, serotonergic axons reach all the forebrain areas, though the terminal maturation, in which external factors are also involved, continues into early postnatal life before it is fully established (Fig. 4b) (Deneris and Gaspar, 2018; Lidov and Molliver, 1982). However, rather than remaining unchanged throughout the lifetime, serotonergic neural circuits are plastic and adaptive in response to environmental challenges, such as stress, traumatic experience, or pharmacological treatments (Azmitia, 2007; Lesch and Waider, 2012).

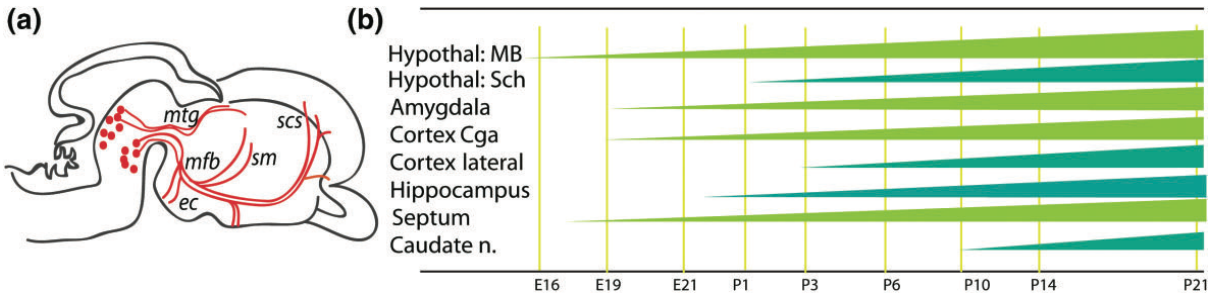

Figure 4. Development of serotonergic axons in rats.
(a) The cell bodies of serotonergic neurons are restricted to the rostral hindbrain, though they send projection axons throughout the whole brain. During the period of axon pathway formation, the growing ascending serotonergic axons travel along preexisting fiber tracts such as the medial forebrain bundle (mfb), the mamillotegmental tract (mtg), the supracallosal striae (scs), external capsule (ec), and the stria medullaris (sm) (Cases et al., 1995). (b) Although the extending axons reach the vicinity of all target structures that are to receive a serotonergic innervation by the end of gestation, the development of axon terminal arborizations proceeds postnatally to three weeks of age. However, terminal arborizations do not develop immediately after the arrival of axons. It is rather region-dependent and seems to be correlated with the maturation of the target regions as shown with light and dark green triangles (representing early and late target invasion, respectively) shading across developmental stages (Lidov and Molliver, 1982). Reprinted from "Serotonin neuron development: shaping molecular and structural identities," by Deneris and Gaspar, 2017. *Wiley Interdisciplinary Reviews: Developmental Biology*, 7(1), p. 26. Copyright (2017), with permission from Wiley (License number: 5112990450410).

In vertebrates and invertebrates, 5-HT is a major modulator of behavior. Imbalances in the serotonergic system are linked to a number of psychiatric, neurodevelopmental, and mood disorders in humans. Although accounting for a small percentage of the total cell number of the brain, serotonergic neurons modulate versatile behavioral processes and brain functions, such as mood, anxiety, stress, fear, reward, aggression, attention and plasticity, among others, each mediated by distinct 5-HT receptors (Berger et al., 2009; Carhart-Harris and Nutt, 2017). In humans, it has been shown that abnormalities in both the central and peripheral serotonergic systems, including elevated whole blood 5-HT level and altered serotonergic innervation, may underlie the pathophysiology of autism spectrum disorder (Lew et al., 2020; Muller et al., 2016). In contrast, early studies found a decrease in blood 5-HT levels among hyperactive and ADHD children (Abdulamir et al., 2018; Coleman, 1971; Spivak et al., 1999). Recent clinical,

neuroanatomical, experimental and genetic studies further furnished evidence which supports the role of 5-HT in ADHD etiology (Banerjee and Nandagopal, 2015; Oades et al., 2008). Moreover, evidence has shown that deficiency of some individual members of the cadherin superfamily resulted in alterations in the serotonergic system. For instance, loss of protocadherin-α family led to altered serotonergic axonal terminal arborizations and cognitive functions in mice (Chen et al., 2017; Katori et al., 2009; Katori et al., 2017). As mentioned above, previous results from our group also showed that CDH13 has a role in the normal development of the serotonergic system in early embryonic stages (Forero et al., 2017). Understanding the function of the serotonergic system will be essential for achieving complementary adaptive and potentially therapeutic outcomes.

1.5 Aim of this study

The function of cell adhesion molecules changes over development. Initially providing spot welds of structural adhesion, they later become dynamic and multifunctional signaling nodes that can eventually exert a profound influence over neurotransmission in the mature CNS. With the previous knowledge that CDH13 is highly expressed by serotonergic neurons in mouse embryos and that loss of CDH13 may impact serotonergic circuit formation, the current study aimed to understand how CDH13 contributes to the generation, maintenance, and pathological dysfunction of brain circuits after birth, with an emphasis on the serotonergic system.

CHAPTER 2 MATERIALS AND METHODS

2.1 Mouse husbandry and handling

2.1.1 Animals

Two mouse lines were used in the study: (1) Most molecular experiments were carried out using a constitutive *Cdh13* knockout (*Cdh13*$^{-/-}$) mouse line on a C57BL/6N background, which was generated by crossing *Cdh13*$^{loxP/loxP}$ mice with a constitutive Cre deleter line. Mice were genotyped by PCR as described in my master's thesis (Ku, 2017). In brief, primer pairs 1 and 2 (sequences listed in Table 1) were used in two independent reactions to detect the Cdh13 wild-type and knockout alleles, respectively. Primer pair 3 was included in both PCR reactions as an internal control of amplification. The conditions of the PCR are shown in Fig. 4. See Rivero et al. (2015) for details on the mouse line. (2) For the behavioral assessments mentioned in this study, a conditional *Cdh13* knockout mouse model was used (in the following referred to as *Cdh13* cKO). The gene of interest, *Cdh13*, was selectively knocked out in the serotonergic system of *Cdh13* cKO mice by crossing *Cdh13*$^{loxP/loxP}$ mice with *Pet1-Cre* mice subsequently. PET-1, also known as FEV, is a transcription factor required for shaping serotonergic neuron identity by regulating expression of genes required for 5-HT biosynthesis, vesicular transport, reuptake, and metabolism (Okaty et al., 2020; Spencer and Deneris, 2017; Wyler et al., 2016). The genotypes of the offspring were identified by PCR analysis of tail DNA for the *Cdh13* floxed allele and the *Cre* transgene in two independent reactions using primer pairs 1 and 4 (the sequences are listed in Table 1), respectively. Primer pair 3 was included in both PCR reactions as an internal control of amplification. The conditions of the PCR are shown in Fig. 5. See Forero et al. (2020) for details of the generation of this serotonergic neuron-specific *Cdh13* knockout (*Cdh13*$^{loxP/loxP}$:*Pet1- Cre*$^{+/-}$).

Table 1 PCR primer pairs used for genotyping.

Primer pair	Primer name	Primer sequence (5'– 3')	Band size (bp)	Purpose
1	Cdh13 forward	TGGTTCTGCTCCAAGACTCAG	See purpose	to detect the *Cdh13* wild-type (233 bp) or Cdh13 floxed (437 bp) alleles
	Cdh13 reverse 1	ATTAGGGACTATCCTGGGCTA		
2	Cdh13 forward	TGGTTCTGCTCCAAGACTCAG	478	to detect the *Cdh13* knockout allele
	Cdh13 reverse 2	CCAGGAAGAGATAAAGCCAGG		
3	Internal control forward	CTAGGCCACAGAATTGAAAGATCT	324	Positive control
	Internal control reverse	GTAGGTGGAAATTCTAGCATCATCC		
4	Cre forward	GCGGTCTGGCAGTAAAAACTATC	100	To detect the *Cre* allele
	Cre reverse	GTGAAACAGCATTGCTGTCACTT		

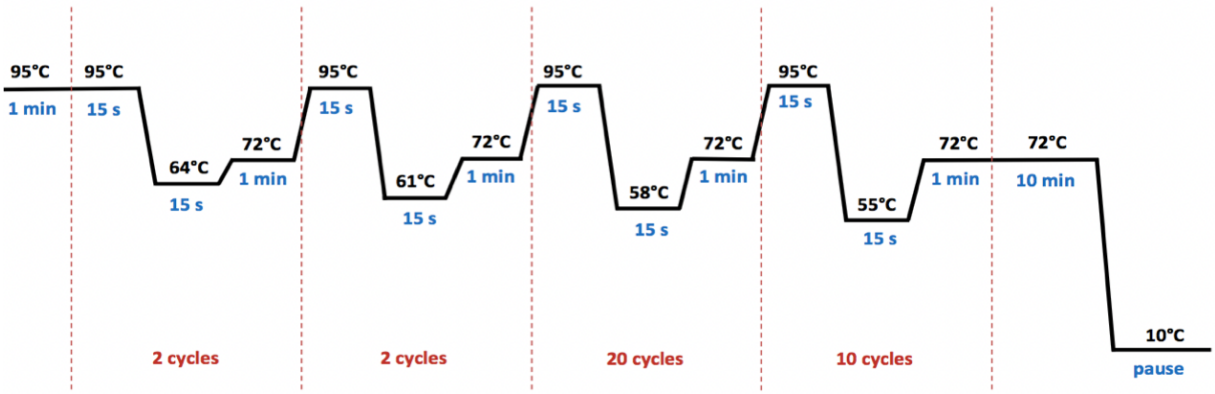

Figure 5 Conditions of the PCR used for genotyping (adapted from Ku (2017))

2.1.2 Perfusion

Isoflurane-anesthetized mice were transcardially perfused with 30 mL ice-cold 0.1 M phosphate-buffered saline (PBS; pH 7.4) pretreated with 20 units/mL heparin, followed by 30 mL ice-cold freshly prepared 4% PFA (paraformaldehyde; prepared from powder, if not stated otherwise) with a flow rate of 2.75 mL/min (18 rpm) for 11 min each. The tissues were post-fixed in 4% PFA for 24 to 48 h at 4°C, and then rinsed in 1x PBS for 3 times, 15 min each.

2.1.3 Mouse tissue preparation (cryoprotection and section)

For the tissue subjected to the immunohistochemistry procedure, incubations in 10% and 20% sucrose solutions for 24 h each were carried out in order to preserve its cellular morphology. Subsequently, the specimens were frozen in dry-ice-cooled isopentane and stored at -80°C until tissue sectioning. Tissue was embedded in Cryo-gel before proceeding to cutting with Cryostat (Leica CM 1950) at -20°C. Coronal slices of 20 µm thickness were collected on HistoBond+ adhesive slides precoated with gelatin. Sections (on slides) were stored at -80°C if not used immediately.

2.2 Immunohistochemistry and tissue labelling

2.2.1 Immunofluorescence staining

After air-drying for one hour at room temperature (RT), tissue sections were treated with citrate buffer (10mM, pH 6.0) in a water bath at 80°C for 20 min for retrieving antigens. To reduce non-specific binding, sections were incubated with a blocking solution (10% normal horse serum and 0.2% Triton X-100 diluted in 1x TBS) at RT for one hour. Primary antibodies were applied overnight at 4°C, and secondary antibodies were applied for 1.5 h at RT (dilutions of individual antibodies are listed in 2.7.2). DAPI was used as a nuclear counterstaining and incubated with secondary antibodies simultaneously. Slides were mounted with Fluoro-Gel before proceeding to microscopy. All incubations were done in a dark humidified chamber; washings with TBS (3 times, each 5 min) were carried out between incubations; primary and secondary antibodies were diluted in 5% blocking solution.

2.2.2 Signal amplification for immunohistochemistry

For the gross examination of CDH13 protein distribution in the adult brain, an additional signal amplification treatment was added, as the CDH13-immunoreactive (-ir) signal would have otherwise been too scant for detection (due to the low expression level in the adult brain). Steps similar to those mentioned in 2.2.1 were performed, except for the following. Firstly, prior to the blocking step, the endogenous peroxidase activity was quenched by incubating sections with 3% hydrogen peroxide (H_2O_2) in methanol for 10 min at RT. Secondly, instead of using fluorophore-conjugated secondary antibodies, biotinylated secondary antibodies were used in a dilution of 1:600. Thirdly, to detect the biotinylated targets, avidin-biotin complex kits (VECTASTAIN® ABC Standard Kit, Vector Labs) were used after the secondary-antibody incubation. Lastly, an amplification was performed by incubating sections with 1:200 Cyanine 3 (diluted in TSA amplification diluent [see 2.7.2]) for 10 min at RT as instructed by the manufacturer (TSA™, PerkinElmer). An unamplified control, an amplified negative control (e.g. a knockout sample) as well as an endogenous biotin/streptavidin blocked control were included to rule out false-positive signal detection (Fig. 6).

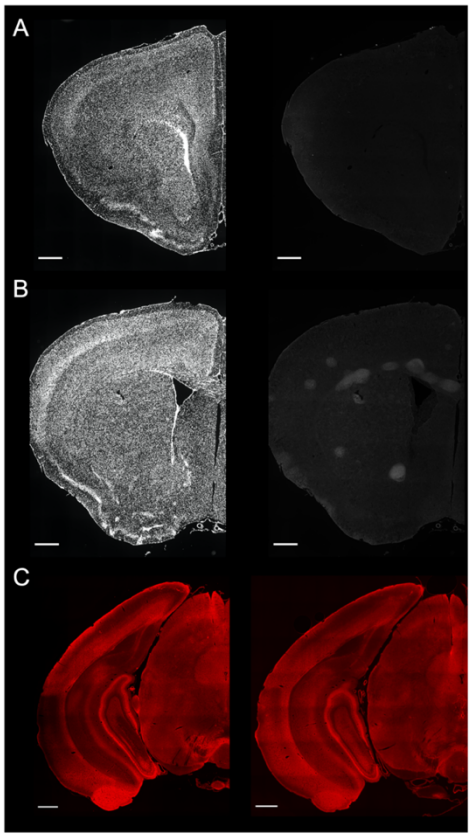

Figure 6. Negative controls for tyramide signal amplification detection that was used for CDH13 protein expression study in adult mouse brain.
(A) No CDH13 immunoreactivity was found in the *Cdh13*-null mouse brain sections stained with CDH13 antibody (right panel). The counter staining with DAPI is shown in the left panel. (B) Minimal CDH13 immunoreactivity was found in the wild-type adult brain section with CDH13 primary antibody omitted (right panel). The counter staining with DAPI is shown in the left panel. (C) Wild-type adult brain section stained with CDH13 antibody using the TSA amplification kit (left panel). Additional blocking solutions were added to block endogenous streptavidin and biotin activities during the staining procedure (right panel). Images were taken with the exact same parameters used for figures 1 and 2. Note that the contrast of the images in the right panels of A and B were enhanced for 0.01% in order to visualize the brain structure. Scale bar = 500 μm.

2.2.3 Whole-mount staining and tissue clearing: passive CLARITY

CLARITY is an acronym for **C**lear **L**ipid-exchanged **A**crylamide-hybridized **R**igid Imaging / **I**mmunostaining / in situ-hybridization-compatible **T**issue h**Y**drogel. This is a hydrogel-based tissue clearing technique, one of the best among all currently available techniques for preserving actual tissue size. The clearing process, however, takes about two to three weeks, which is significantly longer than solvent-based ones. All the procedures were performed following the description in Hu et al. (2017) and Flynn (2016), with minor modifications. In short, the animal was transcardially perfused with 20 mL of ice-cold 1x PBS at 10mL/min, followed with 20 mL of hydrogel solution (see 2.7.2) at the same rate. The brain was dissected out and post-fixed in hydrogel solution at 4°C for three days. The tissue was then transferred to a 5 mL tube filled with hydrogel solution and wrapped with parafilm on a shaker in an incubator at 37°C for 2.5 hours to allow the hydrogel to polymerize. The excess gel was removed around the tissue before washing with 1x PBS for four times. The tissue was transferred in a 10 mL tube filled with clearing solution (see 2.7.2) on a shaker at 37°C for clearing. The clearing solution was changed every three days for two weeks and every 7 days for another two weeks.

2.2.4 **I**mmunolabelling-enabled three-**D**imensional **I**maging of **S**olvent **C**leared **O**rgans: iDISCO+

iDISCO+ is an improved version of iDISCO that reduces sample shrinkage and better preserves brain morphology. All procedures were performed following the methanol protocol provided in Renier et al. (2014) and Renier et al. (2016), as well as their website (http://www.idisco.info). Briefly, mice were perfused transcardially with 20 mL 1x PBS and then 20 mL 4% PFA (prepared from 16% PFA, EMS, #15710-S). The brain tissue was isolated and post-fixed overnight at 4°C followed by 1h RT with shaking. In some instances, the specimen was trimmed sagittally to 1mm thick slices with a vibratome (Leica VT 1000S) sectioning speed of 0.40 mm/s and a frequency of 80 Hz. *Pretreatment* After washing with 1x PBS three times for 30 min each, the tissue was dehydrated with series of methanol/H_2O (20%, 40%, 60%, 80% and 100%) for one hour each. An additional wash with 100% methanol was then carried out to eliminate the H_2O residue. This dehydration treatment removes water, the major light scatterer in tissues. After an overnight incubation in dichloromethane/methanol (2:1) at RT, tissue samples were washed in 100% methanol twice at RT, followed by a short chilling step at 4°C. The tissue was then bleached in chilled freshly prepared 5% H_2O_2 in methanol overnight at 4°C. Rehydration with series of methanol/H_2O (80%, 60%, 40%, 20% and 1xPBS) was performed one hour each at RT. The tissue was then washed in 0.2% (v/v) TritonX-100/PBS twice, one hour each at RT. *Immunolabelling* The samples were incubated in a permeabilization solution (see 2.7.2) at 37°C for 2 days. After blocking in a blocking solution (see 2.7.2) at 37°C for 2 days, the samples were incubated in primary antibody (1:500) for 4 days. The samples were incubated in secondary antibody (1:500) at 37°C for 4 days. Washing steps were carried out before and after the secondary antibody incubation with PTwH (PBS/0.2% Tween-20 with 10 µg/ml heparin) for 5 times with the last washing lasting until the next day. All steps were carried out in a rotating incubator. The tubes were sealed with parafilm with little to no bubbles to prevent oxidation. *Clearing* The samples were dehydrated with series of methanol/H_2O (20%, 40%, 60%, 80% and 100%) for one hour each and 100% overnight at RT. An incubation in dichloromethane /methanol (2:1) at RT for 3 to 5 hours (until the samples sank to the bottom) was followed by two incubations with 100% dichloromethane for 15 min each (until the

samples sank to the bottom). A final incubation was performed in DiBenzyl Ether to clear the samples. All samples were submerged in DiBenzyl Ether and kept in the dark until imaging.

2.3 Gene expression analysis

2.3.1 Laser microdissection (LMD)

For the evaluation of the knockout efficiency of *Cdh13* cKO mice, fresh frozen brain tissue was sectioned at 20 µm and mounted on polyethylene-naphthalate (PEN)-membrane-coated slides. The nucleic acids of these sections were visualized with 0.02% toluidine blue (diluted in ethanol) and dried at 40°C for 10 min. Subsequently, the region of interest was captured with a DM6000B laser microdissection system (Leica Biosystems) and collected in 0.2 mL PCR SoftTubes. Samples were immediately placed at 4°C until completion of LMD. All steps were performed under RNase-free conditions.

To investigate the expression level of *Cdh13* mRNA in subgroups of DR, similar procedures to those mentioned above were used, except for the following: instead of 0.02% toluidine blue, coronal sections were stained with 0.25% cresyl violet (diluted in ethanol) for a better cell nuclei visualization. The region of interest was captured with a LMD 6 laser microdissection system (Leica Biosystems).

2.3.2 RNA extraction and reverse transcription

Total RNA of microdissected tissue were isolated with the Picopure RNA Isolation kit according to the manufacturer's protocols, inclusive of the on-column DNase digestion treatment. For first-strand complementary DNA (cDNA) synthesis, the following mixture was prepared in a thin-walled 0.5-mL tube: 5 µg total RNA, 1 µL random hexamer primer, 0.4 µL dNTPs, 0.2 µL BSA, and RNase-free water to 13 µL. The tube was heated to 65°C for 5 min and put promptly on ice for 2 min in order to denature RNA with high GC content or secondary structures. Subsequently, 4 µL 5× first-strand buffer, 1 µL 0.1M DTT, 1 µL RNasin® Ribonuclease Inhibitors, and 1 µL SuperScript™ III Reverse Transcriptase were added, and mixed by pipetting. The reverse transcription reaction was performed at 25°C for 5 min to allow extension of the random primers, 60 min at 50°C for the reverse transcription step, followed by heat inactivation for 5 min at 95°C. A no-template control that omits RNA and a no-reverse-transcriptase control were included as negative controls. The cDNA products were stored at -20°C until further use.

2.3.3 Real-time PCR

Each cDNA pool was diluted 1:4 prior to usage in a 10 µl reaction including 5 µl SYBR™ Select Master Mix for CFX. Reactions were analyzed upon a Bio-Rad real-time thermal cycler CFX384 using the following cycle conditions: 2 min at 95°C, (5 s 95°C and 30 s 60°C) x45 cycles, and 10 s at 95°C. Primer sequences were: *Cdh13*; forward, 5′-CTGTCCTAAACTTGACCTTC-3′, reverse, 5′-GTTCCTGAGAGCCACTAAG-3′; *B2m* (β_2 microglobulin), QuantiTect Mm_B2m_2_SG Primer Assay; *Rplp0* (ribosomal protein

lateral stalk subunit P0), QuantiTect Mm_Rplp0_1_SG Primer Assay. The relative mRNA expression level of *Cdh13* was normalized to that of *B2m* and *Rplp0*.

2.4 Microscopy

2.4.1 Epifluorescence microscopy

Multichannel fluorescence images were acquired using an Olympus epifluorescence microscope with emission wavelengths 455 nm (DAPI), 519 nm (EGFP), 554 nm (RFP) and/or 668nm (Cy5) with automated exposure time. Stitched images were acquired using a motorized XY-stage with the autofocus option. All images were processed with Olympus CellSense software and/or ImageJ.

2.4.2 Confocal Microscopy

Confocal images were acquired with an Olympus FluoView FV1000 laser scanning biological microscope. For the visualization of immunolabeled serotoninergic and dopaminergic neurons as well as serotonergic fibers, the brain slices were imaged with 10x (/0.4 UPlan SAPO) or 20x (/0.75 UPlanSAPO) air objectives. The upper and lower limits of the z position were visually delimited. Blue (DAPI), green (Alexa Fluor 488) and red (Alexa Fluor 555) channels were obtained through sequential frame scanning with the concurrent collection of fluorescence signal for each individual channel. For the visualization of iDISCO+ cleared brain slices, the sections were placed in closed glass-bottom culture dishes (IBIDI, µ-Dish 35 mm, high glass bottom) filled with dibenzyl ether and imaged with a 10x air objective.

2.4.3 Light sheet fluorescence microscopy (LSFM)

The imaging was performed in collaboration with the group of Professor Katrin G. Heinze at the Rudolf Virchow Center at the University of Würzburg. All the technical details regarding the setup were described in Amich et al. (2020) and Stegner et al. (2017). In short, the light-sheet fluorescence microscopy setup is home-built and fixed with a Hund objective (A10/0.25; Hund, Wetzlar, Germany). All cleared tissue images were acquired with tissue submerged in DiBenzyl ether. A custom fiber coupled laser combiner (BFI OPTiLAS GmbH, Groebenzell, Germany) with required laser lines (autofluorescence, 488 nm; Alexa 647, 640 nm) was used for fluorescence excitation. Exposure time was 200 ms each frame. All image acquiring hardware (laser, camera, lenses) were controlled by IQ 2.9 software (Andor, Belfast, United Kingdom). Images were taken with an Andor sCMOS (Neo 5.5; 2160 × 2560 pixels), saved as TIFF files, and processed as described in Section 2.6.5.

2.5 Behavioral tests

All behavioral testing took place at the facility of the Center of Experimental Molecular Medicine, University Hospital of Würzburg. Mice were group-housed under controlled environmental conditions with ambient temperature of 21±0.5°C, humidity of 50±5% and a 12/12h light/dark cycle. Food and water were given *ad libitum* unless stated otherwise. All experimental procedures were approved by the boards of the University of Würzburg and the Government of Lower Franconia (license 55.2-2531.01-92/13). A cohort of three-to-four-

month-old adult male *Cdh13* cKO mice (n = 14) and their Ctrl littermates (n = 10) were subjected to a battery of behavioral tests to evaluate locomotor activity (open field test), anxiety-related behavior (elevated plus maze, light-dark box, open field), sociability, social memory and preference for novelty (social behavior test), as well as spatial learning and memory (Barnes maze test). In addition, a second cohort of four-to-five-month-old male *Cdh13* cKO mice (n = 13) and Ctrl littermates (n = 7) was subjected to the five-choice serial reaction time task (5-CSRTT) to assess visuospatial attention and motor impulsivity. Details of all conducted behavioral assessments were described previously in Rivero et al. (2015) and Forero et al. (2020). All experiments were conducted in a genotype-blinded fashion.

2.5.1 Open field test (OF)

The open field test is performed to examine general locomotor activity, as well as exploratory and anxiety-related behaviors. This task relies on rodents' natural spontaneous exploratory behaviors in new environments. The subject was put into one of the corners of a 50 x 50 cm square box with an illumination gradient between 50 and 100 lx from the walls to the center of the arena for a duration of 30 min, with a camera installed on top above to monitor its activity. The total distance traveled was used to assess general locomotion, and the time spent in the center versus border areas as well as the latency to enter the center of the arena were recorded as parameters for anxiety-like behavior.

2.5.2 Elevated plus maze (EPM)

The elevated plus maze is used to assess anxiety-related behavior in rodents (Walf and Frye, 2007). The "plus" shape maze is composed of two open and two closed arms (all with the dimension of 30 × 5 cm; the closed arms are equipped with additional 15 cm high walls) that are elevated to about 60 cm above the floor. This task relies on rodents' preference toward dark and enclosed spaces, and an unconditioned fear of heights and open spaces. Briefly, the subject was placed at the junction of the four-armed maze and allowed to explore for 10 min, during which its performance was captured by a CCD camera and tracked by VideoMot2 software (Version 6.04, TSE systems, Germany). The number of entries, the latency to enter, and the time spent in each of the arms as well as the total distance travelled were calculated.

2.5.3 Light-dark box (LDB)

The light-dark box is used to assess anxiety-related behavior in rodents. Similar to the principle mentioned above, it is based on rodents' natural preference toward dark and enclosed spaces, and an innate aversion to brightly illuminated areas(Bourin and Hascoet, 2003). The apparatus is a square box (50 × 50 × 40 cm) consisting of an illuminated (100 lx) compartment and a dark enclosed compartment (about one-third of the total area of the box) with a small opening in between which allows the subject to access the other part. The mouse was placed in the dark compartment and allowed to explore for 10 min, during which its performance was captured by a CCD camera and tracked by VideoMot2 software. The total distance travelled, the number of entries and the latency to enter the lit compartment, as well as the time spent in each compartment recorded.

2.5.4 Object recognition test (OR)

The object recognition test is used to evaluate cognition and recognition memory in rodents. It includes a habituation step for 5 min, together with two phases lasting 10 min each. Two identical objects (50 mL falcon tubes covered with aluminum foil from the inside) were placed on one side of the open field arena (about 30 cm apart from one another) for the first phase, and for the second phase, which was carried out 10 min later, one of the objects was replaced with a novel object (a lego with the same height and top surface area as the 50 mL falcons). The subject was placed in one of the corners of the arena, and the individual performance was recorded by a CCD camera and tracked by VideoMot2 software. The sides to position objects were randomly alternated in order to avoid residual olfactory cues. The time spent on exploring each object and the total distance travelled were measured.

2.5.5 Barnes maze (BM)

The Barnes maze is used to assess spatial learning and memory in rodents. The apparatus consists of a circular platform (120 cm in diameter) with forty evenly spaced holes at the periphery (each 5 cm in diameter); one of the holes was randomly chosen to hold an escape box. Motivated by its natural aversion to bright and open space, the subject is trained to navigate by the visual cues that are placed around the maze at a distance of approximately 10 cm to find and enter the escape box fixed underneath the platform. The subjects were individually placed at the center of the maze and covered with a dark cylinder. The timer started immediately after removing the cylinder, and the subject was allowed to explore the maze for 3 min or until it found the escape hole. Two trials were carried out each day during the total 9-day training period, with a break of testing between days four and five. The mouse was guided by gentle pulling at the tail if it failed to enter the escape hole within 3 min. Each trial was recorded by a camera that was mounted above the testing platform. The latency to enter the hidden box, latency to start exploring the platform as well as the total distance travelled were automatically measured by the VideoMot2 software. The number of primary errors, defined as the number of times the subject poked its head into a wrong hole before locating the escape box for the first time, were manually scored by an examiner in a genotype-blind manner. The time a subject spent in each quadrant was analyzed with the VideoMot2 software by dividing the maze into four equal quadrants with the target hole approximately in the center of the 10 holes assigned to the target quadrant. Clockwise from the target quadrant, the other quadrants were termed as positive, opposite, and negative as described in Attar et al. (2013).

2.5.6 Social behavior test (SB)

Sociability and social novelty were probed using a social behavior test carried out in the open field arena. This test is based on the rodent's natural preference for spending time with another rodent rather than an object (sociability) and for investigating a novel counterpart rather than a familiar one (social novelty). In the first 10-min trial, where probe sociability was probed, the subject was placed at a corner of the arena that contained a grid cage with an unfamiliar mouse and another identical but empty cage. The cages were placed at the upper corners of the arena, and their positions were alternated randomly. Sociability was defined as interaction time with an unfamiliar mouse over an empty cage. After a short break for 5 min, the second 10-min trial was performed to probe social novelty by putting a novel mouse in the originally empty cage.

Preference for social novelty was defined as time spent interacting with the novel mouse over the familiar one. The behavior was captured by a CCD camera and tracked by VideoMot2 software. The total distance travelled, the number of visits and time spent within each interaction zone (animal vs cage; familiar vs novel mouse), as well as the latency to approach each zone were measured.

2.5.7 Five-choice serial reaction time task (5-CSRTT)

This is a cognitive task to evaluate visuospatial attention and motor impulsivity in rodents. Starting from a week prior and up to the end of the test, mice were food-restricted and maintained at 85–90% of their free-feeding body weight, with their target weights adjusted upward every week by 1 g to account for growth. Water was available *ad libitum*. Detailed procedures were described previously in the Methods and Supplementary Information sections of Forero et al. (2020). In short, the task was divided in three main phases: habituation, autoshaping and testing. Details regarding the number of sessions in each training phase and each training day, the duration of each trial, as well as the parameters used for each level were included in Table 1. During the habituation phase, mice were familiarized with the 5-CSRTT chamber and trained to associate nosepoking into a lit aperture with a food pellet as a reward. The autoshaping phase is the main training period when the mice were trained with progressing difficulties to differentiate between rewarding nose-pokes (lit holes) and those that did not lead to a reward (unlit holes). During the testing phase, mice were probed for attention and impulse control deficits with two trial levels at five and two second stimulus durations (StD) each, and one trial level at variable inter-trial interval (ITI). This was only carried out once all mice had reached criteria (>75% accuracy and <15% omission) for three consecutive days at 10-s StD and 10-s ITI within the last autoshaping level. The StD was reduced to increase the attentional load of the task and assess attentional control systematically (Bari et al., 2008; Robbins, 2002). The level of variable ITI (in which the ITI ranging from 6 s to 14 s) occurred pseudo-randomly and was unpredictable to the mice. This was used to probe deficits or enhancements in behavior that are not apparent in well-trained subjects using standard testing parameters (Amitai and Markou, 2011; Robbins, 2002). The 5-CSRTT task was carried out in an operant chamber that was placed within a ventilated, illuminated and sound-attenuating box (5-Hole Box Systems, TSE Systems, Homburg, Germany). All performance was captured with a CCD camera mounted on the ceiling of the box. Measures of correct responses, incorrect responses, premature responses, omissions, latencies to correct and incorrect responses, the number of completed trials, and nose-pokes at each aperture were taken automatically by the TSE Operant behavior software. Rewards earned were manually scored by examiners who were blind to the genotypes. The accuracy and the total number of nose-pokes were calculated from the raw data. The definitions of all the parameters are listed in the following table (Table 2).

Table 2. Training timeline and the corresponding parameters used in each stage of the 5-CSRTT.

Level	Total number sessions	Session (min)	Trials per session	StD (s)	Time out (s)	LH (s)	ITI (s)	H6	remarks
Hab1	2	10	5	(A)	-	-	-	-	(C)
Hab2	5	5	5	(A)	-	-	-	-	(C)
0 (Auto)	3	20	30	(A)	-	-	-	-	(D)
1 (Auto)	1	5	10	(A)	5	-	-	-	
2 (Auto)	4	5	10	(A)	5	-	-	x (B)	
3 (Auto)	3	10	20	(A)	5	-	1	x (B)	
4 (Auto)	1	10	20	50	5	-	2	x (B)	
5 (Auto)	1	10	20	40	5	-	3	x (B)	
6 (Auto)	1	10	20	30	5	-	5	x (B)	
7 (Auto)	1	20	50	20	5	-	5	x (B)	
8 (Auto)	3	20	60	10	5	2	10	x (B)	
9 (Auto)	2	20	60	10	5	2	10	-	
10 (Test 1)	4	20	60	5	5	2	10	-	
11 (Test 2)	4	20	60	2	5	2	10	-	
12 (vITI)	2	20	60	2	5	2	(E)	-	

Abbreviations: StD, stimulus duration; LH, limited hold; ITI, inter-trial interval; H6, hole 6; Hab, habituation; Auto, autoshaping; vITI, variable inter-trial interval; x, the H6 was included; -, not applicable.

(A) Stimulus illuminated until nose-poke

(B) Each trial starts with a nope-poke in hole 6

(C) A reward pellet was delivered in all apertures that were illuminated in the beginning. The light was then off when the first nose-poke was detected.

(D) One aperture was illuminated at a time until a nose-poke was detected, after which the reward pellet was delivered.

(E) The ITI varied randomly between 5 and 15 s, controlled by the TSE operant behavior software on a random schedule.

Table 3. Definition of 5CSRTT parameters.

Critical parameter	Definition
Correct response	A nose-poke into an illuminated aperture during the stimulus duration period or the limited hold period that followed
Incorrect response	A nose-poke into any non-illuminated aperture during the stimulus duration period or the limited hold period that followed
Premature response	A nose-poke into any aperture before the stimulus light was presented
Omission	The mouse failed to respond during the stimulus duration period or the limited hold period that followed
Latency to correct response	The mean delay period from the start of the stimulus phase until the occurrence of a correct nose-poke reaction
Latency to incorrect response	The mean delay period from the start of the stimulus phase until the occurrence of an incorrect nose-poke reaction
Latency to hole 6	The mean delay period from the correct reaction until the next visit to hole 6
Number of nose-pokes	The number of sensor interruptions in an aperture
Accuracy	The total number of correct responses divided by the sum of correct and incorrect responses

2.6 Data analysis

2.6.1 Quantification of serotonergic neurons in the DR

Coronal sections (20 μm) were immunostained for tryptophan hydroxylase 2 (TPH2) — a specific marker for serotonergic neurons of the brain — to reveal the somas of serotonergic neurons. (1) To estimate the number of TPH2-ir neurons in subgroups of DR, images of each hemisphere of the DR were taken at 20x magnification. In total, ten and eight slices (at intervals of 60 μm) of adult and P14 brain, respectively, were included in the analysis. All images were processed with ImageJ (see 2.6.4). After images of the right and left sides were put together using the "montage" option, a vertical line was drawn from the lowest point of the aqueduct to indicate the midline of the brain (Fig. 7). The TPH2-ir cells lying within 80 (lateral to the midline) × 320 (away from the lowest point of the aqueduct) μm or 60 × 290 μm were referred to as the dorso-median clusters (B7d) of the adult and postnatal day (P)14 brain, respectively (the boxed areas); the TPH2-ir cells lying further lateral to the B7d and above the horizontal lines (aligned to the lowest point of the boxes) were referred to as the clusters of lateral wings (B7l); those below the horizontal lines were referred to as the ventral cluster (B7v). For the P14 brains, an additional image of the ventral cluster was taken each section. Given that brains of different developmental stages vary in size, the border limits dividing DR subgroups were carefully estimated in a small set of data (two wild-type brains of the same age) prior to the analyses. TPH2-positive serotonergic neurons showing a labeling above the background with clear outlines were counted manually. (2) To estimate the area occupied by serotonergic

neurons, the images were processed using the same script mentioned above. The area occupied by TPH2-ir neurons was outlined manually using the polygon selection option, and the size of the selected area was measured. All the quantifications were conducted by a single examiner who was blind to the genotypes.

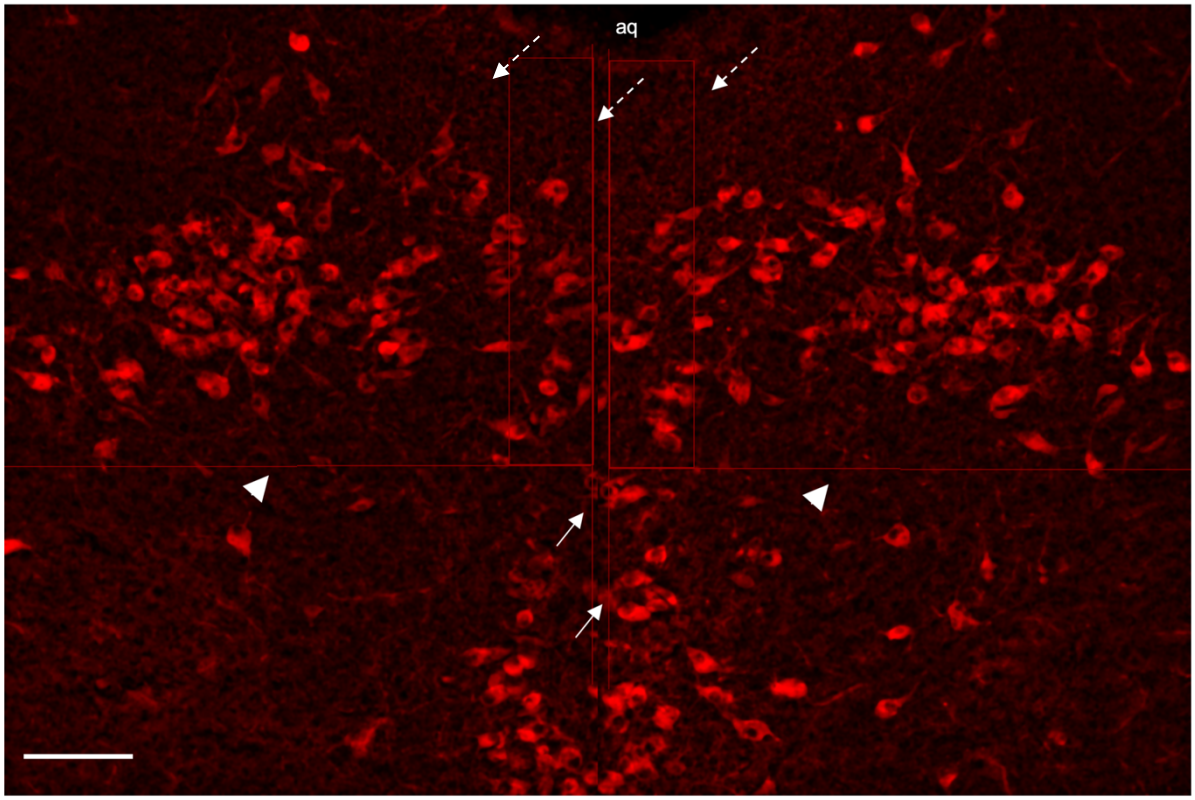

Figure 7. **Representative montaged image of P14 coronal section stained for TPH2.**
First, the left and right sides of the DR images were processed and montaged. Second, vertical lines starting from the lowest point of the aqueduct were laid over on both sides (arrows). Third, two 60 × 290 μm boxes were placed lateral to the midlines with the upper limit aligned to the lowest point of the aqueduct (dashed arrows). Lastly, horizontal lines aligned to the lower limit of the boxes were laid over on both sides (arrowheads). The TPH2-ir cells lying within the boxed areas were referred to as the B7d; those lying lateral to the boxes and above the horizontal lines were referred to as the B7l; those localized below the horizontal lines were referred to as the B7v. aq, aqueduct. Scale bar = 100 μm.

2.6.2 Quantification of serotonergic innervation

Coronal sections were immunostained for 5-HT transporter (5-HTT, also known as SERT) — a marker for presynaptic serotonergic processes — to reveal the serotonergic axons. To estimate the density of 5-HTTir fibers in target areas, images of the infralimbic cortex, cingulate cortex, basolateral complex of amygdala, caudate putamen, dorsal lateral nucleus of thalamus, paraventricular nucleus of thalamus, and cerebellum from both hemispheres of three to four continuous sections at intervals of 120 μm were taken at 20x magnification. A total of six images at a z-depth of 20 μm (1.5 μm step size, 13-16 z-stacks) was acquired for each brain region. All images were processed and analyzed automatically with ImageJ (see 2.6.4). (1) To measure the density of the 5-HTTir fibers, the region of interest (the central region of all brain

areas, except for the cerebellum) of the image was selected and the pixels occupied by the 5-HTT-expressing fibers within the selection were quantified automatically. For the cerebellar cortex, the granular and Purkinje cell layers were manually marked as selections because 5-HTT-ir fibers almost exclusively distribute to those two layers of the cerebellar cortex (based on my observation; Bishop et al., 1985). The density of the 5-HTT-ir fibers was then calculated by dividing the size of the whole selected area into the size occupied by 5-HTT-ir fibers. (2) To measure the number of the 5-HTT-ir fibers, seven vertical lines (70 μm) were randomly drawn in the central area of each image, and the number of 5-HTT-ir fibers crossing through the lines were counted automatically.

2.6.3 Statistics

All the statistical analyses, except for the evaluation of BM and 5-CSRTT results, were performed with GraphPad Prism (version 6.04 or 8.4.3). The normal distribution of the data was first evaluated by D'Agostino-Pearson, Shapiro-Wilk and Kolmogorov-Smirnov normality tests. Statistical significance of normally and non-normally distributed data was assessed with two-tailed unpaired student's t test and nonparametric Mann-Whitney test, respectively. The statistical significance threshold was set at 0.05 and the significance levels were reported as follows: $p < 0.05$ (indicated by *), $p < 0.01$ (indicated by **), $p < 0.001$ (indicated by ***), and $p < 0.0001$ (indicated by ****).

For the BM and 5-CSRTT, the differences between genotypes were analyzed with repeated measures mixed ANOVA, with genotype as the between-subjects factor and test session as the repeated measure. When a statistically significant effect (i.e. main effects and interactions) was observed, a Sidak's post-hoc test with correction for multiple comparisons was performed. Similarly, the learning progress of these two behavioral tasks was assessed with repeated measures mixed ANOVA followed by a Tukey's multiple comparisons test by comparing the performance of each genotype among sessions. The "ROUT method" provided in Prism was used to identify outliers, which were excluded from the analysis.

2.6.4 ImageJ

Prior to each analysis, the corresponding macro script was written using image-sets of two wild-type brains (out of the whole independent data set). In general, all images were processed using pre-written macro scripts that include a combination of several steps as follows: (a) The background was removed using "Subtract background" with the radius of rolling ball set to be the size of the largest object of each image set. For example, the rolling ball radius for processing the TPH2-stained DR images was 20 because the biggest object was the TPH2-ir cell soma with a long-axis diameter of 20 μm; for quantifying the innervation in target areas, the radius of rolling ball was set to be 1.5 or 1.45 depending on the anatomical region, because the thickest part of 5-HTT-ir fibers was estimated to be 1.5 or 1.45 μm. (b) Extreme pixels of the images were ignored using "Median filter", with the radius of the filter set to 2. (c) All slices of a z-stack were collapsed to a single plane using "maximum z-projection" or "average z-projection" to reveal a sharp-looking cellular or fiber-like structure, respectively. (d) The contrast of the images was enhanced for visualization. (e) The threshold of the images was automatically determined using the "IsoData" algorithm before they were binarized.

For quantification of serotonergic neurons in DR, each image was processed automatically with steps a, b, c and d. Subsequently, ROI (region of interest) selections were applied to the image before the neurons in the image were scored manually with the "cell counter" function (see Appendix A for the macro script). For quantification of serotonergic innervation, images were processed automatically in a batch with steps c, a, d and e before the measurements, in which defined numbers of areas or lines were randomly laid over individual images and the desired data was recorded. An additional step could be added after a 2D image was produced (step c) in order to manually delineate the ROI selections for anatomically non-uniform regions. For instance, to exclude the molecular layer of the cerebellar cortex in the analysis, the granular and Purkinje cell layers were manually depicted as the ROI selections with the "polygon selections" option (see Appendix B for the macro script). Note that all the images presented in this thesis are non-processed. For a better visualization, the brightness and contrast of all images were adjusted automatically with the "Brightness/Contrast" tool before scale bars were added.

2.6.5 Imaris

Fluorescent images were collected in z-series throughout the volume of the whole brain or brain slices to generate image stacks. The individual stack was subjected to a mathematical postprocessing method that reassigns out-of-focus light (deconvolution) using Huygens professional software. The deconvoluted stack was then imported into Imaris, with which snapshots of volume images were captured. When required, background subtraction in accordance with the diameter of the cells was employed to eliminate unspecific background signals prior to the acquisition of the snapshots.

2.7 Materials, reagents and equipment

All the materials, solutions, reagents, and equipment were grouped according to the numerical order of Methods mentioned above.

2.7.1 Mouse husbandry and handling

Reagents or Instruments	**Name and Location of Suppliers**
Agarose	Biozym, Vienna, Austraia
Chromium potassium sulfate	Fluka, Steinheim, Germany
Cryo-gel	Leica Biosystems, Nussloch, Germany
Cryomold	Sakura Finetek, Alphen aas den Rijn, Netherlands
Cryostat (Leica CM 1950)	Leica Biosystems, Nussloch, Germany
D-sucrose	AppliChem, Damstadt, Germany
Ethidiumbromide	AppliChem, Damstadt, Germany
Gel loading dye (6x)	New England BioLabs, Frankfurt am Main, Germany
Gelatin	Fluka, Steinheim, Germany
Heparin	Ratiopharm, Ulm, Germany

HistoBond+ adhesive slides	Paul Marienfeld, Lauda-Königshofen, Germany
Isoflurane	CP-Pharma, Burgdorf, Germany
Isopentane	AppliChem, Damstadt, Germany
Paraformaldehyde (PFA)	Roth, Karlsruhe, Germany
PCR machine	Biometra, Goettingen, Germany
Phosphate-buffered saline (PBS), 10x	Lonza, Walkersville, MD, USA
Proteinase K	Qiagen, Hilden, Germany

Buffers and solutions	**Recipe**
4% PFA	4% paraformaldehyde in PBS, pH 7.5
Gelatin-coating solution	0.03% Gelatin, 0.005% chromium potassium sulfate
Lysis buffer (DNA extraction)	1.5M Tris-HCl, pH 8.5, 5M NaCl, 0.5M EDTA, pH 8, 20% SDS in ultrapure water

2.7.2 Immunohistochemistry and tissue labelling

Reagents or Instruments	**Name and Location of Suppliers**
16% PFA (#15710-S)	Electron Microscopy Sciences, Hatfield, PA, USA
Acrylamide, 40%	Bio-Rad Laboratories, Feldkirchen, Germany
Avidin-biotin complex kit	VECTASTAIN® ABC Standard Kit, Vector Labs, Biozol, Eching, Germany
Bis-acrylamide , 2%	Bio-Rad Laboratories, Feldkirchen, Germany
Boric acid	Sigma-Aldrich, Steinheim, Germany
Citrate acid monohydrate	Sigma-Aldrich, Steinheim, Germany
DAPI	Sigma, Steinheim, Germany
DiBenzyl Ether	Sigma, Steinheim, Germany
Dichloromethane	Sigma-Aldrich, Steinheim, Germany
DMSO	Sigma, Steinheim, Germany
Fluoro-gel	Electron Microscopy Sciences, Hatfield, PA, USA
Glycine	Sigma, Steinheim, Germany
HCl	AppliChem, Damstadt, Germany
Hydrogen peroxide (H_2O_2)	Merck, Darmstadt, Germany
IBIDI µ-Dish 35 mm, glass bottom culture dish (Cat. No. 81158)	IBIDI, Gräfelfing, Germany
Methanol	Sigma-Aldrich, Steinheim, Germany
NaCl	Th. Geyer, Renningen, Germany
NaOH	AppliChem, Damstadt, Germany
Normal donkey serum	Jackson Immunoresearch, PA, USA
Normal horse serum	Vector, Peterborough, United Kingdom

SDS	AppliChem, Damstadt, Germany
Tris HCl	Roth, Karlsruhe, Germany
Triton X-100	Sigma, Steinheim, Germany
Tween 20	Sigma, Steinheim, Germany
Tyramide signal amplification kit (Cyanine 3)	PerkinElmer, Rodgau, Germany
Tyramide signal amplification Plus DNP kit	Akoya Biosciences (formerly PerkinElmer Life and Analytical Sciences), Marlborough, MA, USA
Ultrapure water systems (Synergy®)	Merck Millipore, Darmstadt, Germany
VA-044	Fujifilm Wako, Neuss, Germany
Vibratome (Leica VT 1000S)	Leica Biosystems, Nussloch, Germany
Water bath (GLS aqua 12 plus)	Grant, Cambridge, United Kingdom

Buffers and solutions	**Recipe**
TBS	100 mM Tris-HCl, 150 mM NaCl, pH 7.5
Citrate buffer	10 mM citrate acid monohydrate, pH 6.0
10% blocking solution (immunofluorescence labeling)	10% normal horse serum, 0.2% Triton X-100 in TBS
Sodium borate buffer (TSA amplification diluent)	0.3% H_2O_2 in borate, pH 8.5
Hydrogel solution (CLARITY)	4% PFA, 4% acrylamide, 0.05% bis-acrylamide, 0.25% VA-044
Clearing solution (CLARITY)	8% SDS in 200mM sodium borate buffer
Permeabilization solution (iDISCO$^+$)	0.2% Triton X-100, 20% DMSO, 0.3 M glycine in PBS
Blocking solution (iDISCO$^+$)	0.2% Triton X-100, 10% DMSO, 6% donkey serum in PBS
PTwH (iDISCO$^+$)	0.2% Tween-20 with 10 µg/ml heparin in PBS

Primary antibodies					
Antigen	Catalogue number	Suppliers	Host	Concentration	Dilution
5-HTT	PC177L	Calbiochem® Merk Millipore	Rabbit	No data available	1:500
CDH13	AF3264	R&D systems	Goat	0.2 mg/ml	1:400
TH	ab113	Abcam	Sheep	0.15 mg/ml	1:1000
TPH2	Not applicable	Self-produced[101,102]	Rabbit	Not applicable	1:1000

Secondary antibodies		
Antibody	Manufacturer	Dilution
Donkey-anti-rabbit IgG (H+L chains) Alexa Fluor 488 conjugated	Thermo Fisher Scientific, Damstadt, Germany	1:400
Donkey-anti-rabbit IgG (H+L chains) Alexa Fluor 488 conjugated	Abcam, Cambridge, United Kingdom	1:400
Donkey-anti-goat IgG (H+L chains) Alexa Fluor 555 conjugated	Thermo Fisher Scientific, Damstadt, Germany	1:400
Donkey-anti-rabbit IgG (H+L chains) Alexa Fluor 647 conjugated	Thermo Fisher Scientific, Damstadt, Germany	1:400
Cy™5 AffiniPure Donkey Anti-Rabbit IgG (H+L)	Jackson Immunoresearch, Cambridge House, United Kingdom	1:400
Biotinylated horse anti-goat IgG (H+L)	Vector Laboratories, Burlingame, CA, USA	1:400

2.7.3 Gene expression analysis

Reagents or Instruments	**Name and Location of Suppliers**
0.1M DTT	Invitrogen, Carlsbad, CA, USA
0.2 mL PCR SoftTubes	Biozym Scientific, Hessisch Oldendorf, Germany
5× first-strand buffer	Invitrogen, Carlsbad, CA, USA
BSA (20 mg/ml)	New England Biolabs, Frankfurt am Main, Germany
Cresyl violet acetate	Sigma, Steinheim, Germany
Diethylpyrocarbonate (DEPC)	AppliChem, Damstadt, Germany
Ethanol absolute	AppliChem, Damstadt, Germany
Laser microdissection system software (version 8.2.1.7070)	Leica Biosystems, Nussloch, Germany (ZEP, UKW)
Leica DM6000 B laser microdissection system	Leica Biosystems, Nussloch, Germany (Institute of Clinical Neurobiology, UKW)
Leica LMD 6 laser microdissection system	Leica Biosystems, Nussloch, Germany (ZEP, UKW)
PEN-membrane-coated slides	Applied Biosystems, Foster City, CA, USA
Picopure RNA Isolation kit	Thermo Fisher Scientific, Vilnius, Lithuania
QuantiTect Mm_B2m_2_SG Primer Assay (NM_009735)	Qiagen, Hilden, Germany
QuantiTect Mm_Rplp0_1_SG Primer Assay (NM_007475)	Qiagen, Hilden, Germany
random hexamer primer (100 µM)	Thermo Fisher Scientific, Vilnius, Lithuania
Real-time thermal cycler (CFX384)	Bio-Rad Laboratories, Feldkirchen, Germany
RNase away	Thermo Fisher Scientific, Vilnius, Lithuania
RNase-Free DNase Set	Qiagen, Hilden, Germany
RNasin® Ribonuclease Inhibitors	Promega, Madison, WI, USA

Set of dATP, dCTP, dGTP, dTTP (100mM)	Promega, Madison, WI, United States
Silica gel orange	Roth, Karlsruhe, Germany
SuperScript™ III Reverse Transcriptase (200 U/µL)	Invitrogen, Carlsbad, CA, USA
SYBR™ Select Master Mix for CFX	Thermo Fisher Scientific, Vilnius, Lithuania
Toluidine blue	Sigma, Steinheim, Germany

2.7.4 Microscopy

Instruments	**Name and Location of Suppliers**
Epifluorescence microscope (1x2 Ucb)	Olympus, Hamburg, Germany
FluoView FV1000 Confocal microscope	Olympus, Tokyo, Japan
Fluoview software (version 4.1.a)	Olympus, Tokyo, Japan
Olympus CellSense Dimension software (version 1.18)	Olympus, Hamburg, Germany

2.7.5 Behavioral tests

Reagents or Instruments	**Name and Location of Suppliers**
VideoMot2 software 6.04	TSE Systems, Bad Homburg, Germany
5-Hole Box Systems	TSE Systems, Bad Homburg, Germany
TSE Operant behavior software 3.07	TSE Systems, Bad Homburg, Germany

2.7.6 Data and statistical analysis

Softwares	**Name and Location of Suppliers**
ImageJ 2.1.0/1.53c	Open source image processing software http://imagej.net/Contricutors
GraphPad Prism (version 8.4.3 [for data from 2021 on] or 6.04 [for data before Dec. 2020])	GraphPad Software, CA, USA
Bio-Rad CFX manager 3.0 (version 3.0.1222.0925)	Bio-Rad Laboratories, Feldkirchen, Germany
LinRegPCR (version 2018.0)	Heart Failure Research Center Academic Medical Center, Amsterdam, The Netherlands
QBase+ (version 3.1)	Biogazelle, Zwijnaarde, Belgium
Huygens Professional (version 21.04 0p1 64b)	Scientific Volume Imaging B.V., Hilversum, The Netherlands
Imaris x64 (version 9.7.2)	Bitplane AG, CA, USA
Imaris File Converter x64 (version 9.7.0)	Bitplane AG, CA, USA

CHAPTER 3 RESULTS

3.1 Absence of CDH13 impacts the serotonergic circuit in mature brains

3.1.1 CDH13 is widely distributed in the adult mouse brain

Although the mRNA expression data was available in the Allen Brain Atlas, CDH13 protein expression in the adult brain was not yet characterized. The determination of which regions of the CNS express CDH13 and whether it is expressed by neurons or glial cells is of great importance given that protein is the functional endpoint of gene expression and performs the majority of biological actions in a cell (Freeman and Hemby, 2004). Furthermore, numerous studies have shown that mRNA expression may not directly equate with protein expression (Freeman and Hemby, 2004; Gygi et al., 1999). To produce an overview of CDH13 protein expression in the adult brain, immunohistochemistry on 20 µm brain slices at several anatomical levels was performed. Due to the generally low and diffuse expression of CDH13 in the adult brain when compared to expression in embryos, a signal amplification step was carried out in addition to the immunostaining in order to achieve an optimal intensity level for optical visualization. Additional slides, either omitted the primary antibody or pretreated with biotin-streptavidin blocking solutions, were used as negative controls (see Fig. 6 in 2.2.2).

In general, the expressions of *Cdh13* mRNA and protein were mostly related, with a few exceptions. For example, the cell-rich layer II of the piriform cortex and the thalamic reticular nucleus contained only *Cdh13* mRNA labelling, while the lateral posterior nucleus of the thalamus contained only CDH13 protein immunoreactivity. Briefly, intense labelling of *Cdh13* mRNA was present in the cell somas of (1) restricted forebrain regions, such as the limbic, infralimbic and insular cortices, layers V and VI of most six-layered neocortex, the claustrum and dorsal endopiriform; (2) cell groups that use a specific neurotransmitter, such as the GABAergic reticular thalamic nucleus, the dopaminergic ventral tegmental area and substantia nigra, the serotonergic raphe nuclei, and the noradrenergic locus coeruleus. In addition, conspicuous CDH13 protein immunoreactivity was found in the neuropil and often delineated subnuclei within a structure or the lamination in cortical areas. For example, strong CDH13 immunolabelling was found in all layers of the insular cortex, and concentrated in layers I, V, and VI of the limbic, infralimbic, cingulate, and temporal cortices (Fig. 8). Regional variance, for instance, was observed in the thalamus, hippocampus, and amygdala with the paraventricular thalamic nucleus, lateral posterior nucleus of thalamus, lateral amygdalar nucleus, the posteroventral part of medial amygdalar nucleus, the posterior parts of basolateral and basomedial amygdalar nuclei, the stratum lacunosum-moleculare of hippocampal cornu ammonis fields, and the molecular layer of dentate gyrus containing higher levels of CDH13 compared to other subdivisions within the same structure. Moderate CDH13 expression was also detected in distinct brainstem areas, such as the DR, superior colliculi, dorsal and lateral tegmental nuclei, and nucleus prepositus (Fig. 9). In the cerebellum, CDH13 was expressed by a fiber-like structure in the molecular layer that resembled the radial fibers of Bergmann glia morphologically (Fig. 10) (Reeber et al., 2018). The staining was repeated with pretreatment of additional biotin and streptavidin blocking solutions in order to block endogenous biotin and reduce non-specific staining. Similar results were observed, although further immunolabelling or co-localization experiments using another method would be needed to verify this data.

Subcellularly, CDH13 was localized in the rough endoplasmic reticulum and Golgi apparatus, as well as on the membrane of neuronal processes and terminals. These results, together with the data obtained by a former PhD student, Sarah Sich, are planned to be published (manuscript in preparation).

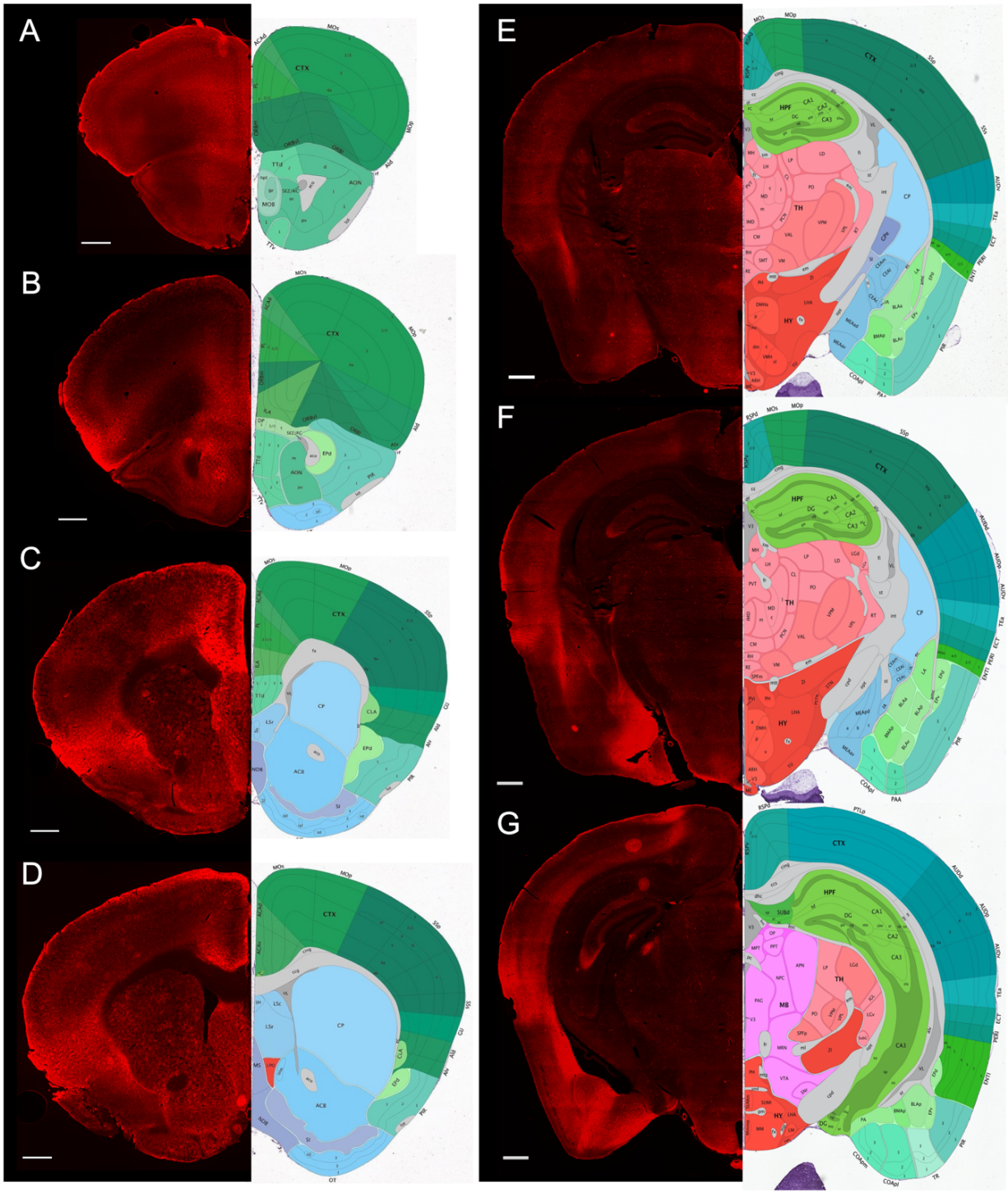

Figure 8. Distribution of CDH13 protein in the rostral adult mouse brain.
Intense CDH13 immunoreactivity was found in the dorsal endopiriform nucleus, claustrum, layer I of the neocortex, the prelimbic, infralimbic (A, B, C), anterior cingulate (D) and insular (B, C, D) cortices. In addition, the stratum lacunosum-moleculare of hippocampal cornu ammonis fields (E, F, G), the molecular layer of dentate gyrus (E, F, G), the lateral amygdalar nucleus (F), the posteroventral part of medial amygdalar nucleus (F), and the posterior parts of basolateral and basomedial amygdalar nuclei (G) were moderately labelled. Scale bar = 500 µm.

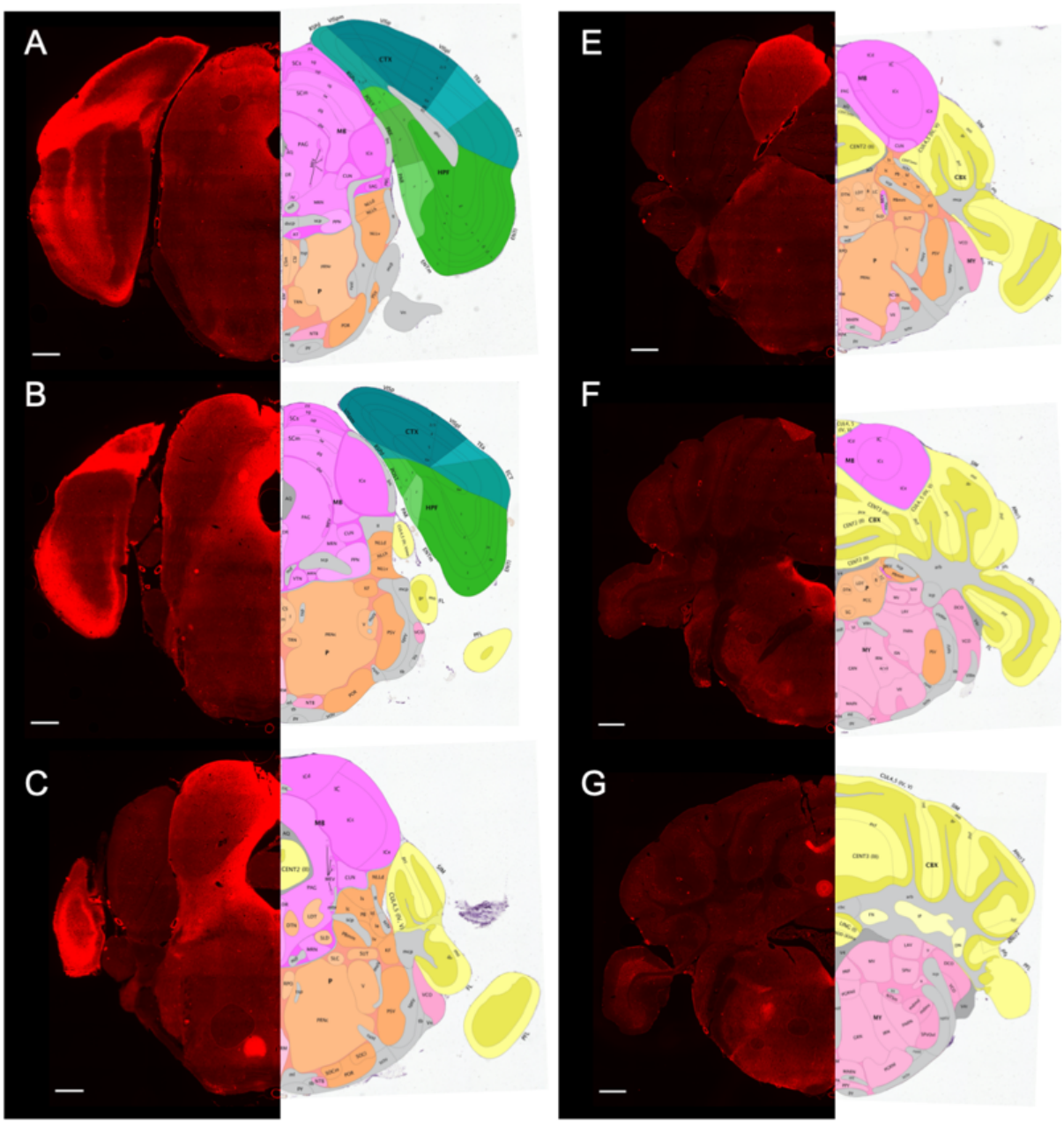

Figure 9. Distribution of CDH13 protein in the caudal adult mouse brain.
Intense CDH13 immunoreactivity was found in layers I and VI of the temporal cortex (A, B), layer II of entorhinal area (A, B), and periaqueductal gray (A, B, C), while moderate labelling was observed in the dorsal raphe (A, B), superior colliculi (B, C, D), dorsal and lateral tegmental nuclei (F), and nucleus prepositus (G). Scale bar = 500 μm.

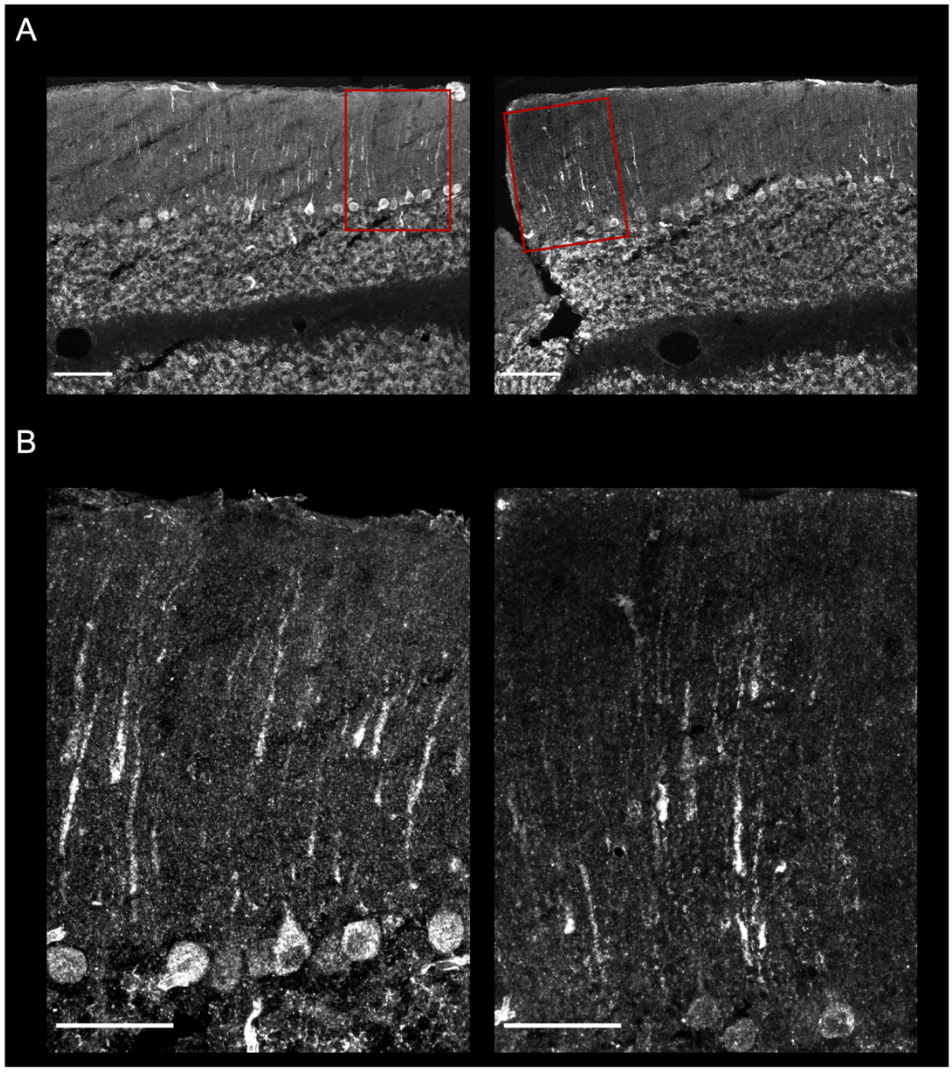

Figure 10. CDH13 is expressed by glia-like cells in the adult cerebellum.
(A) Wild-type adult cerebellar sections stained with CDH13 antibody. A fiber-like structure traversing the molecular layer of the cerebellum radially was detected with TSA kit alone (left panel in A) and TSA kit inclusive of biotin/streptavidin blocking solutions (right panel in A). (B) Higher magnifications of the boxed areas in A. The CDH13-positive signal could be observed at the processes as well as the soma of glia-like cells, which resembled Bergmann glia cells. Scale bar = 100 μm in A; 50 μm in B.

3.1.2 Loss of CDH13 impacts subgroups of DR serotonergic neurons differentially

The widespread ascending serotonergic projections are derived largely from the dorsal and median raphe nuclei in the rostral rhombomeres. The initial examination of the cellular organization of adult serotonergic system disclosed rather unexpected results, with the cell density of DR serotonergic neurons being increased, but with unaltered innervation in the prefrontal cortex (PFC) of *Cdh13*$^{-/-}$ mice compared to their wild-type littermates (Forero et al. (2017); results were partially derived from my master's thesis: Ku (2017)). This finding was largely based on the assumption that the DR serotoninergic neurons represented a single population as viewed by many early functional studies. However, more recent works have pointed to physiological and molecular heterogeneity within the serotonergic system. Both anterograde and retrograde tracing studies have indicated that the DR serotonergic neurons that

project to specific targets have stereotyped locations and vice versa. The serotonergic efferent connections from different raphe nuclei to the major brain regions are distinctive and non-overlapping (Muzerelle et al., 2016; Ren et al., 2019). Therefore, the idea that all the DR serotonergic neurons should be considered a single population that sends projections to the prefrontal cortex is too unspecific and must be refined.

To this end, the data was examined more closely by dividing the DR neurons into three anatomically defined subgroups; ventral cluster (B7v), dorso-median cluster (B7d), and the lateral wings (B7l), following the description in a conditional anterograde tracing study by Muzerelle et al. (2016). To be more precise, B7v refers to the TPH2-ir neurons that together form an open-paper-fan shape together, located above and between the medial longitudinal fasciculi; B7d refers to those that lie above the B7v, below the cerebral aqueduct; B7l refers to those that have the shape of its name, a loosely aggregated group of cells lying lateral to the B7d (Fig. 11A).

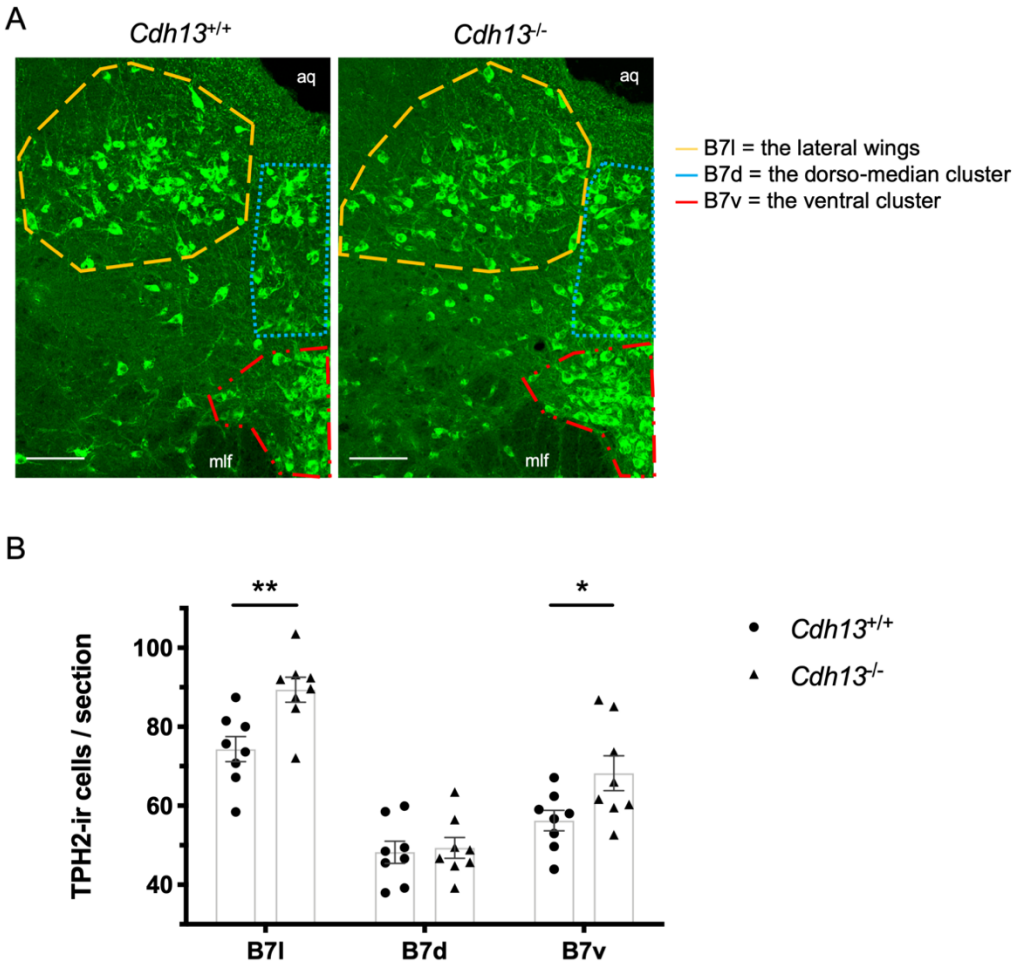

Figure 11. Lacking CDH13 has a differential impact on subgroups of DR serotonergic neurons in the adult brain.
(A) Coronal sections stained for TPH2 showing serotonergic neurons (in green) in the DR with the schematic delineation of subdivided groups, namely, the B7l (yellow dashed line), B7d (blue dotted line) and B7v (red dash-dotted line) clusters. (B) Higher numbers of TPH2-ir cells in B7l ($p = 0.0047$) and B7v ($p = 0.0344$), but not B7d ($p = 0.7762$), were found in *Cdh13*-null mice compared with their wild-type littermates. n = 8 per genotype. Scale bar = 100 µm. aq, cerebral aqueduct; mlf, medial longitudinal fascicle. Data presented as mean ± s.e.m. * $p < 0.05$, ** $p < 0.01$.

The average numbers of TPH2-ir cells per 20 micron brain slices were 74.3166 ± 9.0580, 48.1979 ± 7.9171 and 56.2189 ± 7.3080 in the B7l, B7d and B7v, respectively. Indeed, the analysis showed that the previously observed increase of TPH2-ir cells in *Cdh13*$^{-/-}$ mice was mainly concentrated in the B7l (n = 8; p = 0.0047), with a moderate increase in the B7v (p = 0.0344), whereas no change was found in the B7d (p = 0.7762) (Fig. 11B).

3.1.3 High serotonergic neuronal density leads to hyperinnervation in the laterodorsal nucleus of the thalamus

Brain structural connectivity (and the functional properties of neuronal networks) is highly impacted by cell density, influenced by variations in spatial arrangement and amount of cell-to-cell contact, as well as the global concentration of extrinsic factors (Akum et al., 2004; Beul and Hilgetag, 2019; Biffi et al., 2013; Cullen et al., 2010). In particular, the fibers of serotonergic neurons may travel for long distances across various brain regions, among which the fiber density of an individual region varies. This may reflect the physiological function of the regions and circuit strength of the region, as well as pathological changes. Given that the cell densities of serotonergic neurons in the B7l and B7v of *Cdh13*$^{-/-}$ mice were increased, its impact on the projection was examined. To this end, the target areas of B7l and B7v that contained CDH13 protein expression and, at the same time, that were closely related to ADHD pathophysiology were investigated. The following regions were selected: the infralimbic (IL) and cingulate (CG) cortices, the basolateral complex of the amygdala (AmyBL), and caudate putamen (CPu), which received the majority of projections from the B7v; the laterodorsal nucleus of the thalamus (ThaLD) and the cerebellum (CB), which received projections predominantly originating from the B7l; the paraventricular nucleus of the thalamus (ThaPV) which received projections from both the B7v and B7l. Due to the nature of serotonergic innervation (net- or matrix-like structure), it is rather difficult to look at individual trajectories. After images were taken and processed with ImageJ, they underwent the following two evaluations. To measure the density of serotonergic innervation at individual regions, the size of the whole selected area was divided into the pixels occupied by 5-HTT-ir fibers; to estimate the number of fibers at target regions, the number of intersections where 5-HTT-ir fibers crossed a randomly placed line was noted. All the image processing and measurements were automated in a batch process with ImageJ, and multiple technical replicates were included. For more details, see Materials and Methods. For the macro scripts, see Appendix A and B.

As shown in Fig. 12A, the morphological presentation of 5-HTT-ir fiber at individual regions was distinct. The density of serotonergic innervation varied among examined regions, with the highest found in the AmyBL (11.9349 ± 1.3927 × 10^{-2}/μm^2), followed by the ThaPV (11.2512 ± 0.6109 × 10^{-2}/μm^2), IL (10.5954 ± 1.5196 × 10^{-2}/μm^2), CG (9.6127 ± 1.5504 × 10^{-2}/μm^2), ThaLD (6.6268 ± 0.4426 × 10^{-2}/μm^2), CPu (5.7822 ± 0.6354 × 10^{-2}/μm^2), and CB (1.0668 ± 0.1348 × 10^{-2}/μm^2) in descending order (Fig. 12B)**.** The measured densities of serotonergic fibers were consistent with recent studies that examined TPH2-ir or 5-HTT-ir fibers across brain areas using newly established tissue clearing methods (Awasthi et al., 2020; Maddaloni et al., 2017). Compared to their wild-type littermates, *Cdh13*$^{-/-}$ mice displayed a significantly higher density of 5-HTT-ir fiber in the ThaLD (p = 0.0083), which received the majority of

serotonergic innervations from the B7l neurons (Fig. 12B). This effect, however, was not seen when examining the number of 5-HTT-ir fibers in the ThaLD (p = 0.5906), nor in other examined areas (Fig. 12C). It is likely that increased thickness, but not number, of serotonergic axons contributes to the observed hyperinnervation in the ThaLD.

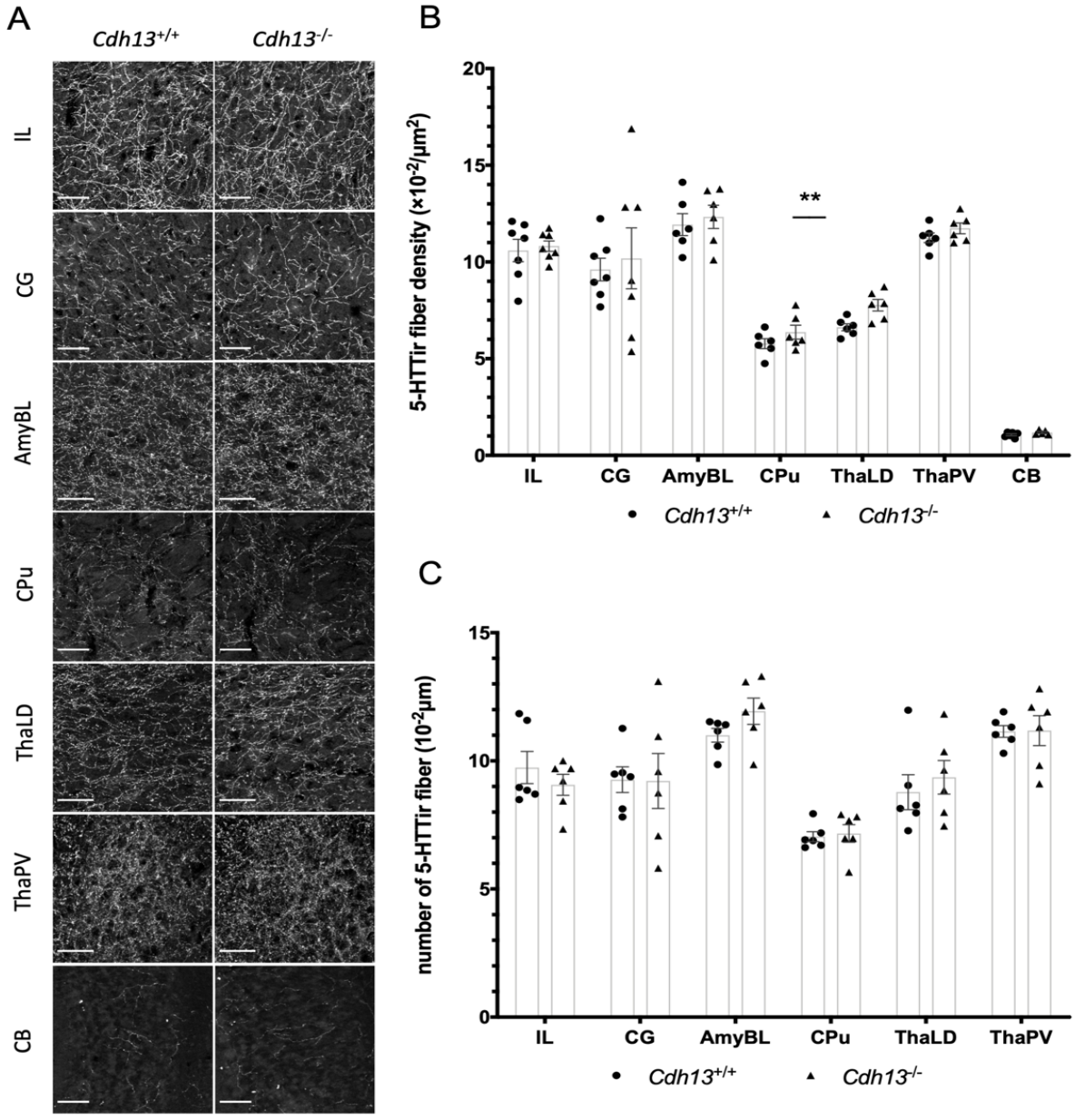

Figure 12. Serotonergic innervation in target areas of B7l and B7v neurons.
(A) Representative images of 5-HTTir fibers in the infralimbic cortex, cingulate cortex, basolateral complex of amygdala, caudate putamen, lateral dorsal nucleus of thalamus, paraventricular nucleus of thalamus, and cerebellum. (B) The density of 5-HTTir fibers in examined brain areas. Compared to their wild-type littermates, the 5-HTTir fiber density was significantly higher in the ThaLD of *Cdh13*-null mice (p = 0.0083). (C) The estimated numbers of 5-HTTir fibers in examined brain areas. Note that the number of 5-HTTir fibers in cerebellum was too low to yield reliable data, which was therefore excluded. IL, infralimbic cortex; CG, cingulate cortex; AmyBL, basolateral complex of amygdala; Cpu, caudate putamen; ThaLD, lateral dorsal nucleus of thalamus; ThaPV, paraventricular nucleus of thalamus; CB, cerebellum. n = 6-7 per genotype. Scale bar = 50 µm. Data presented as mean ± s.e.m. **$p < 0.01$.

3.1.4 System-level visualization of serotonergic circuits in adult mouse brain

Although it had been possible to measure the density of serotonergic fibers with the established protocol (section 3.1.3), it was challenging to acquire confocal images without background. The analysis of the fiber densities heavily relied on several factors, of which two are of special importance in this case. Firstly, in order to reduce the fluorescent signal of the background resulting from non-specific staining or autofluorescence, the quality and condition of the immunolabelling is critical for achieving a high signal-to-noise ratio of the acquired images. Secondly, the digital processing of individual images, which involves subtracting the background, among other operations, can introduce a bias into the measurement of image data, thereby making it susceptible to errors. In the last decade, a wide range of novel tissue clearing technologies, such as CLARITY and iDISCO+, have been developed and employed to overcome these challenges. The benefits of obtaining optical transparency in intact and 3D tissue goes beyond by (1) enabling exploration of spatial relationships between structures or molecules of interest; (2) allowing global visualization of neural networks; (3) being less time-consuming compared with the classic histological analysis of biological tissues by mechanical sectioning into two-dimensional slices.

CLARITY is a hydrogel-based clearing, relying on the removal of lipids with a strong ionic detergent, sodium dodecyl sulfate (SDS), while retaining the protein and DNA of the tissue by fixing them within a solid polymer network using formaldehyde and hydrogel monomers, acrylamide and bisacrylamide (Chung and Deisseroth, 2013; Chung et al., 2013; Gradinaru et al., 2018; Jensen and Berg, 2017). The clearing with SDS can be carried out in active (faster) or passive (slower) processes that rely on electrophoresis and diffusion, respectively. After immunolabelling, the sample is submerged in a refractive index (RI) matched medium for imaging. Due to limited access to the required equipment for active CLARITY, the straightforward and inexpensive passive CLARITY was tested. However, the efficiency turned out to be very low. While highly transparent E13.5 mouse brain tissue was attained, the transparency of whole adult brain tissues was rather poor after one month of submersion in clearing solution that was replaced regularly (Fig. 13A).

Alternatively, solvent-based iDISCO+ was carried out. Developed by Ertürk and colleagues (Erturk et al., 2012; Erturk and Bradke, 2013), DISCO-based tissue clearing offers a rapid and robust protocol that has been widely used in imaging studies of neuronal circuits. Combining immunolabelling with DISCO, the iDISCO+ optimized by Renier et al. improved the sample labeling conditions by reducing the autofluorescence and increasing the signal-to-noise ratio, therefore allowing the visualization of molecularly labeled fine structures within large intact tissues in 3D (Renier et al., 2014). After incubating with TPH2 antibody for seven days and Alexa Fluor 647 for another week, the whole adult mouse brain was sectioned sagittally into 1 mm slices using a vibratome which allowed subsequent imaging with confocal microscopy (Fig. 13B). Strikingly, not only were the TPH2-ir serotonergic neurons of DR captured (Fig. 13E), also the dendrites and axons were also clearly labelled (Fig. 13C and D), despite not being usually visible using conventional immunofluorescence staining with TPH2 antibody due to the background and autofluorescence of the tissue. The pattern and morphology of TPH2-positive signals were highly comparable with that of *Tph2*^{GFP} knock-in brain slices, in which

GFP expression allowed punctual identification of serotonergic neurons and axons (Maddaloni et al., 2017). In addition, compared with confocal microscopy, which has a limited range of imaging depth due to the working distance of the equipped objective lens, LSFM enabled deep-brain volumetric imaging at much higher speeds. This procedure was therefore repeated and 3D images of the whole-brain tissue were taken with LSFM (Fig. 13F and G). Although more experiments are needed to optimize the whole-mount labeling and image acquisition procedures, this powerful technique will allow for generation of new knowledge of the natural architecture and neural connectivity of the serotonergic system.

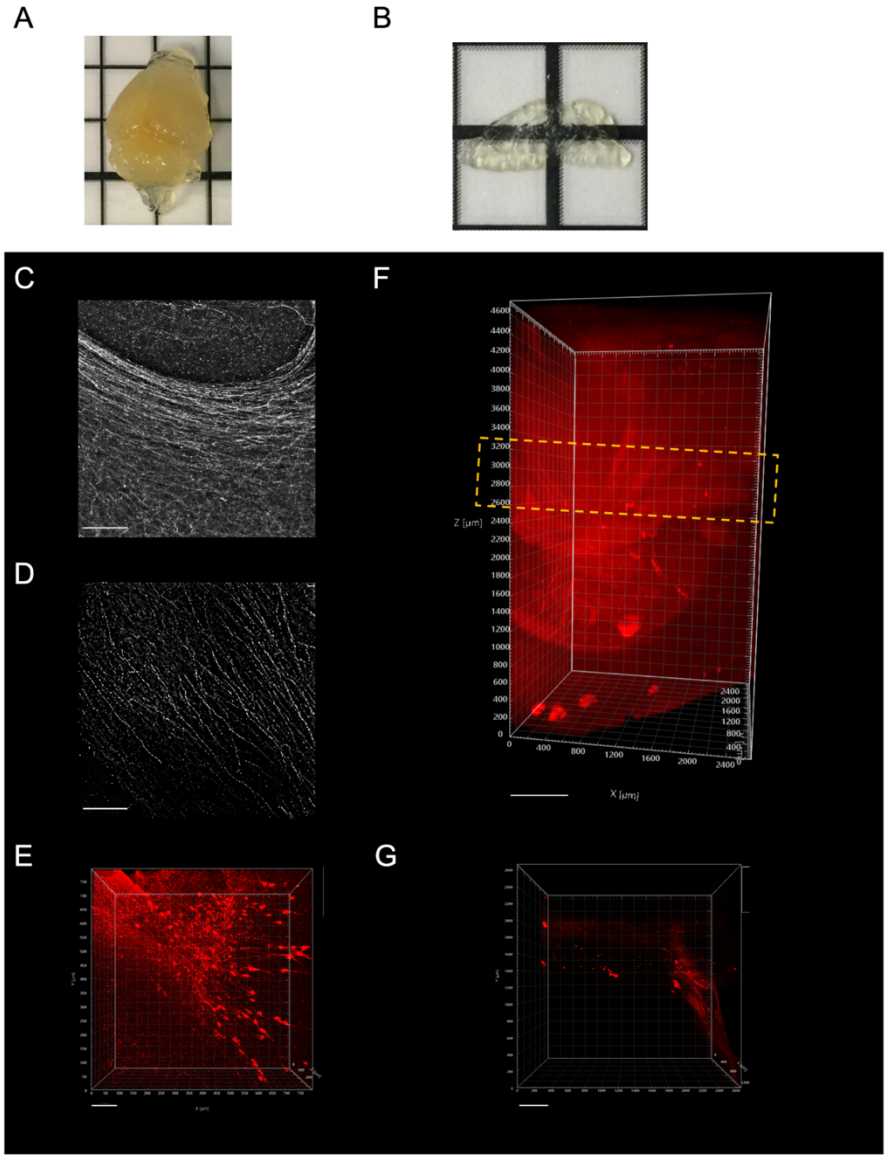

Figure 13. Optical tissue clearing and 3D imaging of the whole-mount TPH2-labelled adult brain.
(A) After a month of immersion in a CLARITY-based clearing solution, the adult mouse brain did not obtain the required transparency for imaging, except for the surface of the tissue. (B) An iDISCO+-cleared sagittal brain slice with a thickness of 1 mm prior to confocal microscope imaging. (C and D) TPH2-labelled fiber tracts of an iDISCO+-cleared brain were visualized by confocal microscopy. (E and F) Examples of 3D-reconstructed images taken by confocal (E) and LSFM (F), which have depths of approximately 300 µm and 4800 µm in z direction, respectively. (G) A cropped slice indicated in F showing details of the TPH2-labelled cells and axons in their natural space. Scale bar = 150 µm in C and D; 100 µm in E; 700 µm in F; 400 µm in G.

3.2 Serotonergic system-specific knockout mice display molecular and cognitive alterations

3.2.1 Molecular alterations in conditional mice were similar to that in the constitutive model

With the availability of serotonergic system-specific CDH13 knockout mice (abbreviated to *Cdh13* cKO), we investigated the impact of CDH13 in the serotonergic system. First, the efficiency of the conditional knockout mice was investigated by semi-qualifying the *Cdh13* mRNA expression of laser-microdissected DR tissue with real-time quantitative reverse transcription PCR (qRT-PCR). In order to reduce the incubation time and to obtain an optimal RNA yield, the sections were rapidly stained with 0.02% toluidine blue before the tissue was dissected out with the anatomical feature. In dorsal DR, where the anatomical localization was most stable and unvaried, the knockout efficiency was calculated to be 65.9% ($p < 0.0001$), while the overall efficiency of DR was 38.3% ($p < 0.0001$) (Fig. 14A and B). Beside serotonergic neurons, there are other types of cells in the DR that express CDH13, including GABAergic, dopaminergic cells as well as astrocytes, which may be the source that contribute to the residual CDH13 expression (Campagnoni et al., 2001; Huang et al., 2019; Huang et al., 2003; Takeuchi et al., 2000).

Moreover, this experiment was later repeated with non-specific cresyl violet staining (also known as Nissl staining) that allowed for better visualization of the size of cells in the DR. Compared with other types of neurons in DR, serotonergic neurons are relatively large in size, and it was therefore easier to recognize the rough localization of serotonergic neurons. Similarly, the aqueduct and medial longitudinal fascicles were also used as anatomical references.

As a result, the levels of *Cdh13* expression were significantly reduced in all the examined DR subregions of *Cdh13* cKO mice (Fig. 14C). The overall conditional knockout efficiency was calculated to be 54.14%, whereas individually in the B7d, B7v and B7l, they were 75.91%, 55.55% and 30.96%, respectively. This might be related to the density of serotonergic neurons in each subgroups, as CDH13 is still expressible by adjacent non-serotonergic cells. Specifically, in the B7l, where serotonergic neurons were relatively sparse distributed compared with that of other two B7 groups, the lowest knockout efficiency among all was observed, which might be the result of the *Cdh13* expression from other cell types.

Furthermore, a two-way ANOVA (with genotype and subregion as the between-subjects factors) was carried out to measure the effect of genotypes and subregions on *Cdh13* expression level. When interactions and/or main effects were detected, the Sidak's multiple comparisons test was performed as the post hoc correction. There was a statistically significant interaction between the genotypes and the subregions on *Cdh13* expression levels (F (2, 39) = 12.06, $p < 0.0001$) (Fig. 14C). The expression levels of *Cdh13* especially differed amongst these three subregions of DR in control mice, with that of B7d significantly higher than the other two areas (B7l vs. B7d: $p = 0.0015$; B7d vs. B7v: $p = 0.0003$).

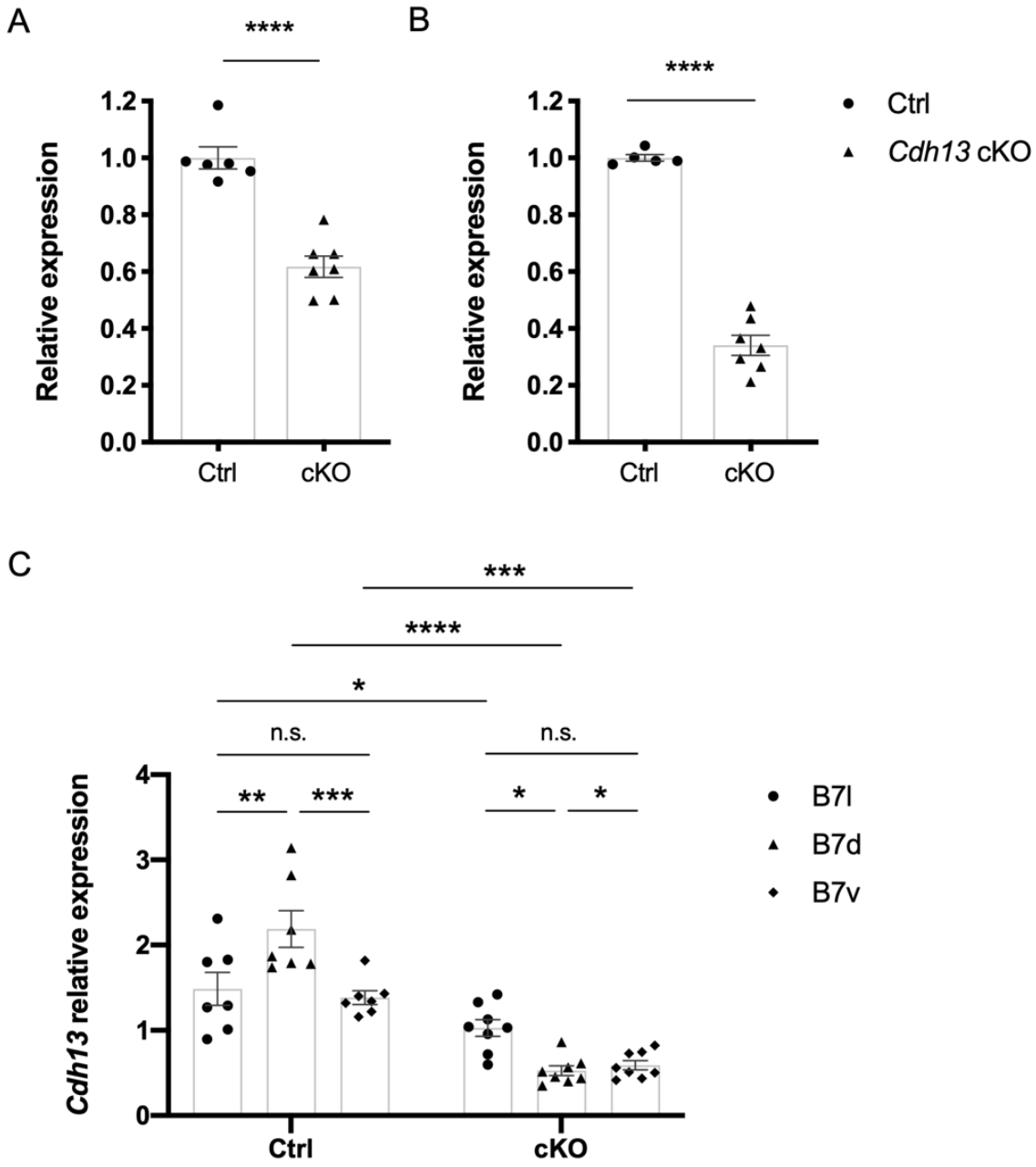

Figure 14. Laser microdissection combined with qRT-PCR showed that *Cdh13* was efficiently knocked out in *Cdh13* cKO mice.

(A) Relative expression of *Cdh13* in the whole DR. The knockout efficiency was calculated to be 38.3% ($p < 0.0001$) (B) Relative expression of *Cdh13* in the B7d. The knockout efficiency was calculated to be 65.9% ($p < 0.0001$). (C) The analysis was repeated with another cohort of naïve brains using Nissl-staining that provided a better visual guidance for recognizing the neurons in DR subregions. The knockout efficiency was calculated to be 30.96% ($p = 0.0422$), 55.55% ($p = 0.0002$), 75.91% ($p < 0.0001$) and 54.14% in the B7l, B7v, B7d, and the whole DR, respectively. Among the subareas, *Cdh13* expression levels in the B7l and B7v significantly differed from that of B7d within genotypes ([Ctrl: B7l vs. B7d, $p = 0.0015$; B7l vs. B7d, $p = 0.9277$; B7l vs. B7d, $p = 0.0003$]; [*Cdh13* cKO: B7l vs. B7d, $p = 0.0182$; B7l vs. B7d, $p = 0.0459$; B7l vs. B7d, $p = 0.9765$]). A, B: n = 6-7 per genotype; C: n = 8 per genotype. Scale bar = 50 µm. Data presented as mean ± s.e.m. * $p < 0.05$, ** $p < 0.01$, *** $p < 0.001$, **** $p < 0.0001$. Adapted from "Serotonin (5-HT) neuron-specific inactivation of Cadherin-13 impacts 5-HT system formation and cognitive function," by Forero et al., 2020. *Neuropsychopharmacology*.

On the other hand, imaging with structured illumination microscopy (SIM), immunofluorescent labelling of CDH13 showed that CDH13 expression was reduced and did not cluster along the processes and cell body of serotonergic cells of *Cdh13* cKO mice (Fig. 15). This work, along with other studies mentioned in this paragraph, was largely performed by my colleagues, Dr. Andrea Forero (a fellow PhD student at the time), and Ana Belén Malpartida (a Master's student at the time). The credit is truly all theirs. As their findings helped substantially explain the rationale of this thesis and the work that continued afterwards, a summary of their work is included as follows. In brief, nearly all results were consistent with those carried out using the constitutive mouse model. More precisely, *Cdh13* cKO mice exhibited increased serotonergic cell density in the DR at E13.5 as well as in adulthood, in which the differential increase of serotonergic neurons in the B7l and B7v was again verified. In addition, the serotonergic hyperinnervation in the developing PFC and somatosensory cortex was consistent in both of the mouse models. Rather unexpectedly, in the adult mouse brain, serotonergic innervation was decreased in the cingulate cortex of *Cdh13* cKO mice, whereas it was increased in the ThaLD of *Cdh13*$^{-/-}$ mice (see Forero et al. (2020) and Chapter 4 for more details). Nonetheless, results from both models were largely consistent and comparable, supporting the notion that knocking out CDH13 in the serotonergic system alone was sufficient to bring about the molecular alterations in the serotonergic circuits.

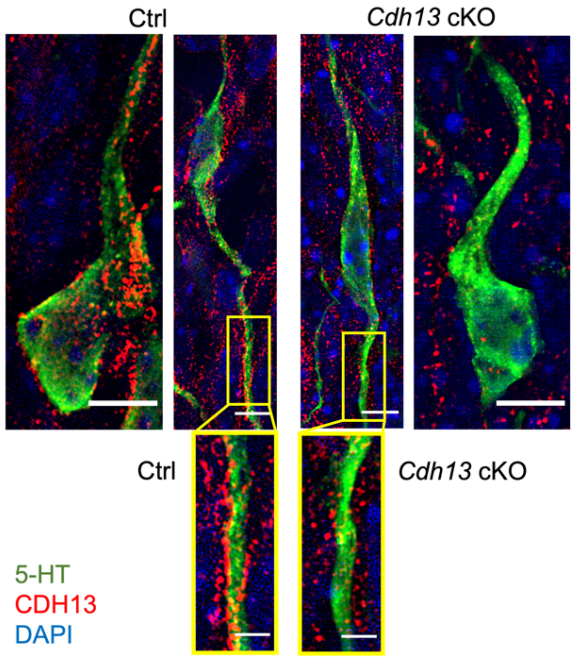

Figure 15. The conditional inactivation of CDH13 was further evidenced by the immunofluorescent labelling of CDH13 in embryonic control and *Cdh13* cKO brains imaged with SIM.
The CDH13 immunoreactivity did not cluster along the soma and extending neurite of 5-HT-labelled neurons in the *Cdh13* cKO brain, suggesting the inactivation of CDH13 expression in serotonergic neurons. This work was done by Dr. Andrea Forero and was included in her dissertation (Forero, 2020). Adapted from "Serotonin (5-HT) neuron-specific inactivation of Cadherin-13 impacts 5-HT system formation and cognitive function," by Forero et al., 2020. *Neuropsychopharmacology,* 168:108018.

3.2.2 Knocking out CDH13 in the serotonergic system alone is sufficient to alter cognitive phenotypes

After characterizing the molecular presentations of the serotonergic system in the *Cdh13* cKO mice (section 3.2.1), the behavioral phenotypes of the *Cdh13* cKO mice were assessed using a battery of behavioral tests for locomotor activity, anxiety-like behavior, spatial learning and memory, sociability and social novelty, and motor impulsivity and attentional control. In order to reduce task-induced chronic stress, the behavioral evaluation was structured in a way that the observational tasks which rely on spontaneous rodent behavior, such as the open field (OF), elevated plus maze (EPM), light-dark box (LDB), and social behavior (SB) tasks, were conducted prior to complex tasks involving training, such as the Barnes Maze (BM). A second cohort of male *Cdh13* cKO mice (n = 13) and Ctrl littermates (n = 7) was subjected to five-choice serial-reaction time task (5-CSRTT). This part of the study was performed together with Dr. Andrea Forero (a fellow PhD student at the time), and Judit Alhama-Riba (a Master's student at the time). For the OF, EPM, LDB, and SB, the differences between genotypes were assessed with two-tailed unpaired student's t test or the nonparametric Mann-Whitney test; for the BM and 5-CSRTT, the differences in the performance were analyzed with repeated measures mixed ANOVA, with genotype as the between-subjects factor and test session as the within-subjects factor. When significant main effects and/or interactions were observed, a Sidak post-hoc test was used to follow up.

In general, the student's t test detected no difference between genotypes in the total distance traveled in the OF, EPM, and LDB, indicating normal locomotor capability (Fig. 16). Similarly, no signs of anxiety-like behavior were observed in the *Cdh13* cKO mice as the latency until center zone entry ($p = 0.6764$), time spent at the border ($p = 0.3219$) and in center zone ($p = 0.3381$) in the OF (Fig. 16A), latency until light compartment entry ($p = 0.1792$) and percentage of time spent in the light compartment ($p = 0.9482$) in the LDB (Fig. 16B), and latency to open arm ($p = 0.5875$) and percentage of time spent in the open arm ($p = 0.9581$) in the EPM (Fig. 16C) were unaltered. Additionally, in the first trial of SB, all mice regardless of genotypes displayed significantly higher tendency for the social stimulus (*Cdh13* cKO: $p < 0.0001$; Ctrl: $p = 0.0005$), which was an age- and sex-matched mouse in a cage, as opposed to a non-social stimulus that was an empty cage, indicating normal sociability (Fig. 17A). No differences in the time spent with social stimulus ($p = 0.5004$) or non-social stimulus ($p = 0.3594$) were found between genotypes. Notably, the *Cdh13* cKO mice approached the social stimulus significantly faster (i.e. reduced latency) compared to their control littermates (Ctrl: n = 8; *Cdh13* cKO: n = 9; $p = 0.0085$). In the second trial, a novel mouse, previously unencountered by the subject animal, was placed in the originally empty cage. All mice demonstrated a higher preference for the unfamiliar mouse over the familiar one (*Cdh13* cKO: $p = 0.0101$; Ctrl: $p = 0.0.0053$), suggesting normal social recognition and novelty preference (Fig. 17B). Likewise, no differences in the time spent with familiar ($p = 0.8174$) or unfamiliar ($p = 0.4643$) mouse were found between genotypes.

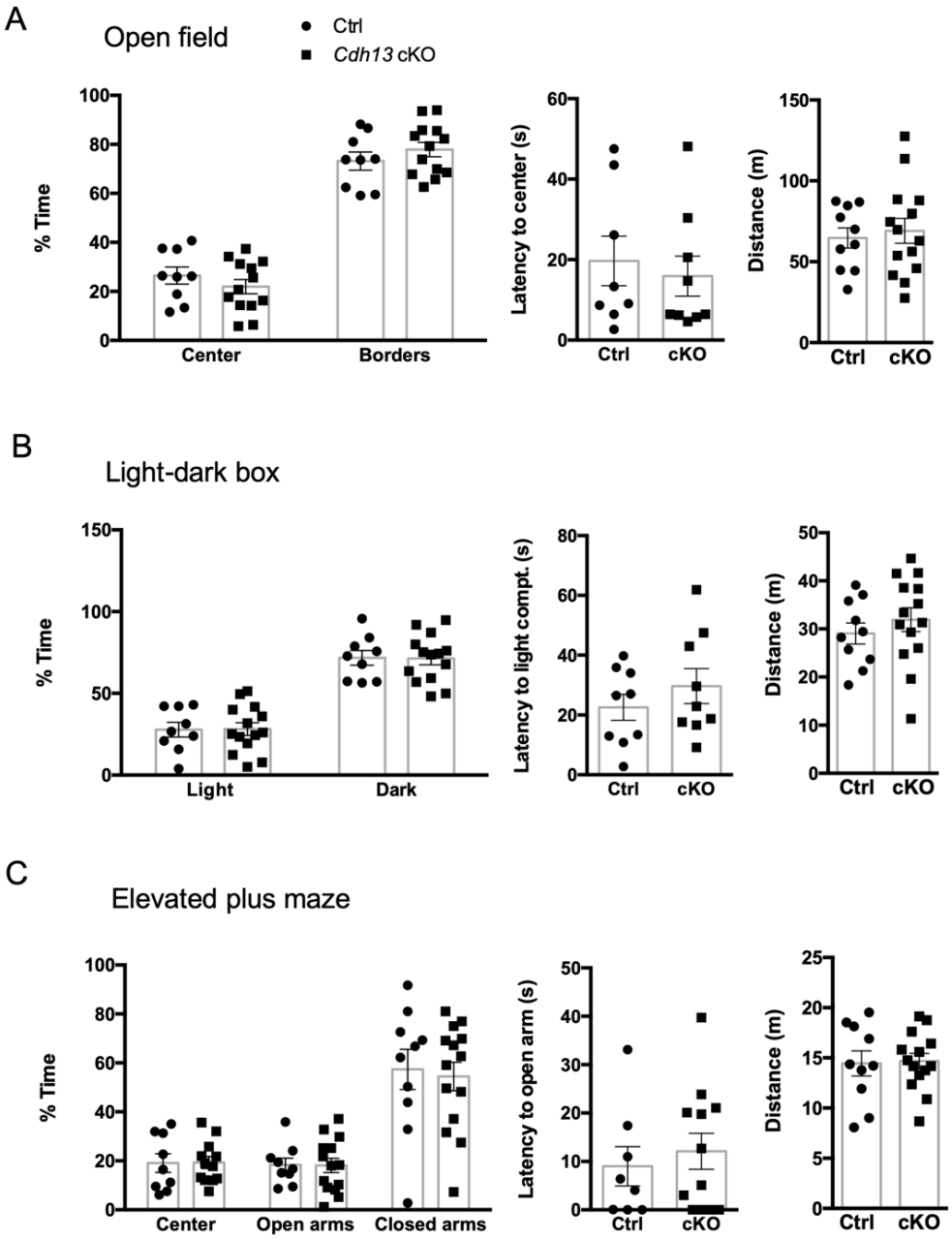

Figure 16. Behavioral assessments of locomotor activity and anxiety-like behaviors in *Cdh13* cKO and control mice.

The behavior of both groups of mice was similar in the open field (A), light-dark box (B) and elevated plus maze tests (C). The *Cdh13* cKO mice displayed normal locomotor activity as was indicated by comparable total distance traveled to the controls in all three paradigms. Analysis of anxiety-related parameters, including the time spent in the center of the arena and the latency to enter the center area in the open field test (A), time spent in the lid area in the light-dark box test (B), and time spent in the open arm in the elevated-plus maze test (C), indicated no differences between genotypes. Ctrl: n = 10; *Cdh13* cKO: n = 14. Data presented as mean ± s.e.m. These assessments were carried out together with Dr. Andrea Forero who was a fellow PhD student and therefore, they were also included in her dissertation (Forero, 2020). Adapted from "Serotonin (5-HT) neuron-specific inactivation of Cadherin-13 impacts 5-HT system formation and cognitive function," by Forero et al., 2020. *Neuropsychopharmacology,* 168:108018.

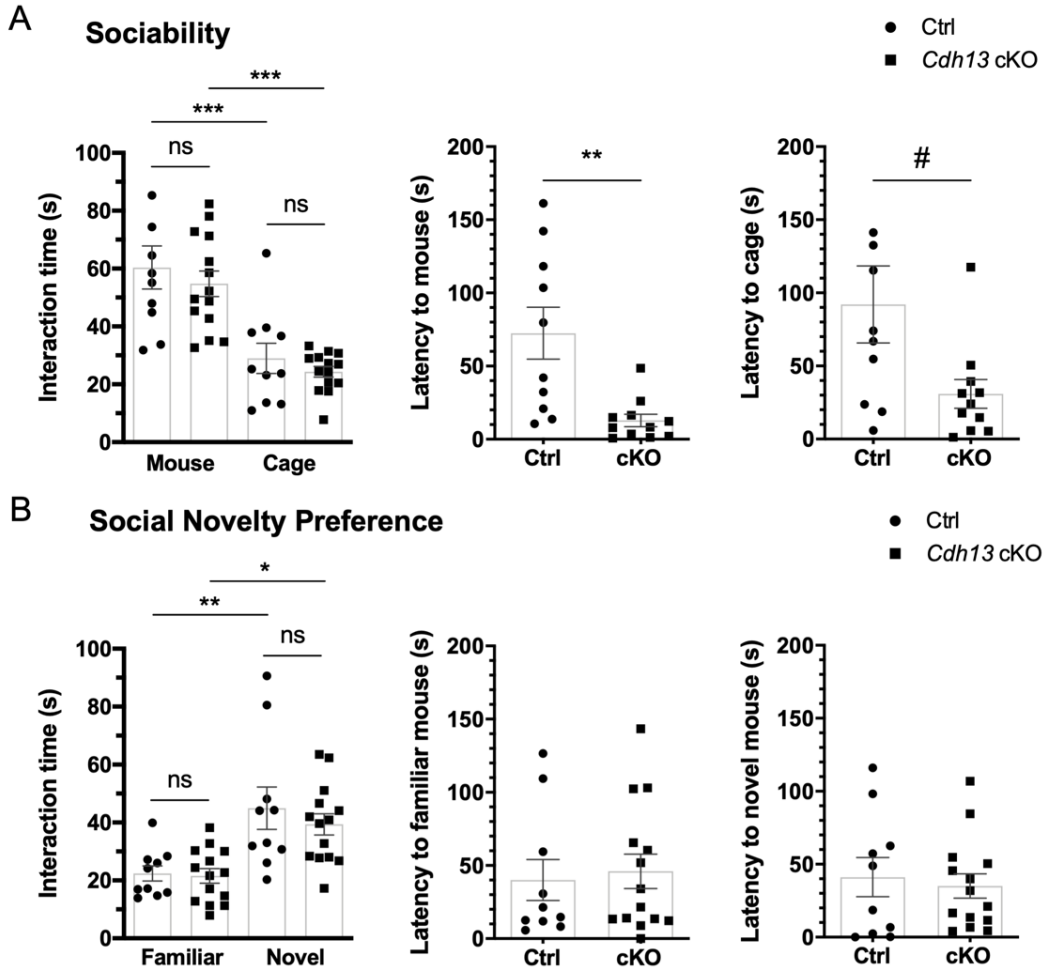

Figure 17. Assessment of sociability and social novelty preference in *Cdh13* cKO mice.
(A) All mice showed a higher preference for a social stimulus (an age- and sex-matched mouse) over a non-social stimulus (an empty cage), indicating normal sociability. Nonetheless, the *Cdh13* cKO showed a significantly reduced latency to approach the social stimulus (Ctrl: n = 8; *Cdh13* cKO: n = 9; p = 0.0085). (B) The *Cdh13* cKO mice exhibited normal social novelty preference as was shown by the preference for the novel social stimulus over the familiar one. Data presented as mean ± s.e.m. #$p < 0.1$, *$p < 0.05$, **$p < 0.01$, ***$p < 0.001$. These assessments were carried out together with Dr. Andrea Forero who was a fellow PhD student and therefore, they were also included in her dissertation (Forero, 2020). Adapted from "Serotonin (5-HT) neuron-specific inactivation of Cadherin-13 impacts 5-HT system formation and cognitive function," by Forero et al., 2020. *Neuropsychopharmacology,* 168:108018.

Moreover, in cognitive tasks involving active learning and memory of the subjects, the *Cdh13* cKO mice required longer time for the acquisition of paradigms compared with their control littermates. For instance, although all mice learned to find the escape hole within the given time period, the *Cdh13* cKO mice made significantly more primary errors on day two and four of the Barnes maze testing phase (day two: p = 0.0066; day four: p = 0.0086) (Fig. 18A). Interestingly, the *Cdh13* cKO mice became mobile sooner than control counterparts in the testing platform (i.e. reduced latency to start), both in the pre-pause (p = 0.014) and post-pause (p = 0.001) phases (Fig. 18B). However, the percentages of time spent in each quadrant did not differ between genotypes (Fig. 19). Another example would be their performance in the 5-

CSRTT, in which the *Cdh13* cKO mice displayed significantly lower attentional accuracy in terms of making more incorrect responses (main effect of genotype: F (1, 18) = 7.984, p = 0.0112; day six: p = 0.0135) during Stage 2 of the autoshaping phase (Fig. 21C). This resembled the delays and gaps in the process of acquiring and appropriating basic skills for learning in ADHD-affected individuals with or without other comorbid learning disabilities (Berger et al., 2013; Dyck and Piek, 2014; Schmidt and Petermann, 2009). No alterations in all measured parameters between genotypes were observed in the habituation phase in the 5-CSRTT (Fig. 20).

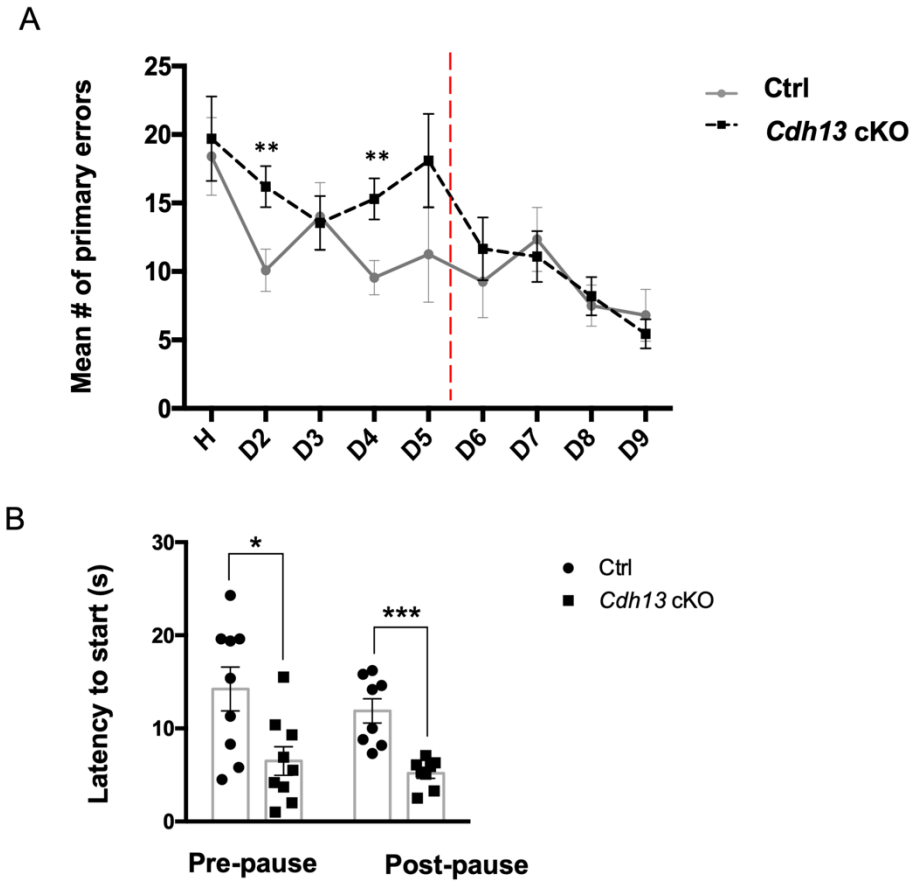

Figure 18. Spatial learning and memory deficits of *Cdh13* cKO mice was revealed by the Barnes maze.
(A) The *Cdh13* cKO mice made a significantly higher number of primary errors on day two and four (n = 10 per genotype; day two: p = 0.0066; day four: p = 0.0086) during the pre-pause phase. (B) Compared to the controls, *Cdh13* cKO mice showed reduced latency to start, that is, becoming mobile faster in the arena, in the pre-pause (n = 9 per genotype; p = 0.014) and post- pause (n = 8 per genotype; p = 0.001) phases. H, habituation phase; D, day. Data presented as mean ± s.e.m. *p < 0.05, **p < 0.01, ***p < 0.001. These assessments were carried out together with Dr. Andrea Forero who was a fellow PhD student and therefore, they were also included in her dissertation (Forero, 2020). Adapted from "Serotonin (5-HT) neuron-specific inactivation of Cadherin-13 impacts 5-HT system formation and cognitive function," by Forero et al., 2020. *Neuropsychopharmacology,* 168:108018.

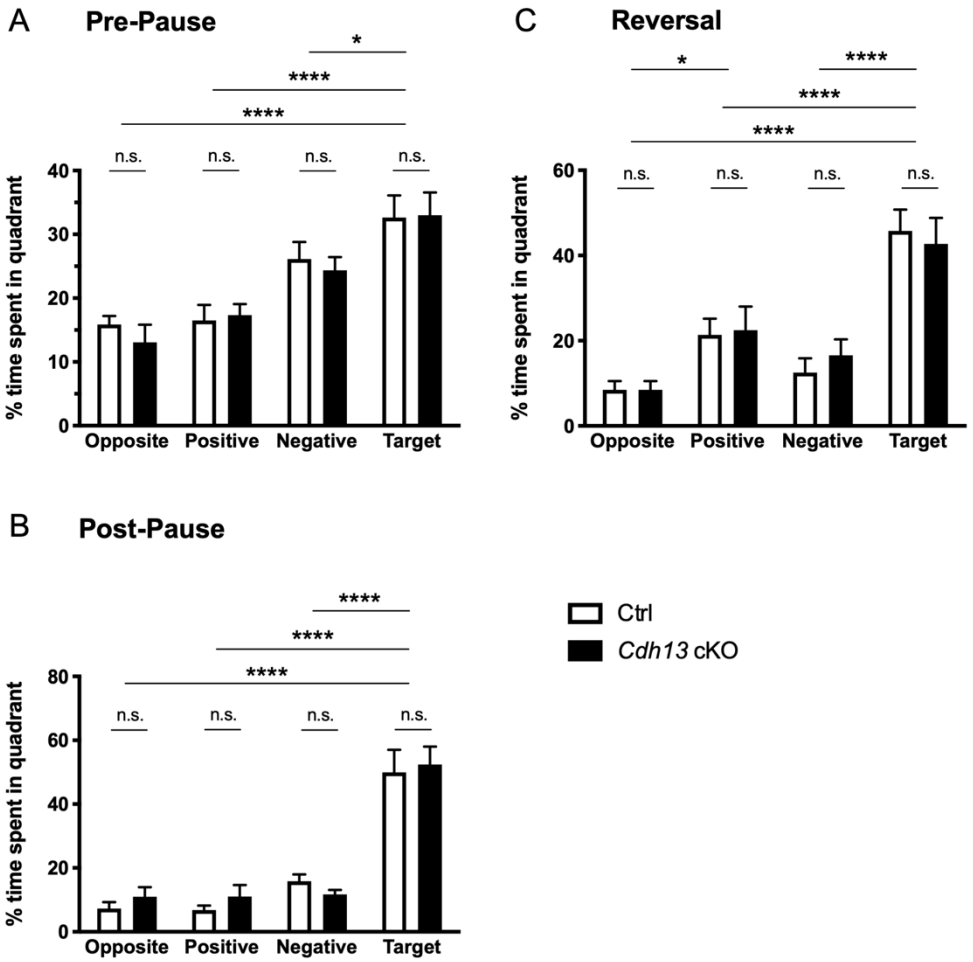

Figure 19. The percentage of time spent in each quadrant within pre-, post-pause, and reversal phases of the Barnes maze test.
The maze is divided into four quadrants with the escape hole being in the center of the Target quadrant; the other quadrants are labeled clockwisely from the Target quadrant as Positive, Opposite, and Negative. No difference in the averaged % time spent in each quadrant was found between genotypes in all three phases. As expected, during the pre-pause (A) and post-pause (B) phases, all mice spent significantly more time in the Target quadrant. However, during the reversal phase (C), all mice were equally inflexible as they spent most of the time in the Target quadrant as they did in the previous two phases and less than 10% of the time in the Opposite quadrant where the escape box was placed. n = 9 per genotype. Data presented as mean ± s.e.m. $*p < 0.05$, $****p < 0.0001$. Adapted from "Serotonin (5-HT) neuron-specific inactivation of Cadherin-13 impacts 5-HT system formation and cognitive function," by Forero et al., 2020. *Neuropsychopharmacology,* 168:108018.

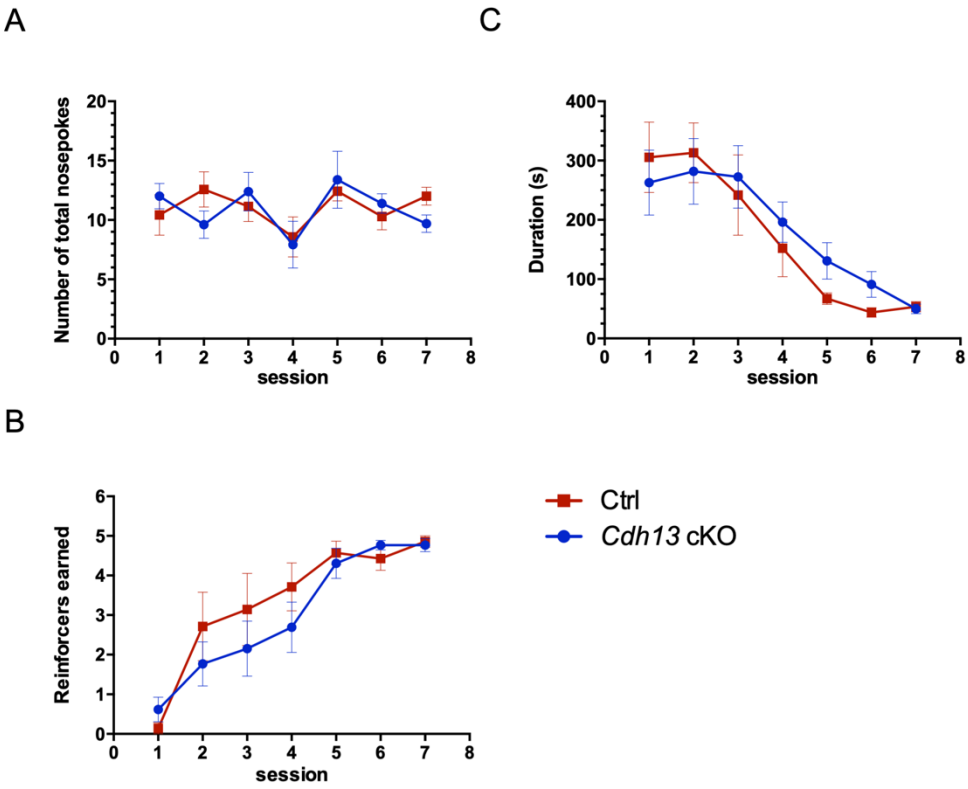

Figure 20. Performance measures of the habituation phase of the 5-CSRTT.
Prior to initiating training, mice were habituated to the operant chamber for seven sessions in total and learned to complete the session gradually with decreased duration of time and increased number of reward pellets. Two-way repeated measure ANOVA revealed no differences between genotypes in the number of total nose-pokes (A), the number of earned reinforcers (B) and the duration to poke at least once at each aperture (C). Ctrl: n = 10; *Cdh13* cKO: n = 14. Data presented as mean ± s.e.m. Adapted from "Serotonin (5-HT) neuron-specific inactivation of Cadherin-13 impacts 5-HT system formation and cognitive function," by Forero et al., 2020. *Neuropsychopharmacology,* 168:108018.

Furthermore, the *Cdh13* cKO mice showed signs of impulsive-like behaviors in subjected behavioral tasks, including the BM and 5-CSRTT. Specially, the *Cdh13* cKO mice became mobile in the testing arena or platform significantly sooner than their counterparts as was evident by the decreased latencies to start in the pre-pause (p = 0.014) and post-pause (p = 0.001) phases of BM (Fig. 18B). During stage 2 of the autoshaping phase of 5-CSRTT, the *Cdh13* cKO mice made significantly more premature responses (genotype by session interaction: F (3, 54) = 12.29, p < 0.0001; day eight: p < 0.0001) (Fig. 21G), a widely used measure of motor impulsivity that is one of the hallmarks of ADHD (Bari et al., 2008; Robbins, 2002; Volkow and Swanson, 2013; Wilens and Spencer, 2010; Winstanley et al., 2006). Unexpectedly, during the testing phase of the 5-CSRTT, *Cdh13* cKO mice showed enhanced attentional performance in terms of higher numbers of correct responses (Stage 1: session × genotype interaction, F (3, 54) = 5.480, p = 0.0023; Stage 2: genotype, F (1, 18) = 5.133, p = 0.0360) (Fig. 22A) during stage 2 as well as a decreased number of omissions (Stage 2: genotype, F (1, 18) = 4.745, p = 0.0429) (Fig. 22F) on the last testing day. However, no differences between genotypes were found in the final level of the testing phase, in which the inter-trial interval was variable and unpredictable to the subject animal (Fig. 23). For more details, see Forero et al. (2020).

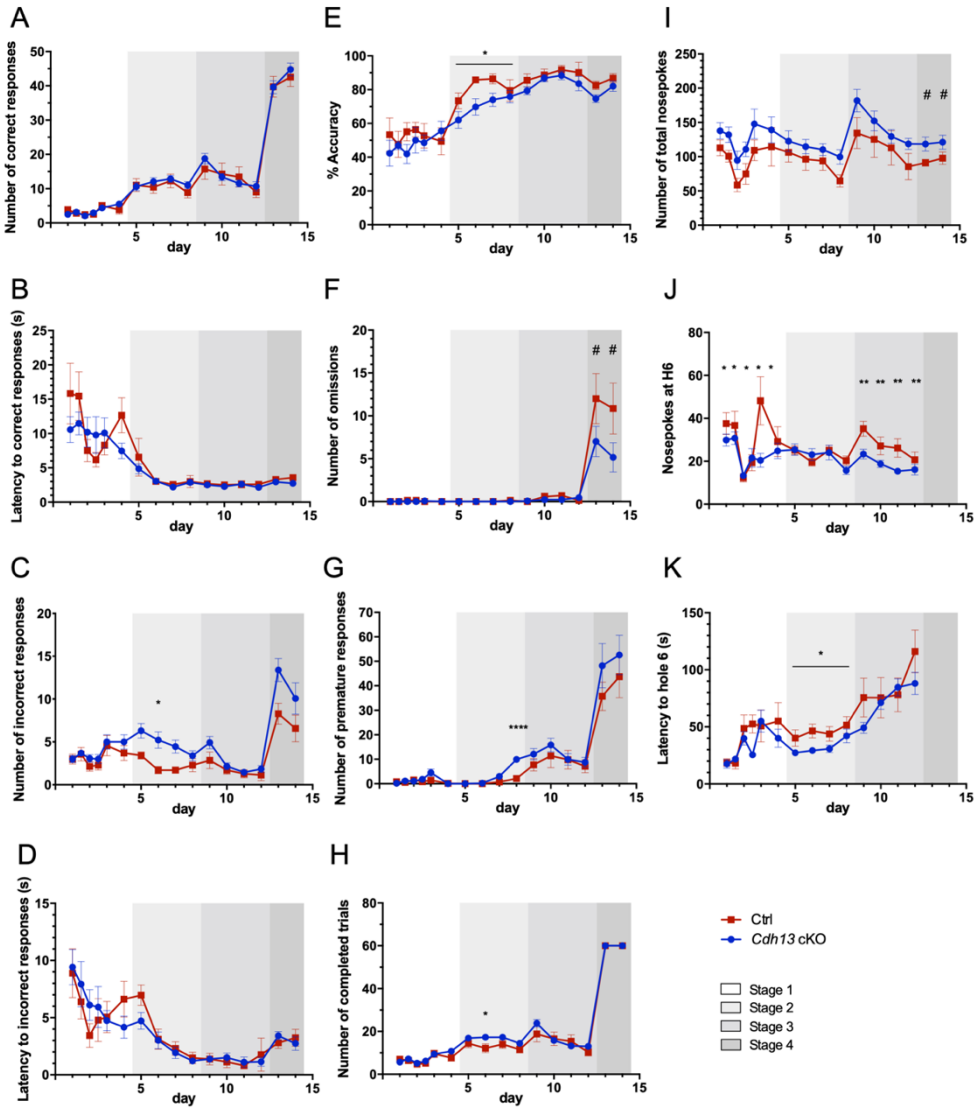

Figure 21. Performance measures of the autoshaping phase of the 5-CSRTT.
For the autoshaping phase, mice were trained with increasing levels of difficulty for over two weeks. The number of and latency to correct response (A and B, respectively), number of and latency to incorrect response (C and D, respectively), percentage of accuracy (E), number of omission (F), premature response (G), completed trials (H), total nose-pokes (I), and nose-poke at hole 6 (J), as well as the latency to hole 6 (K) were recorded and analyzed. Both groups of mice were able to respond to the stimuli within 5 s after six days of training (in Stage 2), despite the performance fluctuations in the first stage. During stage 2, the *Cdh13* cKO mice made significantly more incorrect responses (C; main effect of genotype: F (1, 18) = 7.984, p = 0.0112; day six: p = 0.0135) and premature responses (G; genotype by session interaction: F (3, 54) = 12.29, $p < 0.0001$; day eight: $p < 0.0001$). Although the percentage of accuracy during the same stage decreased significantly in *Cdh13* cKO mice (E; main effect of genotype: F (1, 18) = 5.319, p = 0.0332), the number of completed trials increased (H; F (1, 18) = 5.023, p = 0.0379) compared to controls. In the same stage, the *Cdh13* cKO mice needed less time to initiate the next trial (K; main effect of genotype: F (1, 18) = 5.782, p = 0.0272) as was indicated by reduced latency to H6. Noticeably, the average value of total nose-pokes made by the *Cdh13* cKO mice was higher than the controls during the entire period of autoshaping phase, although it was only close to significant (F (1, 18) = 3.362, p = 0.0833) in the last stage (I). Note that in the last stage of autoshaping, the mice did not have to initiate the trial themselves (hence no data point of nose-poke at and latency to hole 6 available [J and K, respectively]) and were able to complete 60 trials within 20 min (H). Ctrl: n = 10; *Cdh13* cKO: n = 14. Data presented as mean ± s.e.m. #$p < 0.1$, *$p < 0.05$, **$p <$ 0.01, ***$p < 0.001$, ****$p < 0.0001$. Adapted from "Serotonin (5-HT) neuron-specific inactivation of Cadherin-13 impacts 5-HT system formation and cognitive function," by Forero et al., 2020. *Neuropsychopharmacology,* 168:108018.

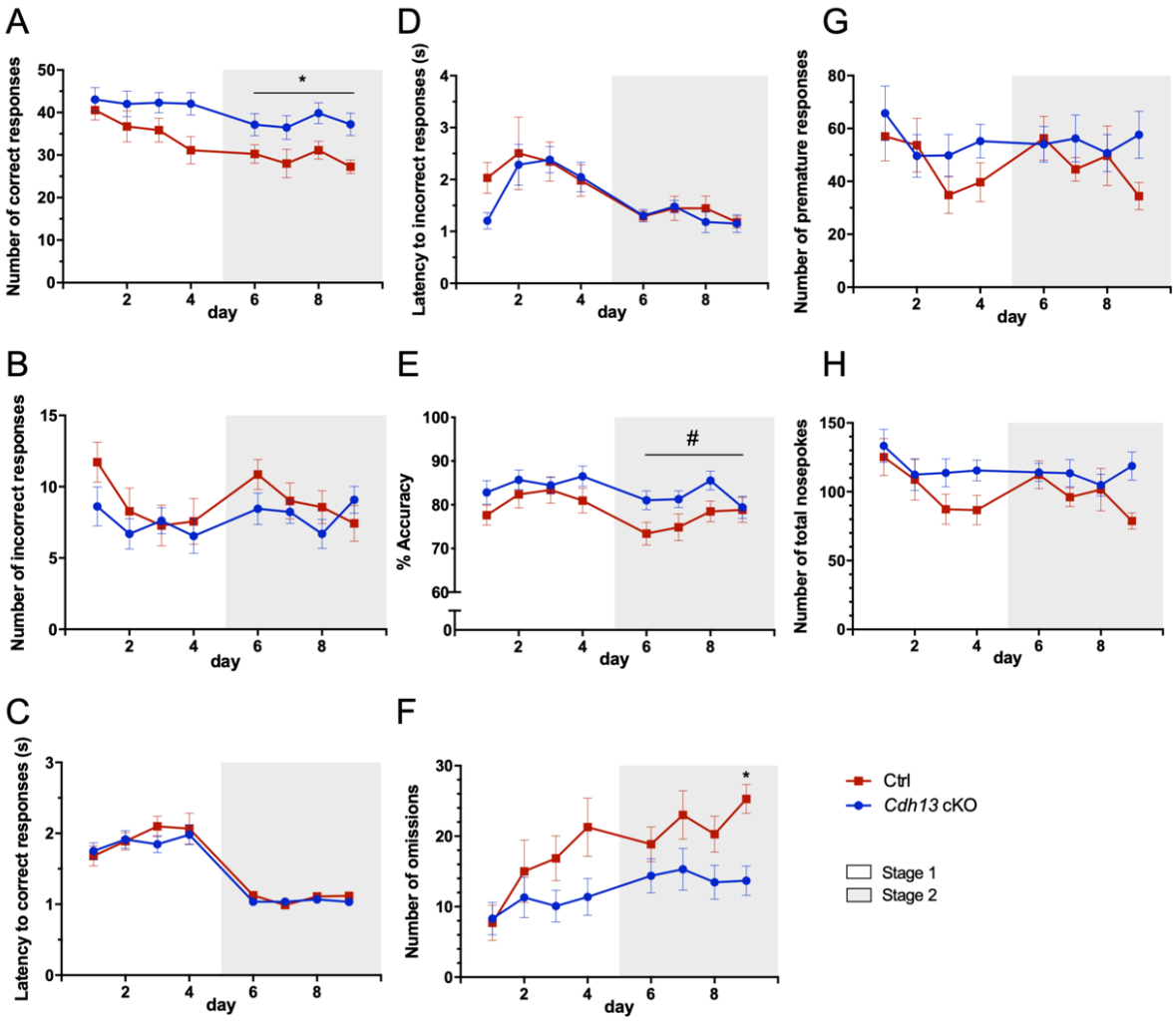

Figure 22. Performance measures of the testing phase of the 5-CSRTT.
Once all mice had reached criteria (>75% accuracy and <15% omission) for three consecutive days at 10-s StD and 10-s ITI within the last autoshaping level, they were subjected to two levels of testing. The number of correct and incorrect responses (A and B, respectively), latency to correct and incorrect responses (C and D, respectively), percentage of accuracy (E), number of omission (F), premature response (G), and total nose-pokes (H) were recorded and analyzed. The stimulus duration was shortened from 5 s in stage one to 2 s in stage two, hence the lower latencies in the second testing stage (C and D). Interestingly, *Cdh13* cKO mice performed better in terms of making more correct responses (Stage 1: session × genotype interaction, F (3, 54) = 5.480, p = 0.0023; Stage 2: genotype, F (1, 18) = 5.133, p = 0.0360) and fewer omissions (Stage 2: genotype, F (1, 18) = 4.745, p = 0.0429) than the controls in the testing phase. The number of total nose-pokes and the latencies to correct and incorrect responses did not differ between genotypes. Note that the number of completed trials and nose-poke at hole 6 were not included as part of the measurements because the mice were exposed to equal number of trials at each stage and were not required to initiate the trial by themselves with a nose-poke at hole 6 during all the period of the testing phase. Ctrl: n = 10; *Cdh13* cKO: n = 14. Data presented as mean ± s.e.m. #p < 0.1, *p < 0.05. Adapted from "Serotonin (5-HT) neuron-specific inactivation of Cadherin-13 impacts 5-HT system formation and cognitive function," by Forero et al., 2020. *Neuropsychopharmacology,* 168:108018.

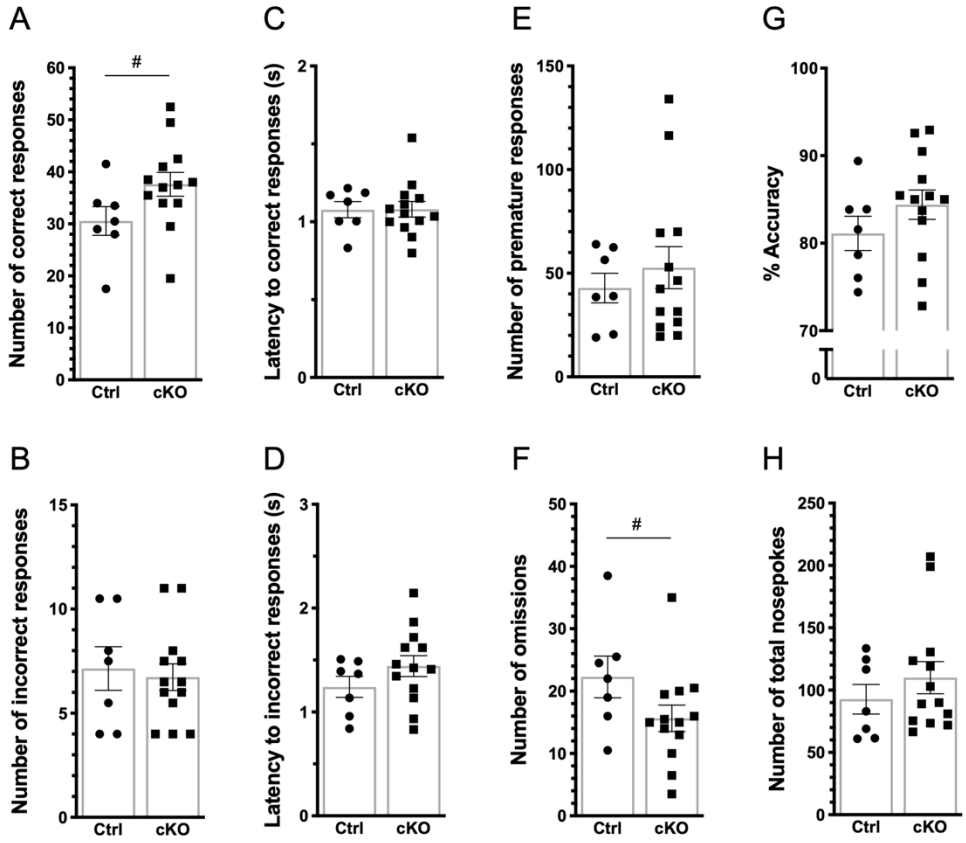

Figure 23. Performance measures of the final level of the testing phase, in which the inter-trial interval was variable and randomly presented.
After the testing phase, all mice were probed with one level of variable ITI in which the ITI occurred pseudorandomly. The number of correct and incorrect responses (A and B, respectively), latency to correct and incorrect responses (C and D, respectively), number of premature response (E), omission (F), percentage of accuracy (G), and number of total nose-pokes (H) were recorded and analyzed. While the *Cdh13* cKO mice did not exhibit any significant changes in most of the measured parameters, trends were observed toward an increased number of correct responses (p = 0.0757) and reduced number of omissions (p = 0.0967). Ctrl: n = 10; *Cdh13* cKO: n = 14. Data presented as mean ± s.e.m. #p < 0.1. Adapted from "Serotonin (5-HT) neuron-specific inactivation of Cadherin-13 impacts 5-HT system formation and cognitive function," by Forero et al., 2020. *Neuropsychopharmacology,* 168:108018.

3.3 Insights into the role of CDH13 during postnatal development

3.3.1 No differences in the innervation of serotonergic neurite at P14

After reaching their target regions at birth, the maturation of serotonergic neurons takes another three to four weeks. Depending on the target region, serotonergic fibers either transiently or progressively increase their density before it stabilizes to the adult level. In the prefrontal cortices, serotonergic innervation peaks at P7 and gradually decreases up to P28, possibly resulting from changes in the length, but not the diameter, of the fibers (Maddaloni et al., 2017). Given that the alterations in the density of serotonergic fibers were observed only in embryonic brains, the analysis was therefore extended to the postnatal stages when the remodeling and maturation of the serotonergic innervation take place. To identify the timing of the disappearance of the observed abnormalities, P14 brains were first investigated for the following reasons: as mentioned above, the remodeling or terminal maturation of serotonergic neurons takes place during the first three weeks of life; the temporal expression of CDH13 in the whole brain peaks at P7, therefore making P14 the first timepoint at which the expression levels reduce and remodeling begins to take place (Deneris and Gaspar, 2018; Lidov and Molliver, 1982; Rivero et al., 2015). To this end, the density of serotonergic neurons in the DR as well as the density of serotonergic innervation in the infralimbic (IL) and cingulate (CG) cortices were examined using P14 conditional mice and their control littermates.

As revealed by the two-tailed unpaired student's t test, the serotonergic innervation in terms of the density of the 5-HTT-ir fibers (IL: $p = 0.1821$; CG: $p = 0.4881$; n = 6 per genotype) and the number of the 5-HTT-ir fibers (IL: $p = 0.3102$; CG: $p = 0.6155$; n = 6 per genotype) did not differ between *Cdh13* cKO mice and their control littermates at P14 (Fig. 24B and C), indicating that the compensation of excess serotonergic innervation in the prefrontal cortex might take place before P14 and that the differences in the innervation become indistinguishable by P14. This is consistent with the observation by Maddaloni et al. (2017), which showed that the innervation index (i.e. the length of fibers) of medial PFC decreased between P7 and P14. On the other hand, no differences in the number of TPH2-ir neurons in individual subareas of DR (B7l: $p = 0.4719$; B7d: $p = 0.9904$; B7v: $p = 0.9993$; n = 6 per genotype) and in whole DR ($p = 0.5208$; n = 6 per genotype) were found, unexpectedly (Fig. 24A).

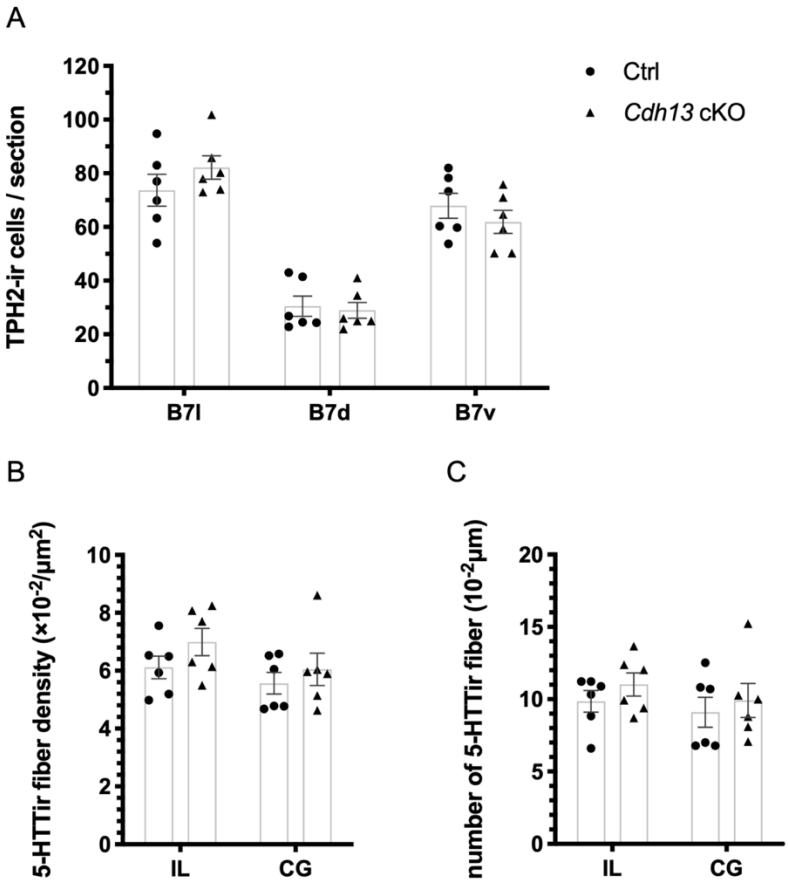

Figure 24. No alteration was found in the numbers of serotonergic neurons and their innervation to prefrontal cortices in P14 brains of *Cdh13* cKO mice.
(A) The number of TPH2-ir neurons in B7l, B7d and B7v of *Cdh13* cKO mice did not differ from that of the controls (p = 0.1270, 0.3013 and 0.8734, respectively). (B and C) Neither the density nor the number of 5-HTT-ir fiber in IL and CG was changed in the *Cdh13* cKO mice (IL: p = 0.2762 for the density and p = 0.4370 for the number of 5-HTT-ir fibers; CG: p = 0.5864 for the density and p = 0.6816 for the number of 5-HTT-ir fibers). n = 6 per genotype. Data presented as mean ± s.e.m.

3.3.2 CDH13 has no effect on the dopaminergic cell density in the ventral tegmental area

Interaction among monoaminergic neuronal systems, both during development as well as in the adult CNS, produces a wide variety of behavioral phenotypes, of which alteration may lead to neuropsychiatric disorders (Gantz et al., 2015). Dopaminergic and serotonergic neurons are anatomically proximal; they have shared afferent inputs originating from the same regions as well as common efferent target regions in the forebrain that are implicated in the pathophysiology of neurodevelopmental disorders; they develop in parallel and in close apposition (Di Giovanni, 2010; Niederkofler et al., 2015). Electrophysiological and neurochemical data have demonstrated that, via its various receptor subtypes, 5-HT can exert complex effects on the activity of midbrain dopaminergic neurons (Di Giovanni, 2010). In particular, the serotonergic input from the DR to the ventral tegmental area (VTA) synapses predominantly onto dopaminergic neurons lying in the medial part of the VTA, which, in turn, send projections to the mPFC, nucleus accumbens and amygdala, which are important players in the pathophysiology of ADHD (Beier, 2015). To find out whether alterations of the serotonergic system early in the development impact its neighboring dopaminergic neural

population, the cell density of the dopaminergic neurons of VTA was measured in the P15 wild-type mice and their *Cdh13*$^{-/-}$ littermates.

The expression pattern of CDH13 at P15 was similar to that of an adult brain. That is, CDH13-ir signal was observed in all cortical layers, except for layer IV, with the strongest in the superficial layer I. While the immunolabelling was found across all layers in the dorsal and lateral agranular parts of the retrosplenial area, it appeared to be weaker in the ventral portion. In the hippocampal formation, intense CDH13 protein expression was observed in the stratum lacunosum-moleculare as well as the molecular layer of the dentate gyrus (DG) and ventral subiculum, with weaker but moderate expression in the stratum lucidum of CA3, and the hilus of the DG (Fig. 25A). In the parahippocampal regions (i.e. the perirhinal and entorhinal cortices), CDH13-positive signal was found across all layers with the strongest being in the layer I. In the brainstem, the superior colliculi and midbrain reticular nucleus expressed higher levels of CDH13 compared with the neighboring thalamus and red nucleus. Notably, a low-to-moderate level of CDH13 expression was found in the VTA, whereas a slightly higher level was observed in the adjacent substantia nigra (Fig. 25A).

The dopaminergic neurons in the midbrain slices were visualized by immunolabelling with the catecholamine-specific enzyme tyrosine hydroxylase (TH). The dopaminergic neurons of the VTA in this study referred to the TH-ir neurons that were localized medial to the medial lemniscus and were therefore captured by confocal microscopy (Fig. 25C). The acquisition of the images, the counting of the positive cells, and the analyses were carried out as described above with minor modifications. No difference in the density of TH-ir neurons in the VTA between genotypes was found (p = 0.5676; n = 4 per genotype) (Fig. 25B and D).

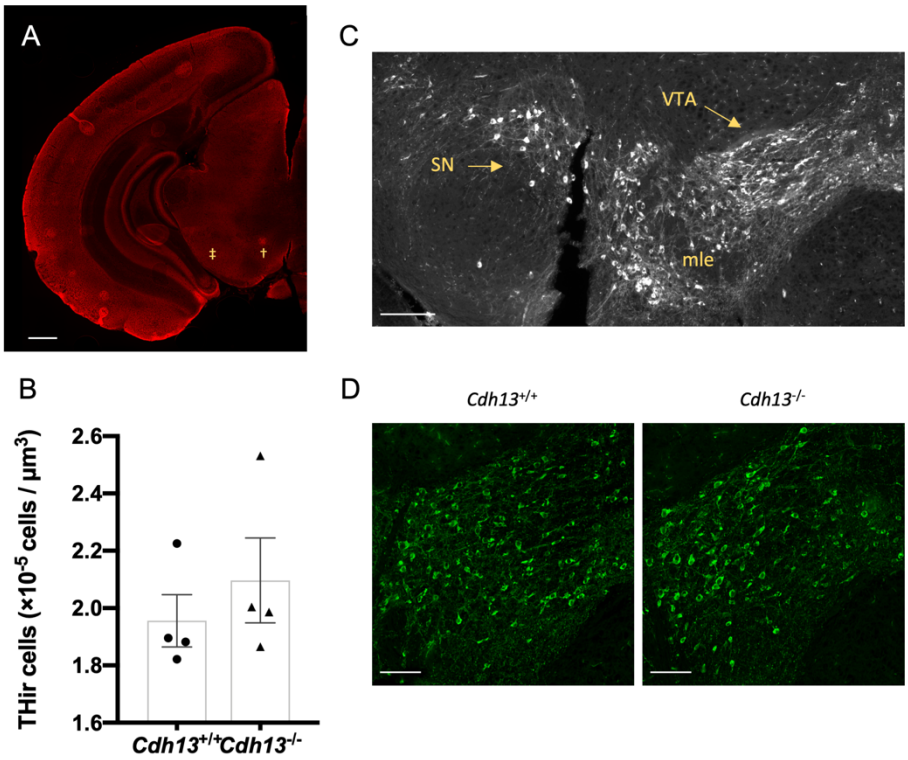

Figure 25. At P15, no dopaminergic alteration in terms of cell density in VTA was detected in *Cdh13*-null mice.
(A) Coronal midbrain section stained for CDH13 protein showing that the distribution of CDH13 in P15 wild-type brains was similar to that in adults. Compared with the adjacent substantia nigra (‡), CDH13 expression at the VTA (†) was faint but visible. (B) At P15, no difference was observed in the density of TH-ir cells in the VTA between genotypes. (C) TH-ir cells in the VTA and adjacent SN in coronal midbrain section. (D) Representative images of TH-stained VTA of both genotypes. VTA, ventral tegmental area; SN, substantia nigra; mle, medial lemniscus. n = 4 per genotype. Scale bars = 500 µm in A; 200 µm in C; 100 µm in D. Data presented as mean ± s.e.m.

CHAPTER 4 DISCUSSION AND OUTLOOK

Taken together, the results demonstrated: (1) Compared to embryonic developmental stages, CDH13 is widely distributed in the mature murine brain. Visualized by immunohistochemistry, CDH13 is detected in distinct brain structures with variable expression levels, both among and within regions. It is also expressed by neurons using neurotransmitters other than 5-HT, such as GABA, dopamine, norepinephrine. (2) The loss of CDH13 impacts serotonergic circuitries and this imapct persists into adulthood. Specifically, within the DR, a differential effect on subgroups of serotonergic neurons in the absence of CDH13 was observed, which may be explained by differential expression of Cdh13 among subgroups of the DR. (3) Hyperinnervation in the dorsal lateral nucleus of the thalamus, but not the prefrontal cortices, in adult mice deficient for CDH13. These findings indicate the relevance of CDH13 in the accurate formation and refinement of serotonergic circuitries in the brain. Furthermore, similar observations were found in the serotonergic-specific knockout model, indicating that those effects are exclusive to the serotonergic system. Probed by multiple behavioral assessments, these mice also showed altered cognitive functions, such as deficits in learning and memory as well as impulsive-like behavior that are closely related to clinical phenotypes of ADHD. Lastly, a closer look at postnatal serotonergic development has narrowed the compensation window to the first two weeks of life, which is a critical period for circuit refinement and terminal field maturation of serotonergic neurons. CDH13 may play a more subtle role in dopaminergic neurons of the VTA, as observed at P15.

Recent single cell transcriptomics studies have reported expression levels of *Cdh13* mRNA in the DR, with variation among its anatomically defined subareas of DR (Huang et al., 2019; Okaty et al., 2020; Ren et al., 2019). Okaty et al. (2020) demonstrated that all Pet1-lineage neurons, which are predominantly serotonergic, express *Cdh13* with various expression levels. Further studies by Ren et al. (2019) and Huang et al. (2019) confirmed that *Cdh13* is expressed by all TPH2-expressing neurons in the DR, which are believed to represent most, if not all, serotonergic neurons in the brain, and by GABAergic and dopaminergic neurons to a lesser extent. Within serotonergic populations in the DR, *Cdh13*-expressing cells are not distributed uniformly throughout the DR. Instead, they are spatially heterogenous along the medial-lateral axis, with the lateral cluster containing more *Cdh13*-expressing cells than the medial ones (Huang et al., 2019). Conversely, in this study, a higher level of *Cdh13* was observed in the B7d rather than the B7l and B7v in the *Cdh13* cKO mice, which may be explained by the different methodologies used. The studies mentioned above focused only on Cdh13 expression in serotonergic neurons, while by cutting out slices of the DR, samples included in this study contained mixed population of cell types. Neuronal cells represent only a minority of cells in the DR, which, in fact, contains mostly non-neuronal cells including astrocytes, oligodendrocyte precursor cells (or polydendrocytes), and differentiating and mature oligodendrocytes, among others (Huang et al., 2019). Evidence suggests that many types of non-neuronal cells, such as astrocytes, also express CDH13 (Campagnoni et al., 2001; Huang et al., 2003; Takeuchi et al., 2000). Additionally, among all neurons in the DR, serotonergic neurons comprise only 30% to 50% of the neuronal population, and many release other neurotransmitters including GABA, glutamate and dopamine, the gaseous signaling molecule nitric oxide, and a variety of peptides (Fu et al., 2010; Huang et al., 2019). Therefore, expression

levels of control mice represent the overall Cdh13 expression in the surrounding cells, whereas the levels of *Cdh13* cKO mice represent *Cdh13* expression by non-serotonergic neurons in the DR (Fig. 13). One would expect that the knockout efficiency of a serotonergic-specific mouse model could reflect the levels of *Cdh13* expressed by DR serotonergic neurons in those three subgroups. However, the data presented in this study may not be seen as the total level of *Cdh13* expressed by all serotonergic neurons of each anatomically defined subregion. This is because the B7l, B7d, and B7v contain different total numbers of serotonergic neurons and in order to control the final yield of total mRNA, the size of microdissected areas of each subregion had to be constant. In other words, these calculated deficiencies represent the averaged expression levels of a certain and identical number of serotonergic neurons in the region rather than the overall expression levels by all serotonergic neurons in the region. This means that *Cdh13* is expressed more highly in the surrounding cells, which in turn inversely controls the density of serotonergic neurons in the DR, whereas the serotonergic neurons in the B7l presumably express higher levels of *Cdh13*, indicating the prominence of CDH13 function in this area. Thus, loss of CDH13 may have a considerably greater effect on the serotonergic neurons in the B7l, but not those in the B7d.

The developmental patterns of serotonergic fiber density are region-specific and occur with interrelated timing, with some areas (e.g. caudate putamen, basolateral amygdala, geniculate nucleus and substantia nigra) presenting a linear and progressive colonization, while other areas (e.g. medial prefrontal cortex, globus pallidus, somatosensory cortex and hippocampus) displaying a transient increase in fiber density (Maddaloni et al., 2017). While the differences in timing of serotonergic innervation are correlated with the maturation of targets, the processes that lead to the formation of regional fiber densities or patterns remain poorly understood (Deneris and Gaspar, 2018). Bian et al. (2015) reported that the pruning of existing connections between neurons, an important process in the refinement of neural circuits, may be coordinated by cadherin/catenin cell adhesion complex in somatosensory circuitries of the murine brain. Although the mechanism for how CDH13 is involved in proper serotonergic innervation patterns remains unknown, it is likely that CDH13-deficient serotonergic neurons are not able to properly sense attractive or repulsive signals that could guide 5-HT axons. This could explain the alteration observed in *Cdh13* cKO mice, as several molecules have been implicated in regulating serotonergic axon outgrowth and terminal arborization, including members of the cadherin superfamily. For example, loss of function studies pointed out that the protocadherin alpha (Pcdhα) c2, the only Pcdhα isoform expressed in serotonergic neurons, was required for serotonergic axon diffusion, axonal tiling, and the assembly of serotonergic circuitries (Chen et al., 2017; Katori et al., 2017). The growth-associated protein-43 (GAP-43) that is expressed on growing serotonergic axons may be a key regulator in normal pathfinding and arborization of serotonergic axons during early brain development, as the absence of GAP-43 resulted in aberrant serotonergic innervation pattern in the forebrain (Donovan et al., 2002). Further axon guidance molecules, such as the erythropoietin-producing hepatocellular carcinoma receptor A5 (EphA5) and its corresponding ephrin ligand, have been shown to repel axon ingrowth of a subset of DR serotonergic neurons, suggesting their roles in region-specific targeting of raphe neurons (Teng et al., 2017). However, in the case of *Cdh13*$^{-/-}$ mice that did not express CDH13 in the whole system, other influences might come into play, as the formation of the

serotoninergic axon terminals is likely dependent on the maturation of other elements in the local neuronal circuitry (Lidov and Molliver, 1982).

Furthermore, the positive outgrowth of serotoninergic terminals is linked to the presence of a number of neurotrophic factors in target tissues, including brain-derived neurotrophic factor (BDNF) and S100 calcium binding protein B (S100B), which have reciprocal interactions with 5-HT. Being the most prevalent neurotrophic factor in the brain, BDNF has been shown to play a role in neurogenesis, differentiation, and synaptic plasticity (Autry and Monteggia, 2012). Research has shown that BDNF promotes development and establishment of serotonergic neural circuitry, and that serotonergic transmission, on the other hand, regulates BDNF expression (Mamounas et al., 1995; Martinowich and Lu, 2008; Migliarini et al., 2013). S100B is known to play a role in tissue development and synaptic plasticity, among others (Nishiyama et al., 2002; Sorci et al., 2013). Early pharmacological studies and experimental evidence indicate the interconnection between the S100B and serotonergic system (Azmitia et al., 1990). It is believed that S100B release from astroglial cells is stimulated by 5-HT binding to the 5-HT1A receptor and that S100B may promote growth and development of serotoninergic neurons, although the underlying molecular mechanism remains to be elucidated (Donato et al., 2009; Whitaker-Azmitia et al., 1990). In addition, 5-HT autoregulates neurite formation and branch morphology of its own axons (Daubert and Condron, 2010; Whitaker-Azmitia and Azmitia, 1986). 5-HT is stored not only in the axon collaterals and terminals, but also in the non-synaptic vesicles of the somata, dendrites, and axonal varicosities (De-Miguel and Trueta, 2005). Although the exact mechanism of the release of 5-HT into the extracellular space of the DR is unclear, evidence suggests that there may be different pathways, including (1) action potential-dependent release from storage vesicles by exocytosis and (2) nonexocytotic 5-HT release occurring without neuronal activity, Ca^{2+} influx, or vesicular monoamine transporter 2–mediated vesicular accumulation of 5-HT (Colgan et al., 2009; Matos et al., 1996; Mlinar et al., 2015). Nonetheless, serotonergic neurons are self-inhibitory, via the activation of 5-HT_{1A} autoreceptors situated on their cell soma and dendrites (Adell et al., 2002). Thus, activation of excessive afferent excitatory fibers or increased number of serotonergic neurons in the DR may result in an increased level of 5-HT in the extracellular space of the DR, which, in turn, can act upon 5-HT_{1A} autoreceptors on the same or other serotonergic neurons to maintain the homeostasis of the system (Adell et al., 2002). Given that the preliminary data suggested elevated 5-HT levels in the developing DR and PFC of the *Cdh13* cKO embryos (data not shown), it will therefore be interesting to examine the levels of 5-HT and various growth factors in the DR as well as target brain areas, such as the prefrontal cortices and thalamic nuclei in CDH13-deficient mouse models.

Alterations in the densities or patterns of serotonergic innervation have been implicated in neuropsychiatric disorders including depression, anxiety, and autism spectrum disorder (Lew et al., 2020; Mann, 1999). For example, the density of serotonergic fibers was unusually higher in the cerebral cortex of individuals diagnosed with autism spectrum disorders compared with age-paired healthy subjects (Azmitia et al., 2011). Similarly, alteration in the density of serotonergic fibers in the ThaLD was observed in the *Cdh13*$^{-/-}$ mice in this study. The thalamus is an important interface between the cortex and its numerous input regions, providing sensory and subcortical information to almost every part of the cortex (Sherman, 2017). Although the

function of the ThaLD remains largely unexplored, studies in rats pointed out its involvement in spatial learning and memory, especially related to somatosensory cues (Bezdudnaya and Keller, 2008; Perry and Mitchell, 2019). Specifically, lesion or inactivation of the ThaLD impaired the performance of spatial memory and learning tasks (i.e. water maze in both publications) in terms of choice accuracy or escape latency in rats (Mizumori et al., 1994; van Groen et al., 2002). In this study, the *Cdh13*$^{-/-}$ mice that displayed hyperinnervation of serotonergic fibers in the ThaLD, made significantly more primary errors than their wild-type littermates in Barnes maze spatial memory task, though only during the reversal phase (Rivero et al., 2015). These suggest the importance of CDH13 in the circuit formation and refinement, and, ultimately, in appropriate cognitive function. However, the effect of the altered serotonergic innervation on ThaLD function remains to be investigated.

There are a few limitations in this study that are worth addressing. Conventional immunofluorescence labelling techniques provide realistic visualizations of the cellular and organizational morphology when an optimal signal-to-noise ratio is achieved, which is unfortunately not always possible. For instance, due to the low abundance of CDH13 in the mature brain, an additional amplification step on top of the usual immunofluorescence staining was required to boost the visualization of CDH13-positive signal. Despite the robust and clear results, Horling et al. (2012) has pointed out pitfalls of the signal amplification technique, such as it being error-prone and leading to loss of localization precision. This may result from displacing the fluorophore from the target and/or the existence of endogenous streptavidin and biotin that serve as targets for antibodies used in the signal amplification machinery. Taking this into consideration, this study performed unamplified and amplified negative controls as well as streptavidin-biotin endogenous activity-blocked amplified controls to affirm the acquired CDH13 protein expression data. As a further example, analysis involving fine structures, such as the density measurement of fluorescently labeled neuronal fibers (in this study 5-HTT-ir fibers), relies largely on the quality of the acquired images due to the low labelling densities on thin fibers. It is challenging to technically and digitally eradicate the background (or autofluorescence) of the tissue, which then contributes to additional noise in the images and may also sometimes significantly influence the estimated outcome, though the period of incubation, the acquiring time of the images (within 48 hours of the immunofluorescence staining procedure), and overall condition of the experiments were tightly controlled and consistent over time. In both of the cases, the application of classical histological approaches together with more recently established tissue clearing approaches will serve as an ideal alternative by maximizing the signal-to-noise ratio. Furthermore, employing a direct method, such as viral tracing and/or tissue clearing techniques, will refine our understanding of the topographic organization of serotonergic axonal projections and further support the notion that the hyperinnervation of serotonergic fibers of the ThaLD arise from neurons lying in the B7l of the DR.

This study has broadened the understanding of the role of CDH13 in the developing and mature murine serotonergic system through the continuing application of classical histological approaches, combined with more recently developed laser microdissection techniques. The behavioral assessments used have also uncovered alterations in the cognitive functions of CDH13-deficient mice, suggesting that CDH13 is important for normal brain function. Two

remaining and relevant questions are what role CDH13 plays in patterning and terminal maturation of serotonergic neurons at postnatal stages as well as in the regulation of neurotransmission at mature synapses. In recent years, focus is beginning to shift to the study of how experience shapes the brain and eventually affects behaviors. An essential characteristic of the development of the human brain is that sensory, cognitive, and emotional experiences influence the development of synapses and neural circuits. In response to sensory and motor experience during postnatal life, neural activity triggers local changes in the number, strength, or connectivity of synapses, which are crucial pathways for learning and memory, as well as for adaptive behavioral responses (Benson et al., 2001; Ebert and Greenberg, 2013). In the adult brain, neuronal gene expression is dynamically changed in response to neuronal activity, which affects adult behavior (McClung and Nestler, 2008; Turrigiano, 2008). Given that CDH13 is also involved in synaptic transmission and the E/I balance (Mossink et al., 2021; Rivero et al., 2015), understanding how the altered serotonergic circuitries adapt during activity-dependent plasticity in the CDH13-inactivated mouse models will provide important insights into the genesis of aberrant states and potential therapeutic targets for neurodevelopmental disorders.

CHAPTER 5 REFERENCES

Abdulamir, H. A., Abdul-Rasheed, O. F., & Abdulghani, E. A. (2018). Serotonin and serotonin transporter levels in autistic children. *Saudi Med J, 39*(5), 487-494. doi:10.15537/smj.2018.5.21751

Adell, A., Celada, P., Abellan, M. T., & Artigas, F. (2002). Origin and functional role of the extracellular serotonin in the midbrain raphe nuclei. *Brain Res Brain Res Rev, 39*(2-3), 154-180. doi:10.1016/s0165-0173(02)00182-0

Akum, B. F., Chen, M., Gunderson, S. I., Riefler, G. M., Scerri-Hansen, M. M., & Firestein, B. L. (2004). Cypin regulates dendrite patterning in hippocampal neurons by promoting microtubule assembly. *Nat Neurosci, 7*(2), 145-152. doi:10.1038/nn1179

Amich, J., Mokhtari, Z., Strobel, M., Vialetto, E., Sheta, D., Yu, Y., . . . Beilhack, A. (2020). Three-dimensional light sheet fluorescence microscopy of lungs to dissect local host immune-aspergillus fumigatus interactions. *mBio, 11*(1). doi:10.1128/mBio.02752-19

Amitai, N., & Markou, A. (2011). Comparative effects of different test day challenges on performance in the 5-choice serial reaction time task. *Behav Neurosci, 125*(5), 764-774. doi:10.1037/a0024722

Arias-Vasquez, A., Altink, M. E., Rommelse, N. N., Slaats-Willemse, D. I., Buschgens, C. J., Fliers, E. A., . . . Buitelaar, J. K. (2011). Cdh13 is associated with working memory performance in attention deficit/hyperactivity disorder. *Genes Brain Behav, 10*(8), 844-851. doi:10.1111/j.1601-183X.2011.00724.x

Arnemann, J., Sultani, O., Hasgun, D., & Coerdt, W. (2006). T-/h-cadherin (cdh13): A new marker for differentiating podocytes. *Virchows Arch, 448*(2), 160-164. doi:10.1007/s00428-005-0055-7

Attar, A., Liu, T., Chan, W. T., Hayes, J., Nejad, M., Lei, K., & Bitan, G. (2013). A shortened barnes maze protocol reveals memory deficits at 4-months of age in the triple-transgenic mouse model of alzheimer's disease. *PLoS One, 8*(11), e80355. doi:10.1371/journal.pone.0080355

Autry, A. E., & Monteggia, L. M. (2012). Brain-derived neurotrophic factor and neuropsychiatric disorders. *Pharmacol Rev, 64*(2), 238-258. doi:10.1124/pr.111.005108

Awasthi, J. R., Tamada, K., Overton, E. T. N., & Takumi, T. (2020). Comprehensive topographical map of the serotonergic fibers in the male mouse brain. *J Comp Neurol*. doi:10.1002/cne.25027

Azmitia, E. C. (2007). Serotonin and brain: Evolution, neuroplasticity, and homeostasis. *Int Rev Neurobiol, 77*, 31-56. doi:10.1016/S0074-7742(06)77002-7

Azmitia, E. C., Dolan, K., & Whitaker-Azmitia, P. M. (1990). S-100b but not ngf, egf, insulin or calmodulin is a cns serotonergic growth factor. *Brain Res, 516*(2), 354-356. doi:10.1016/0006-8993(90)90942-5

Azmitia, E. C., Singh, J. S., & Whitaker-Azmitia, P. M. (2011). Increased serotonin axons (immunoreactive to 5-ht transporter) in postmortem brains from young autism donors. *Neuropharmacology, 60*(7-8), 1347-1354. doi:10.1016/j.neuropharm.2011.02.002

Banerjee, E., & Nandagopal, K. (2015). Does serotonin deficit mediate susceptibility to adhd? *Neurochem Int, 82*, 52-68. doi:10.1016/j.neuint.2015.02.001

Bari, A., Dalley, J. W., & Robbins, T. W. (2008). The application of the 5-choice serial reaction time task for the assessment of visual attentional processes and impulse control in rats. *Nat Protoc, 3*(5), 759-767. doi:10.1038/nprot.2008.41

Benes, F. M., Taylor, J. B., & Cunningham, M. C. (2000). Convergence and plasticity of monoaminergic systems in the medial prefrontal cortex during the postnatal period: Implications for the development of psychopathology. *Cereb Cortex, 10*(10), 1014-1027. doi:10.1093/cercor/10.10.1014

Benson, D. L., Colman, D. R., & Huntley, G. W. (2001). Molecules, maps and synapse specificity. *Nat Rev Neurosci, 2*(12), 899-909. doi:10.1038/35104078

Berger, I., Slobodin, O., Aboud, M., Melamed, J., & Cassuto, H. (2013). Maturational delay in adhd: Evidence from cpt. *Front Hum Neurosci, 7*, 691. doi:10.3389/fnhum.2013.00691

Berger, M., Gray, J. A., & Roth, B. L. (2009). The expanded biology of serotonin. *Annu Rev Med, 60*, 355-366. doi:10.1146/annurev.med.60.042307.110802

Beul, S. F., & Hilgetag, C. C. (2019). Neuron density fundamentally relates to architecture and connectivity of the primate cerebral cortex. *Neuroimage, 189*, 777-792. doi:10.1016/j.neuroimage.2019.01.010

Bezdudnaya, T., & Keller, A. (2008). Laterodorsal nucleus of the thalamus: A processor of somatosensory inputs. *J Comp Neurol, 507*(6), 1979-1989. doi:10.1002/cne.21664

Bian, W. J., Miao, W. Y., He, S. J., Qiu, Z., & Yu, X. (2015). Coordinated spine pruning and maturation mediated by inter-spine competition for cadherin/catenin complexes. *Cell, 162*(4), 808-822. doi:10.1016/j.cell.2015.07.018

Biffi, E., Regalia, G., Menegon, A., Ferrigno, G., & Pedrocchi, A. (2013). The influence of neuronal density and maturation on network activity of hippocampal cell cultures: A methodological study. *PLoS One, 8*(12), e83899. doi:10.1371/journal.pone.0083899

Bourin, M., & Hascoet, M. (2003). The mouse light/dark box test. *Eur J Pharmacol, 463*(1-3), 55-65. doi:10.1016/s0014-2999(03)01274-3

Campagnoni, C. W., Landry, C. F., Pribyl, T. M., Schonmann, V., Kampf, K., Handley, V. W., . . . Campagnoni, A. T. (2001). Identification of genes in the oligodendrocyte lineage through the analysis of conditionally immortalized cell lines. *Dev Neurosci, 23*(6), 452-463. doi:10.1159/000048732

Carhart-Harris, R. L., & Nutt, D. J. (2017). Serotonin and brain function: A tale of two receptors. *J Psychopharmacol, 31*(9), 1091-1120. doi:10.1177/0269881117725915

Cases, O., Seif, I., Grimsby, J., Gaspar, P., Chen, K., Pournin, S., . . . et al. (1995). Aggressive behavior and altered amounts of brain serotonin and norepinephrine in mice lacking maoa. *Science, 268*(5218), 1763-1766. doi:10.1126/science.7792602

Chen, W. V., Nwakeze, C. L., Denny, C. A., O'Keeffe, S., Rieger, M. A., Mountoufaris, G., . . . Maniatis, T. (2017). Pcdhalphac2 is required for axonal tiling and assembly of serotonergic circuitries in mice. *Science, 356*(6336), 406-411. doi:10.1126/science.aal3231

Childress, A. C., & Berry, S. A. (2012). Pharmacotherapy of attention-deficit hyperactivity disorder in adolescents. *Drugs, 72*(3), 309-325. doi:10.2165/11599580-000000000-00000

Chung, K., & Deisseroth, K. (2013). Clarity for mapping the nervous system. *Nat Methods, 10*(6), 508-513. doi:10.1038/nmeth.2481

Chung, K., Wallace, J., Kim, S. Y., Kalyanasundaram, S., Andalman, A. S., Davidson, T. J., . . . Deisseroth, K. (2013). Structural and molecular interrogation of intact biological systems. *Nature, 497*(7449), 332-337. doi:10.1038/nature12107

Ciatto, C., Bahna, F., Zampieri, N., VanSteenhouse, H. C., Katsamba, P. S., Ahlsen, G., . . . Shapiro, L. (2010). T-cadherin structures reveal a novel adhesive binding mechanism. *Nat Struct Mol Biol, 17*(3), 339-347. doi:10.1038/nsmb.1781

Coleman, M. (1971). Serotonin concentrations in whole blood of hyperactive children. *J Pediatr, 78*(6), 985-990. doi:10.1016/s0022-3476(71)80428-6

Colgan, L. A., Putzier, I., & Levitan, E. S. (2009). Activity-dependent vesicular monoamine transporter-mediated depletion of the nucleus supports somatic release by serotonin neurons. *J Neurosci, 29*(50), 15878-15887. doi:10.1523/JNEUROSCI.4210-09.2009

Conacci-Sorrell, M., Zhurinsky, J., & Ben-Ze'ev, A. (2002). The cadherin-catenin adhesion system in signaling and cancer. *J Clin Invest, 109*(8), 987-991. doi:10.1172/JCI15429

Corominas, J., Klein, M., Zayats, T., Rivero, O., Ziegler, G. C., Pauper, M., . . . Lesch, K. P. (2020). Identification of adhd risk genes in extended pedigrees by combining linkage analysis and whole-exome sequencing. *Mol Psychiatry, 25*(9), 2047-2057. doi:10.1038/s41380-018-0210-6

Cullen, D. K., Gilroy, M. E., Irons, H. R., & Laplaca, M. C. (2010). Synapse-to-neuron ratio is inversely related to neuronal density in mature neuronal cultures. *Brain Res, 1359*, 44-55. doi:10.1016/j.brainres.2010.08.058

Daubert, E. A., & Condron, B. G. (2010). Serotonin: A regulator of neuronal morphology and circuitry. *Trends Neurosci, 33*(9), 424-434. doi:10.1016/j.tins.2010.05.005

De-Miguel, F. F., & Trueta, C. (2005). Synaptic and extrasynaptic secretion of serotonin. *Cell Mol Neurobiol, 25*(2), 297-312. doi:10.1007/s10571-005-3061-z

Demontis, D., Lescai, F., Borglum, A., Glerup, S., Ostergaard, S. D., Mors, O., . . . Franke, B. (2016). Whole-exome sequencing reveals increased burden of rare functional and disruptive variants in candidate risk genes in individuals with persistent attention-deficit/hyperactivity disorder. *J Am Acad Child Adolesc Psychiatry, 55*(6), 521-523. doi:10.1016/j.jaac.2016.03.009

Deneris, E., & Gaspar, P. (2018). Serotonin neuron development: Shaping molecular and structural identities. *Wiley Interdisciplinary Reviews-Developmental Biology, 7*(1). doi:ARTN e301
10.1002/wdev.301

Di Giovanni, G. (2010). Dopamine interaction with other neurotransmitter systems: Relevance in the pathophysiology and treatment of cns disorders. *CNS Neurosci Ther, 16*(3), 125-126. doi:10.1111/j.1755-5949.2010.00143.x

Donato, R., Sorci, G., Riuzzi, F., Arcuri, C., Bianchi, R., Brozzi, F., . . . Giambanco, I. (2009). S100b's double life: Intracellular regulator and extracellular signal. *Biochim Biophys Acta, 1793*(6), 1008-1022. doi:10.1016/j.bbamcr.2008.11.009

Donovan, S. L., Mamounas, L. A., Andrews, A. M., Blue, M. E., & McCasland, J. S. (2002). Gap-43 is critical for normal development of the serotonergic innervation in forebrain. *J Neurosci, 22*(9), 3543-3552. doi:20026295

Doyle, D. D., Goings, G. E., Upshaw-Earley, J., Page, E., Ranscht, B., & Palfrey, H. C. (1998). T-cadherin is a major glycophosphoinositol-anchored protein associated with noncaveolar detergent-insoluble domains of the cardiac sarcolemma. *J Biol Chem, 273*(12), 6937-6943. doi:10.1074/jbc.273.12.6937

Dyck, M. J., & Piek, J. P. (2014). Developmental delays in children with adhd. *J Atten Disord, 18*(5), 466-478. doi:10.1177/1087054712441832

Ebert, D. H., & Greenberg, M. E. (2013). Activity-dependent neuronal signalling and autism spectrum disorder. *Nature, 493*(7432), 327-337. doi:10.1038/nature11860

Emch, M., von Bastian, C. C., & Koch, K. (2019). Neural correlates of verbal working memory: An fmri meta-analysis. *Front Hum Neurosci, 13*, 180. doi:10.3389/fnhum.2019.00180

Eriksson, J., Vogel, E. K., Lansner, A., Bergstrom, F., & Nyberg, L. (2015). Neurocognitive architecture of working memory. *Neuron, 88*(1), 33-46. doi:10.1016/j.neuron.2015.09.020

Erturk, A., Becker, K., Jahrling, N., Mauch, C. P., Hojer, C. D., Egen, J. G., . . . Dodt, H. U. (2012). Three-dimensional imaging of solvent-cleared organs using 3disco. *Nat Protoc, 7*(11), 1983-1995. doi:10.1038/nprot.2012.119

Erturk, A., & Bradke, F. (2013). High-resolution imaging of entire organs by 3-dimensional imaging of solvent cleared organs (3disco). *Exp Neurol, 242*, 57-64. doi:10.1016/j.expneurol.2012.10.018

Faraone, S. V., & Larsson, H. (2019). Genetics of attention deficit hyperactivity disorder. *Mol Psychiatry, 24*(4), 562-575. doi:10.1038/s41380-018-0070-0

Flynn, J. M., A.; Palmer, W. (2016). 3d tissue clearing with passive clarity: A handbook for hmri/uon researchers. https://openspim.org/documents/3D_Tissue_Clearing_Handbook_3rd_Ed.pdf

Forero, A. (2020). *Impact of cadherin-13 deficiency on the brain serotonin system using mouse models and human ipsc-derived neurons.* (Doctoral degree), Julius-Maximilians-Universität Würzburg, Würzburg, Germany.

Forero, A., Ku, H. P., Malpartida, A. B., Waldchen, S., Alhama-Riba, J., Kulka, C., . . . Lesch, K. P. (2020). Serotonin (5-ht) neuron-specific inactivation of cadherin-13 impacts 5-ht system formation and cognitive function. *Neuropharmacology, 168*, 108018. doi:10.1016/j.neuropharm.2020.108018

Forero, A., Rivero, O., Waldchen, S., Ku, H. P., Kiser, D. P., Gartner, Y., . . . Lesch, K. P. (2017). Cadherin-13 deficiency increases dorsal raphe 5-ht neuron density and prefrontal cortex innervation in the mouse brain. *Front Cell Neurosci, 11*, 307. doi:10.3389/fncel.2017.00307

Franke, B., Neale, B. M., & Faraone, S. V. (2009). Genome-wide association studies in adhd. *Hum Genet, 126*(1), 13-50. doi:10.1007/s00439-009-0663-4

Fredette, B. J., Miller, J., & Ranscht, B. (1996). Inhibition of motor axon growth by t-cadherin substrata. *Development, 122*(10), 3163-3171.

Fredette, B. J., & Ranscht, B. (1994). T-cadherin expression delineates specific regions of the developing motor axon-hindlimb projection pathway. *J Neurosci, 14*(12), 7331-7346.

Freeman, W. M., & Hemby, S. E. (2004). Proteomics for protein expression profiling in neuroscience. *Neurochem Res, 29*(6), 1065-1081. doi:10.1023/b:nere.0000023594.21352.17

Fu, W., Le Maitre, E., Fabre, V., Bernard, J. F., David Xu, Z. Q., & Hokfelt, T. (2010). Chemical neuroanatomy of the dorsal raphe nucleus and adjacent structures of the mouse brain. *J Comp Neurol, 518*(17), 3464-3494. doi:10.1002/cne.22407

Gantz, S. C., Levitt, E. S., Llamosas, N., Neve, K. A., & Williams, J. T. (2015). Depression of serotonin synaptic transmission by the dopamine precursor l-dopa. *Cell Rep, 12*(6), 944-954. doi:10.1016/j.celrep.2015.07.005

Gradinaru, V., Treweek, J., Overton, K., & Deisseroth, K. (2018). Hydrogel-tissue chemistry: Principles and applications. *Annu Rev Biophys, 47*, 355-376. doi:10.1146/annurev-biophys-070317-032905

Greven, C. U., Bralten, J., Mennes, M., O'Dwyer, L., van Hulzen, K. J., Rommelse, N., . . . Buitelaar, J. K. (2015). Developmentally stable whole-brain volume reductions and developmentally sensitive caudate and putamen volume alterations in those with attention-deficit/hyperactivity disorder and their unaffected siblings. *JAMA Psychiatry, 72*(5), 490-499. doi:10.1001/jamapsychiatry.2014.3162

Gygi, S. P., Rochon, Y., Franza, B. R., & Aebersold, R. (1999). Correlation between protein and mrna abundance in yeast. *Mol Cell Biol, 19*(3), 1720-1730. doi:10.1128/mcb.19.3.1720

Hawi, Z., Tong, J., Dark, C., Yates, H., Johnson, B., & Bellgrove, M. A. (2018). The role of cadherin genes in five major psychiatric disorders: A literature update. *Am J Med Genet B Neuropsychiatr Genet, 177*(2), 168-180. doi:10.1002/ajmg.b.32592

Hawthorne, A. L., Wylie, C. J., Landmesser, L. T., Deneris, E. S., & Silver, J. (2010). Serotonergic neurons migrate radially through the neuroepithelium by dynamin-mediated somal translocation. *J Neurosci, 30*(2), 420-430. doi:10.1523/JNEUROSCI.2333-09.2010

Hayano, Y., Zhao, H., Kobayashi, H., Takeuchi, K., Norioka, S., & Yamamoto, N. (2014). The role of t-cadherin in axonal pathway formation in neocortical circuits. *Development, 141*(24), 4784-4793. doi:10.1242/dev.108290

Hirano, S., & Takeichi, M. (2012). Cadherins in brain morphogenesis and wiring. *Physiol Rev, 92*(2), 597-634. doi:10.1152/physrev.00014.2011

Hoogman, M., Bralten, J., Hibar, D. P., Mennes, M., Zwiers, M. P., Schweren, L. S. J., . . . Franke, B. (2017). Subcortical brain volume differences in participants with attention deficit hyperactivity disorder in children and adults: A cross-sectional mega-analysis. *Lancet Psychiatry, 4*(4), 310-319. doi:10.1016/S2215-0366(17)30049-4

Horling, L., Neuhuber, W. L., & Raab, M. (2012). Pitfalls using tyramide signal amplification (tsa) in the mouse gastrointestinal tract: Endogenous streptavidin-binding sites lead to false positive staining. *J Neurosci Methods, 204*(1), 124-132. doi:10.1016/j.jneumeth.2011.11.009

Hu, W., Tamadon, A., Hsueh, A. J. W., & Feng, Y. (2017). Three-dimensional reconstruction of the vascular architecture of the passive clarity-cleared mouse ovary. *J Vis Exp*(130). doi:10.3791/56141

Huang, K. W., Ochandarena, N. E., Philson, A. C., Hyun, M., Birnbaum, J. E., Cicconet, M., & Sabatini, B. L. (2019). Molecular and anatomical organization of the dorsal raphe nucleus. *Elife, 8*. doi:10.7554/eLife.46464

Huang, Z. Y., Wu, Y., Hedrick, N., & Gutmann, D. H. (2003). T-cadherin-mediated cell growth regulation involves g2 phase arrest and requires p21(cip1/waf1) expression. *Mol Cell Biol, 23*(2), 566-578. doi:10.1128/MCB.23.2.566-578.2003

Jacobs, B. L., & Azmitia, E. C. (1992). Structure and function of the brain serotonin system. *Physiol Rev, 72*(1), 165-229. doi:10.1152/physrev.1992.72.1.165

Jensen, K. H. R., & Berg, R. W. (2017). Advances and perspectives in tissue clearing using clarity. *J Chem Neuroanat, 86*, 19-34. doi:10.1016/j.jchemneu.2017.07.005

Katori, S., Hamada, S., Noguchi, Y., Fukuda, E., Yamamoto, T., Yamamoto, H., . . . Yagi, T. (2009). Protocadherin-alpha family is required for serotonergic projections to appropriately innervate target brain areas. *J Neurosci, 29*(29), 9137-9147. doi:10.1523/JNEUROSCI.5478-08.2009

Katori, S., Noguchi-Katori, Y., Okayama, A., Kawamura, Y., Luo, W., Sakimura, K., . . . Yagi, T. (2017). Protocadherin-alphac2 is required for diffuse projections of serotonergic axons. *Sci Rep, 7*(1), 15908. doi:10.1038/s41598-017-16120-y

Katzman, M. A., Bilkey, T. S., Chokka, P. R., Fallu, A., & Klassen, L. J. (2017). Adult adhd and comorbid disorders: Clinical implications of a dimensional approach. *BMC Psychiatry, 17*(1), 302. doi:10.1186/s12888-017-1463-3

Killen, A. C., Barber, M., Paulin, J. J. W., Ranscht, B., Parnavelas, J. G., & Andrews, W. D. (2017). Protective role of cadherin 13 in interneuron development. *Brain Struct Funct, 222*(8), 3567-3585. doi:10.1007/s00429-017-1418-y

Konrad, K., & Eickhoff, S. B. (2010). Is the adhd brain wired differently? A review on structural and functional connectivity in attention deficit hyperactivity disorder. *Hum Brain Mapp, 31*(6), 904-916. doi:10.1002/hbm.21058

Ku, H. P. (2017). *Effect of cadherin 13 deficiency in the development of the serotonergic system with emphasis on prefrontal cortex innervation.* (Master's degree), Julius-Maximilians-Universität Würzburg, Würzburg, Germany.

Lai, M. C., Lombardo, M. V., & Baron-Cohen, S. (2014). Autism. *Lancet, 383*(9920), 896-910. doi:10.1016/S0140-6736(13)61539-1

Lesch, K. P., & Waider, J. (2012). Serotonin in the modulation of neural plasticity and networks: Implications for neurodevelopmental disorders. *Neuron, 76*(1), 175-191. doi:10.1016/j.neuron.2012.09.013

Lew, C. H., Groeniger, K. M., Hanson, K. L., Cuevas, D., Greiner, D. M. Z., Hrvoj-Mihic, B., . . . Semendeferi, K. (2020). Serotonergic innervation of the amygdala is increased in autism spectrum disorder and decreased in williams syndrome. *Mol Autism, 11*(1), 12. doi:10.1186/s13229-019-0302-4

Lidov, H. G., & Molliver, M. E. (1982). An immunohistochemical study of serotonin neuron development in the rat: Ascending pathways and terminal fields. *Brain Res Bull, 8*(4), 389-430. doi:10.1016/0361-9230(82)90077-6

Maddaloni, G., Bertero, A., Pratelli, M., Barsotti, N., Boonstra, A., Giorgi, A., . . . Pasqualetti, M. (2017). Development of serotonergic fibers in the post-natal mouse brain. *Front Cell Neurosci, 11*, 202. doi:10.3389/fncel.2017.00202

Mamounas, L. A., Blue, M. E., Siuciak, J. A., & Altar, C. A. (1995). Brain-derived neurotrophic factor promotes the survival and sprouting of serotonergic axons in rat brain. *J Neurosci, 15*(12), 7929-7939.

Mann, J. J. (1999). Role of the serotonergic system in the pathogenesis of major depression and suicidal behavior. *Neuropsychopharmacology, 21*(2 Suppl), 99S-105S. doi:10.1016/S0893-133X(99)00040-8

Martinowich, K., & Lu, B. (2008). Interaction between bdnf and serotonin: Role in mood disorders. *Neuropsychopharmacology, 33*(1), 73-83. doi:10.1038/sj.npp.1301571

Matos, F. F., Urban, C., & Yocca, F. D. (1996). Serotonin (5-ht) release in the dorsal raphe and ventral hippocampus: Raphe control of somatodendritic and terminal 5-ht release. *J Neural Transm (Vienna), 103*(1-2), 173-190. doi:10.1007/BF01292626

Matsunaga, E., Nambu, S., Oka, M., & Iriki, A. (2013). Differential cadherin expression in the developing postnatal telencephalon of a new world monkey. *J Comp Neurol, 521*(17), 4027-4060. doi:10.1002/cne.23389

Matsunami, N., Hadley, D., Hensel, C. H., Christensen, G. B., Kim, C., Frackelton, E., . . . Hakonarson, H. (2013). Identification of rare recurrent copy number variants in high-risk autism families and their prevalence in a large asd population. *PLoS One, 8*(1), e52239. doi:10.1371/journal.pone.0052239

Mavroconstanti, T., Johansson, S., Winge, I., Knappskog, P. M., & Haavik, J. (2013). Functional properties of rare missense variants of human cdh13 found in adult attention deficit/hyperactivity disorder (adhd) patients. *PLoS One, 8*(8), e71445. doi:10.1371/journal.pone.0071445

McClung, C. A., & Nestler, E. J. (2008). Neuroplasticity mediated by altered gene expression. *Neuropsychopharmacology, 33*(1), 3-17. doi:10.1038/sj.npp.1301544

Migliarini, S., Pacini, G., Pelosi, B., Lunardi, G., & Pasqualetti, M. (2013). Lack of brain serotonin affects postnatal development and serotonergic neuronal circuitry formation. *Mol Psychiatry, 18*(10), 1106-1118. doi:10.1038/mp.2012.128

Mizumori, S. J., Miya, D. Y., & Ward, K. E. (1994). Reversible inactivation of the lateral dorsal thalamus disrupts hippocampal place representation and impairs spatial learning. *Brain Res, 644*(1), 168-174. doi:10.1016/0006-8993(94)90361-1

Mlinar, B., Montalbano, A., Baccini, G., Tatini, F., Berlinguer Palmini, R., & Corradetti, R. (2015). Nonexocytotic serotonin release tonically suppresses serotonergic neuron activity. *J Gen Physiol, 145*(3), 225-251. doi:10.1085/jgp.201411330

Mossink, B., van Rhijn, J. R., Wang, S., Linda, K., Vitale, M. R., Zoller, J. E. M., . . . Nadif Kasri, N. (2021). Cadherin-13 is a critical regulator of gabaergic modulation in human stem-cell-derived neuronal networks. *Mol Psychiatry*. doi:10.1038/s41380-021-01117-x

Muller, C. L., Anacker, A. M. J., & Veenstra-VanderWeele, J. (2016). The serotonin system in autism spectrum disorder: From biomarker to animal models. *Neuroscience, 321*, 24-41. doi:10.1016/j.neuroscience.2015.11.010

Muzerelle, A., Scotto-Lomassese, S., Bernard, J. F., Soiza-Reilly, M., & Gaspar, P. (2016). Conditional anterograde tracing reveals distinct targeting of individual serotonin cell groups (b5-b9) to the forebrain and brainstem. *Brain Struct Funct, 221*(1), 535-561. doi:10.1007/s00429-014-0924-4

Neale, B. M., Lasky-Su, J., Anney, R., Franke, B., Zhou, K., Maller, J. B., . . . Faraone, S. V. (2008). Genome-wide association scan of attention deficit hyperactivity disorder. *Am J Med Genet B Neuropsychiatr Genet, 147B*(8), 1337-1344. doi:10.1002/ajmg.b.30866

Neale, B. M., Medland, S., Ripke, S., Anney, R. J., Asherson, P., Buitelaar, J., . . . Group, I. I. C. (2010). Case-control genome-wide association study of attention-deficit/hyperactivity disorder. *J Am Acad Child Adolesc Psychiatry, 49*(9), 906-920. doi:10.1016/j.jaac.2010.06.007

Neale, B. M., Medland, S. E., Ripke, S., Asherson, P., Franke, B., Lesch, K. P., . . . Psychiatric, G. C. A. S. (2010). Meta-analysis of genome-wide association studies of attention-deficit/hyperactivity disorder. *J Am Acad Child Adolesc Psychiatry, 49*(9), 884-897. doi:10.1016/j.jaac.2010.06.008

Niederkofler, V., Asher, T. E., & Dymecki, S. M. (2015). Functional interplay between dopaminergic and serotonergic neuronal systems during development and adulthood. *ACS Chem Neurosci, 6*(7), 1055-1070. doi:10.1021/acschemneuro.5b00021

Nishiyama, H., Knopfel, T., Endo, S., & Itohara, S. (2002). Glial protein s100b modulates long-term neuronal synaptic plasticity. *Proc Natl Acad Sci U S A, 99*(6), 4037-4042. doi:10.1073/pnas.052020999

Oades, R. D., Lasky-Su, J., Christiansen, H., Faraone, S. V., Sonuga-Barke, E. J., Banaschewski, T., . . . Asherson, P. (2008). The influence of serotonin- and other genes on impulsive behavioral aggression and cognitive impulsivity in children with attention-deficit/hyperactivity disorder (adhd): Findings from a family-based association test (fbat) analysis. *Behav Brain Funct, 4*, 48. doi:10.1186/1744-9081-4-48

Okaty, B. W., Sturrock, N., Escobedo Lozoya, Y., Chang, Y., Senft, R. A., Lyon, K. A., . . . Dymecki, S. M. (2020). A single-cell transcriptomic and anatomic atlas of mouse dorsal raphe pet1 neurons. *Elife, 9*. doi:10.7554/eLife.55523

Paradis, S., Harrar, D. B., Lin, Y., Koon, A. C., Hauser, J. L., Griffith, E. C., . . . Greenberg, M. E. (2007). An rnai-based approach identifies molecules required for glutamatergic and gabaergic synapse development. *Neuron, 53*(2), 217-232. doi:10.1016/j.neuron.2006.12.012

Perry, B. A. L., & Mitchell, A. S. (2019). Considering the evidence for anterior and laterodorsal thalamic nuclei as higher order relays to cortex. *Front Mol Neurosci, 12*, 167. doi:10.3389/fnmol.2019.00167

Philippova, M., Ivanov, D., Joshi, M. B., Kyriakakis, E., Rupp, K., Afonyushkin, T., . . . Resink, T. J. (2008). Identification of proteins associating with glycosylphosphatidylinositol- anchored t-cadherin on the surface of vascular endothelial cells: Role for grp78/bip in t-cadherin-dependent cell survival. *Mol Cell Biol, 28*(12), 4004-4017. doi:10.1128/MCB.00157-08

Philippova, M., Ivanov, D., Tkachuk, V., Erne, P., & Resink, T. J. (2003). Polarisation of t-cadherin to the leading edge of migrating vascular cells in vitro: A function in vascular cell motility? *Histochem Cell Biol, 120*(5), 353-360. doi:10.1007/s00418-003-0584-6

Ranscht, B., & Dours-Zimmermann, M. T. (1991). T-cadherin, a novel cadherin cell adhesion molecule in the nervous system lacks the conserved cytoplasmic region. *Neuron, 7*(3), 391-402. doi:10.1016/0896-6273(91)90291-7

Reeber, S. L., Arancillo, M., & Sillitoe, R. V. (2018). Bergmann glia are patterned into topographic molecular zones in the developing and adult mouse cerebellum. *Cerebellum, 17*(4), 392-403. doi:10.1007/s12311-014-0571-6

Ren, J., Isakova, A., Friedmann, D., Zeng, J., Grutzner, S. M., Pun, A., . . . Luo, L. (2019). Single-cell transcriptomes and whole-brain projections of serotonin neurons in the mouse dorsal and median raphe nuclei. *Elife, 8*. doi:10.7554/eLife.49424

Renier, N., Adams, E. L., Kirst, C., Wu, Z., Azevedo, R., Kohl, J., . . . Tessier-Lavigne, M. (2016). Mapping of brain activity by automated volume analysis of immediate early genes. *Cell, 165*(7), 1789-1802. doi:10.1016/j.cell.2016.05.007

Renier, N., Wu, Z., Simon, D. J., Yang, J., Ariel, P., & Tessier-Lavigne, M. (2014). Idisco: A simple, rapid method to immunolabel large tissue samples for volume imaging. *Cell, 159*(4), 896-910. doi:10.1016/j.cell.2014.10.010

Rivero, O., Selten, M. M., Sich, S., Popp, S., Bacmeister, L., Amendola, E., . . . Lesch, K. P. (2015). Cadherin-13, a risk gene for adhd and comorbid disorders, impacts gabaergic function in hippocampus and cognition. *Transl Psychiatry, 5*, e655. doi:10.1038/tp.2015.152

Rivero, O., Sich, S., Popp, S., Schmitt, A., Franke, B., & Lesch, K. P. (2013). Impact of the adhd-susceptibility gene cdh13 on development and function of brain networks. *Eur Neuropsychopharmacol, 23*(6), 492-507. doi:10.1016/j.euroneuro.2012.06.009

Robbins, T. W. (2002). The 5-choice serial reaction time task: Behavioural pharmacology and functional neurochemistry. *Psychopharmacology (Berl), 163*(3-4), 362-380. doi:10.1007/s00213-002-1154-7

Sacristan, M. P., Vestal, D. J., Dours-Zimmermann, M. T., & Ranscht, B. (1993). T-cadherin 2: Molecular characterization, function in cell adhesion, and coexpression with t-cadherin and n-cadherin. *J Neurosci Res, 34*(6), 664-680. doi:10.1002/jnr.490340610

Salatino-Oliveira, A., Genro, J. P., Polanczyk, G., Zeni, C., Schmitz, M., Kieling, C., . . . Hutz, M. H. (2015). Cadherin-13 gene is associated with hyperactive/impulsive symptoms in attention/deficit hyperactivity disorder. *Am J Med Genet B Neuropsychiatr Genet, 168B*(3), 162-169. doi:10.1002/ajmg.b.32293

Sanders, S. J., He, X., Willsey, A. J., Ercan-Sencicek, A. G., Samocha, K. E., Cicek, A. E., . . . State, M. W. (2015). Insights into autism spectrum disorder genomic architecture and biology from 71 risk loci. *Neuron, 87*(6), 1215-1233. doi:10.1016/j.neuron.2015.09.016

Schmidt, S., & Petermann, F. (2009). Developmental psychopathology: Attention deficit hyperactivity disorder (adhd). *BMC Psychiatry, 9*, 58. doi:10.1186/1471-244X-9-58

Shapiro, L., & Weis, W. I. (2009). Structure and biochemistry of cadherins and catenins. *Cold Spring Harb Perspect Biol, 1*(3), a003053. doi:10.1101/cshperspect.a003053

Sherman, S. M. (2017). Functioning of circuits connecting thalamus and cortex. *Compr Physiol, 7*(2), 713-739. doi:10.1002/cphy.c160032

Sibille, E., Wang, Y., Joeyen-Waldorf, J., Gaiteri, C., Surget, A., Oh, S., . . . Lewis, D. A. (2009). A molecular signature of depression in the amygdala. *Am J Psychiatry, 166*(9), 1011-1024. doi:10.1176/appi.ajp.2009.08121760

Sodhi, M. S., & Sanders-Bush, E. (2004). Serotonin and brain development. *Int Rev Neurobiol, 59*, 111-174. doi:10.1016/S0074-7742(04)59006-2

Sorci, G., Riuzzi, F., Arcuri, C., Tubaro, C., Bianchi, R., Giambanco, I., & Donato, R. (2013). S100b protein in tissue development, repair and regeneration. *World J Biol Chem, 4*(1), 1-12. doi:10.4331/wjbc.v4.i1.1

Spencer, T. J. (2006). Adhd and comorbidity in childhood. *J Clin Psychiatry, 67 Suppl 8*, 27-31.

Spencer, W. C., & Deneris, E. S. (2017). Regulatory mechanisms controlling maturation of serotonin neuron identity and function. *Front Cell Neurosci, 11*, 215. doi:10.3389/fncel.2017.00215

Spivak, B., Vered, Y., Yoran-Hegesh, R., Averbuch, E., Mester, R., Graf, E., & Weizman, A. (1999). Circulatory levels of catecholamines, serotonin and lipids in attention deficit hyperactivity disorder. *Acta Psychiatr Scand, 99*(4), 300-304. doi:10.1111/j.1600-0447.1999.tb07229.x

Stegner, D., vanEeuwijk, J. M. M., Angay, O., Gorelashvili, M. G., Semeniak, D., Pinnecker, J., . . . Heinze, K. G. (2017). Thrombopoiesis is spatially regulated by the bone marrow vasculature. *Nat Commun, 8*(1), 127. doi:10.1038/s41467-017-00201-7

Tak, Y. G., & Farnham, P. J. (2015). Making sense of gwas: Using epigenomics and genome engineering to understand the functional relevance of snps in non-coding regions of the human genome. *Epigenetics Chromatin, 8*, 57. doi:10.1186/s13072-015-0050-4

Takeuchi, T., Misaki, A., Liang, S. B., Tachibana, A., Hayashi, N., Sonobe, H., & Ohtsuki, Y. (2000). Expression of t-cadherin (cdh13, h-cadherin) in human brain and its characteristics as a negative growth regulator of epidermal growth factor in neuroblastoma cells. *J Neurochem, 74*(4), 1489-1497. doi:10.1046/j.1471-4159.2000.0741489.x

Teng, T., Gaillard, A., Muzerelle, A., & Gaspar, P. (2017). Ephrina5 signaling is required for the distinctive targeting of raphe serotonin neurons in the forebrain. *eNeuro, 4*(1). doi:10.1523/ENEURO.0327-16.2017

Terracciano, A., Sanna, S., Uda, M., Deiana, B., Usala, G., Busonero, F., . . . Costa, P. T., Jr. (2010). Genome-wide association scan for five major dimensions of personality. *Mol Psychiatry, 15*(6), 647-656. doi:10.1038/mp.2008.113

Tiihonen, J., Rautiainen, M. R., Ollila, H. M., Repo-Tiihonen, E., Virkkunen, M., Palotie, A., . . . Paunio, T. (2015). Genetic background of extreme violent behavior. *Mol Psychiatry, 20*(6), 786-792. doi:10.1038/mp.2014.130

Turrigiano, G. G. (2008). The self-tuning neuron: Synaptic scaling of excitatory synapses. *Cell, 135*(3), 422-435. doi:10.1016/j.cell.2008.10.008

Uhl, G. R., Drgon, T., Johnson, C., Li, C. Y., Contoreggi, C., Hess, J., . . . Liu, Q. R. (2008). Molecular genetics of addiction and related heritable phenotypes: Genome-wide association approaches identify "connectivity constellation" and drug target genes with pleiotropic effects. *Ann N Y Acad Sci, 1141*, 318-381. doi:10.1196/annals.1441.018

Uhl, G. R., Drgon, T., Liu, Q. R., Johnson, C., Walther, D., Komiyama, T., . . . Lin, S. K. (2008). Genome-wide association for methamphetamine dependence: Convergent results from 2 samples. *Arch Gen Psychiatry, 65*(3), 345-355. doi:10.1001/archpsyc.65.3.345

Valera, E. M., Faraone, S. V., Murray, K. E., & Seidman, L. J. (2007). Meta-analysis of structural imaging findings in attention-deficit/hyperactivity disorder. *Biol Psychiatry, 61*(12), 1361-1369. doi:10.1016/j.biopsych.2006.06.011

van Groen, T., Kadish, I., & Wyss, J. M. (2002). The role of the laterodorsal nucleus of the thalamus in spatial learning and memory in the rat. *Behav Brain Res, 136*(2), 329-337. doi:10.1016/s0166-4328(02)00199-7

Volkow, N. D., & Swanson, J. M. (2013). Clinical practice: Adult attention deficit-hyperactivity disorder. *N Engl J Med, 369*(20), 1935-1944. doi:10.1056/NEJMcp1212625

Walf, A. A., & Frye, C. A. (2007). The use of the elevated plus maze as an assay of anxiety-related behavior in rodents. *Nat Protoc, 2*(2), 322-328. doi:10.1038/nprot.2007.44

Whitaker-Azmitia, P. M. (2001). Serotonin and brain development: Role in human developmental diseases. *Brain Res Bull, 56*(5), 479-485. doi:10.1016/s0361-9230(01)00615-3

Whitaker-Azmitia, P. M., & Azmitia, E. C. (1986). Autoregulation of fetal serotonergic neuronal development: Role of high affinity serotonin receptors. *Neurosci Lett, 67*(3), 307-312. doi:10.1016/0304-3940(86)90327-7

Whitaker-Azmitia, P. M., Murphy, R., & Azmitia, E. C. (1990). Stimulation of astroglial 5-ht1a receptors releases the serotonergic growth factor, protein s-100, and alters astroglial morphology. *Brain Res, 528*(1), 155-158. doi:10.1016/0006-8993(90)90210-3

Wilens, T. E., & Spencer, T. J. (2010). Understanding attention-deficit/hyperactivity disorder from childhood to adulthood. *Postgrad Med, 122*(5), 97-109. doi:10.3810/pgm.2010.09.2206

Winstanley, C. A., Eagle, D. M., & Robbins, T. W. (2006). Behavioral models of impulsivity in relation to adhd: Translation between clinical and preclinical studies. *Clin Psychol Rev, 26*(4), 379-395. doi:10.1016/j.cpr.2006.01.001

Wyler, S. C., Spencer, W. C., Green, N. H., Rood, B. D., Crawford, L., Craige, C., . . . Deneris, E. (2016). Pet-1 switches transcriptional targets postnatally to regulate maturation of serotonin neuron excitability. *J Neurosci, 36*(5), 1758-1774. doi:10.1523/JNEUROSCI.3798-15.2016

Xu, W., Cohen-Woods, S., Chen, Q., Noor, A., Knight, J., Hosang, G., . . . Vincent, J. B. (2014). Genome-wide association study of bipolar disorder in canadian and uk populations corroborates disease loci including syne1 and csmd1. *BMC Med Genet, 15*, 2. doi:10.1186/1471-2350-15-2

Yoshida, C., & Takeichi, M. (1982). Teratocarcinoma cell adhesion: Identification of a cell-surface protein involved in calcium-dependent cell aggregation. *Cell, 28*(2), 217-224. doi:10.1016/0092-8674(82)90339-7

Zhou, K., Asherson, P., Sham, P., Franke, B., Anney, R. J., Buitelaar, J., . . . Faraone, S. V. (2008). Linkage to chromosome 1p36 for attention-deficit/hyperactivity disorder traits in school and home settings. *Biol Psychiatry, 64*(7), 571-576. doi:10.1016/j.biopsych.2008.02.024

Zhou, K., Dempfle, A., Arcos-Burgos, M., Bakker, S. C., Banaschewski, T., Biederman, J., . . . Asherson, P. (2008). Meta-analysis of genome-wide linkage scans of attention deficit hyperactivity disorder. *Am J Med Genet B Neuropsychiatr Genet, 147B*(8), 1392-1398. doi:10.1002/ajmg.b.30878

APPENDIX A

Macro Script for Quantification of TPH2-ir Neurons in the DR

```
imageTitle=getTitle();
run("Split Channels");
if (isOpen("C3-"+imageTitle)) {
    selectWindow("C3-"+imageTitle);
run("Close");};
selectWindow("C1-"+imageTitle);
run("Close");

selectWindow("C2-"+imageTitle);
run("Duplicate...", "title=Dup_C2-"+imageTitle+" duplicate");
run("Subtract Background...", "rolling=20");
run("Subtract Background...", "rolling=20 stack");
run("Median...", "radius=2 stack");
run("Z Project...", "projection=[Average Intensity]");
run("Enhance Contrast...", "saturated=0.3");
run("Rotate 90 Degrees Right");
rename("AVG_L.oib");

selectWindow("C2-"+imageTitle);
run("Rotate 90 Degrees Right");
rename("L.oib");

selectWindow("Dup_C2-"+imageTitle);
run("Close");

imageTitle=getTitle();
run("Split Channels");
if (isOpen("C3-"+imageTitle)) {
    selectWindow("C3-"+imageTitle);
run("Close");};
selectWindow("C1-"+imageTitle);
run("Close");

selectWindow("C2-"+imageTitle);
run("Duplicate...", "title=Dup_C2-"+imageTitle+" duplicate");
run("Subtract Background...", "rolling=20");
run("Subtract Background...", "rolling=20 stack");
run("Median...", "radius=2 stack");
run("Z Project...", "projection=[Average Intensity]");
run("Enhance Contrast...", "saturated=0.3");
run("Rotate 90 Degrees Right");
rename("AVG_R.oib");

selectWindow("C2-"+imageTitle);
run("Rotate 90 Degrees Right");
rename("R.oib");

selectWindow("Dup_C2-"+imageTitle);
run("Close");

run("Images to Stack", "name=Stack title=[] use");
run("Make Montage...", "columns=2 rows=1 scale=0.80");
run("Fire");

selectWindow("Stack");
run("Close");

run("Cell Counter");
```

APPENDIX B

Macro Script for Quantification of 5-HTT-ir Fibers

```
//should install the PeakFinderTool first
//Plugins->macros->install...

imageTitle=getTitle();
run("Split Channels");
selectWindow("C1-"+imageTitle);
close();

run("Z Project...", "projection=[Average Intensity]");
run("Subtract Background...", "rolling=1.45");
/*
the thresholding and the contrast of all the regions are set to be IsoData and 0.01, respectively.
The rolling ball radius of background subtraction (line 7 in the macro)
for the PFC, amyBL and ThaPV, it is 1.5;  for cPu and ThaDL, it is 1.45.
*/
run("Enhance Contrast...", "saturated=0.01 normalize");
setAutoThreshold("IsoData dark");
run("Make Binary");

//makeOval(74, 150, 863, 482);// for amyBL
//makeRectangle(45, 45, 710, 710);//for CPu
//makeRectangle(74, 109, 880, 557);//ThaDL
//makeRectangle(119, 37, 787, 668);//ThaPV
//makeRectangle(220, 222, 358, 358);//PFC
//makeOval(101, 19, 683, 618);//CG
//makeOval(69, 72, 872, 603);//IL

{
 run("Select None");

 saveSettings();
 original=getTitle();
 setForegroundColor(255,0,0);

 width = getWidth()-120;   // width of the randomly placed ROI
 height = getHeight()-120; // height of the randomly placed ROI
 RoisN =7; // number of ROIs
 trials=500 ; //maximum trials to avoid infinite loop

 i=0;
 j=0;

 xa=newArray(RoisN);
 ya=newArray(RoisN);

 run("Duplicate...", "title=Reference");

 selectWindow("Reference");
 run("8-bit"); //makes it greyscale
 run("RGB Color"); //RGB to display colours
 run("Restore Selection");
 run("Make Inverse");
 run("Fill");
 run("Select None");


 while (i<RoisN && j<trials){
     w = 120;
```

```
        h = 120;
        x = random()*width;
        y = random()*height;
        j++;
        //Check for pixels with value (255,0,0):
        flag= -1;
        makeRectangle(x, y, w, h);
        //Scanning the rectangle perimeter should be faster than scanning the whole box.
        //This is slower, as checks all the points in the box:
        for (xs=x;xs<x+w;xs++){
           for (ys=y;ys<y+h;ys++){
              if (getPixel(xs,ys)==-65536) // pixel is (255,0,0)
                 flag=0;
           }
        }
        if (flag==-1){
           xa[i]=x;
           ya[i]=y;
           run("Fill");
           i++;
        }
   }


  close();
  selectWindow(original);
  setForegroundColor(255,255,0);
     nFiber=newArray(i);
  for (j=0;j<i;j++){
            linew = 100;
    makeLine(xa[j], ya[j], xa[j], ya[j]+linew);
     //run("Area to Line");
     //run("Measure");
     //run("Label");
     run("Find Peaks [3]");
     nFiber[j]=getValue("selection.size")-2;
     run("Draw");
  }
N=nResults;
setResult("Name", N, imageTitle);
for (j = 0; j < i; j++) {
 k=j+1;
setResult("No.Fiber"+k, N, nFiber[j]);
}

updateResults();
}
run("Close All");
```

List of publications

Forero A, Rivero O, Wäldchen S, **Ku HP**, Kiser DP, Gärtner Y, Pennington LS, Waider J, Gaspar P, Jansch C, Edenhofer F, Resink TJ, Blum R, Sauer M, Lesch K.P. Cadherin-13 Deficiency Increases Dorsal Raphe 5-HT Neuron Density and Prefrontal Cortex Innervation in the Mouse Brain. Front Cell *Neurosci*. 2017 Sep 26;11:307. doi: 10.3389/fncel.2017.00307. PMID: 29018333; PMCID: PMC5623013.

Forero A, **Ku HP**, Malpartida AB, Wäldchen S, Alhama-Riba J, Kulka C, Aboagye B, Norton WHJ, Young AMJ, Ding YQ, Blum R, Sauer M, Rivero O, Lesch K.P. Serotonin (5-HT) neuron-specific inactivation of Cadherin-13 impacts 5-HT system formation and cognitive function. *Neuropharmacology*. 2020 May 15;168:108018. doi: 10.1016/j.neuropharm.2020.108018. Epub 2020 Feb 28. PMID: 32113967.

Rivero O, Alhama-Riba J, **Ku HP**, Fischer M, Ortega G, Álmos P, Diouf D, van den Hove DL, Lesch K.P. (submitted). Haploinsufficiency of the ADHD risk gene St3gal3 in mice causes alterations in cognition and expression of genes involved in myelination and sialylation.

Ziegler GC, Ehlis AC, Weber H, Vitale MR, Zöller JEM, **Ku HP**, Schiele MA, Kürbitz LI, Romanos M, Pauli P, Kalisch R, Zwanzger P, Domschke K, Fallgatter AJ, Reif A, Lesch K.P. (submitted). A common CDH13 variant is associated with low agreeableness and neural responses to working memory tasks in ADHD.

Ku HP, Sich S, Rivero O, Pennington L, Schmitt A, Asan E, Lesch K.P. (manuscript in preparation). Regional and transmitter system-related expression of Cadherin-13 in murine brain.

Affidavit

I hereby confirm that my thesis entitled "Cadherin-13 Deficiency Impacts Murine Serotonergic Circuitries and Cognitive Functions" is the result of my own work. I did not receive any help or support from commercial consultants. All sources and / or materials applied are listed and specified in the thesis.

Furthermore, I confirm that this thesis has not yet been submitted as part of another examination process neither in identical nor in similar form.

_____ _____

Place, Date Signature

Eidesstattliche Erklärung

Hiermit erkläre ich an Eides statt, die Dissertation mit dem Titel "Cadherin-13 Defizienz beeinflusst serotonerge Netzwerke und kognitive Funktionen der Maus" eigenständig, d.h. insbesondere selbständig und ohne Hilfe eines kommerziellen Promotionsberaters, angefertigt und keine anderen als die von mir angegebenen Quellen und Hilfsmittel verwendet zu haben.

Ich erkläre außerdem, dass die Dissertation weder in gleicher noch in ähnlicher Form bereits in einem anderen Prüfungsverfahren vorgelegen hat.

_____ _____

Ort, Datum Unterschrift